Università degli Studi di Padova

Dipartimento di Ingegneria Industriale

Corso di Laurea Magistrale in Ingegneria Energetica

Tesi di Laurea Magistrale

Commissioning of a test section for the measurement of in-tube heat transfer coefficient

Collaudo di un impianto per la misura del coefficiente di scambio termico entro tubi

Relatore: Prof. Ing. Davide Del Col (DII-Università di Padova)

Co-Relatore: Prof. Ing.Luke Andrea (TTK Universität Kassel)

Supervisore: Ing. Severin Skusa (TTK Universität Kassel)

Candidato: Imprescia Stefano (1036965)

Anno Accademico 2013/2014

Sommario

L'efficienza energetica è una tematica importante nell'ottica della riduzione delle emissioni di anidride carbonica. In questo contesto il miglioramento degli scambiatori di calore è una componente essenziale e vede come scopo ultimo la scelta di compromesso tra calore scambiato e perdite di carico. Particolare applicazione dove questo risulta determinante è la liquefazione del gas naturale. Questa avviene attraverso due stadi di raffreddamento e poiché le temperature in gioco sono molto basse, i rendimenti di primo ma soprattutto secondo principio risultano pesantemente influenzati. Al fine di migliorare l'efficienza del primo stadio di raffreddamento del gas naturale, è stato approntato un impianto sperimentale atto a simulare il processo in questione. Particolarità di questo impianto è l'essere provvisto di una pompa multifase che permette il funzionamento dello scambiatore di test (tubo in tubo) con diversi tipi di fluido, anche contemporaneamente. Sarà dunque possibile effettuare test riguardanti lo scambio termico mono- e bifase, in questo caso di solo calore sensibile, per simulare le diverse condizioni operative del sistema. Durante la fase di collaudo dell'impianto, oggetto di questo lavoro, i fluidi coinvolti nei test saranno isopropanolo per la fase liquida e azoto per la fase gassosa.

Inizialmente vengono riportati i concetti teorici di base utili per le misure affrontate, poi viene mostrata la composizione dell'impianto sperimentale, soffermandosi sulle sue componenti, quindi è stata presentata la metodologia di riduzione dei dati con la quale sarà possibile comprendere i risultati dei test riportati di seguito.

Una sessione di misure preliminari ha dato risultati inaspettati, che si discostavano eccessivamente da quanto riportato in letteratura, perciò è stata pianificata una serie di test atti a comprendere la natura delle discrepanze riscontrate. Componente principale del lavoro sono i test effettuati con la sola fase liquida, in quanto più semplice da analizzare. Grazie a questi sono stati evidenziati dei difetti intrinseci nella costruzione della sezione di misura. Nella sezione esterna i tubi capillari, che introducono le termocoppie sulla superficie esterna del tubo interno, generano una turbolenza che altera lo scambio termico, rendendo il profilo di temperatura della parete esterna non continuo. Inoltre i tubi che portano ed estraggono il refrigerante nello scambiatore sono posizionati in prossimità della prima ed ultima sezione di misura, influenzandone i valori registrati. Alla luce di queste problematiche viene consigliata una costruzione diversa dello scambiatore. Infine vengono riportati i risultati di misure con fluido primario azoto e con una miscela bifase di isopropanolo e azoto.

Abstract

Energy efficiency plays an important role in the reduction of CO_2-emmissions. The improvement of heat exchangers is one of the essential topics in this context and has the final goal the pay off between exchanged heat and pressure drop. Particular application where this choice is determinant is the liquefy of natural gas. This process is done using two cooling cycles and since the needed temperatures are very low, the energy and especially exergy efficiency is strongly affected.

With the purpose of improving the efficiency of the first cycle, a test facility is built in order to simulate this process. Particularity of this plant is that it is run by a multiphase pump, which allows the flow of liquid and gas phase, even of two different fluids, in the heat exchanger (a tube shell heat exchanger). In this way it is possible to measure single and multi-phase heat transfer coefficient (non-condensing flow), so as to simulate the various operative conditions of the system. During the commissioning of the test rig, object of this work, the fluids used are isopropanol for liquid phase and nitrogen for gaseous phase.

Theoretical basis of the phenomena occurring in the test rig are explained in the first chapter. Then the experimental setup is showed, focusing on the components and sensors consisting the facility. Afterwards, the data reduction methods are explained, followed by the test performed during the commissioning phase.

A preliminary measurement session is carried out, showing results far from literature. Thus, a list of test has been made in order to understand this discrepancy. Main part of the tests are recorded using liquid isopropanol as working fluid. These test brought to light that the shell side has some intrinsic construction problem. In fact the construction that allows the thermocouple to reach the outer wall are causing turbulence that changes the htc in the shell side and so the temperature profile. Furthermore the sub-pipes supplying the coolant in the shell side are mounted in the proximity of the first and last measurement section. The fluid flows direct on the sensor spoiling the results. In order to avoid this problems a different configuration of the shell side is suggested. Anyway, as result of this work it was possible to reduct data with an extended method. In this way gaseous and 2-phase tests are made and the both of them brought a different behavior of the test section. Outer wall temperature trends are different between gas and liquid tests, theoretically due to the great difference in mass flow. Two phase tests brought plausible results according to literature analogies and to the previous tests. The comprehension of these phenomena are still object of test.

To my beloved family
and to all the people
that kept on believe in me

Alla mia amata famiglia
e a tutte le persone
che hanno creduto in me

Padua, 09 October 2014

Table of Contents

Nomenclature

Latin Symbols

A	Considered Surface	$[m^2]$
A, B, C	Constant of polynomial interpolation	
C	General constant values	
c_p	Isobaric heat capacity	$\left[\frac{W}{kg \cdot K}\right]$
D	Considered Diameter	$[m]$
f	Friction factor	
G	Specific mass flow	$\left[\frac{kg}{s \cdot m^2}\right]$
L	Characteristic length	$[m]$
m, n	General coefficients for Nusselt correlation	
$\dot{m}$	Mass flow	$\left[\frac{kg}{s}\right]$
p	Pressure	$[bar, mbar]$
P	Perimeter	$[m]$
q	Specific heat flow	$\left[\frac{W}{m^2}\right]$
Q	Heat	$[J]$
$\dot{Q}$	Heat flow	$[W]$
R	Thermal resistance	$\left[\frac{m^2 \cdot K}{W}\right]$
t	Temperature	[°C]
w	fluid speed	$\left[\frac{m}{s}\right]$
x	vapor quality	
X	Martinelli parameter	
z	General length	

Greek Symbols

α	Heat Transfer Coefficient	$\left[\frac{W}{m^2 \cdot K}\right]$
β	Pitch angle of pipe	$[°]$
∂	Partial differential	
Δ	General difference	
ε	Void Fraction	
λ	Thermal Conductivity	$\left[\frac{W}{m \cdot K}\right]$
μ	Dynamic Viscosity	$\left[\frac{Pa}{s}\right]$
ν	Specific volume	$\left[\frac{m^3}{kg}\right]$
ρ	Density	$\left[\frac{kg}{m^3}\right]$
φ	Circumferential coordinate	
Φ	Phase multiplicator	

Subscripts

- Boundaries

in	Inlet
out	Outlet
$i-o$	From inlet to outlet
int	Internal
ext	External
$1,2,3$	Reference numeration for measurement section
$1-3$	From first to third section
$\overline{1-3}$	From first to third section considering the shell side

- Correlations

DB	Dittus Bölter
Gn	Gnielinski
Ha	Hausen
PP	Petukhov Popov

- Substance

g	Gas
G	Gas only

l	Liquid
L	Liquid only
OM	Homogeneous model
th	Therminol
WF	Working fluid

- Others

$fluid$	Fluid reference
h	Hydraulic reference
i, j	Cursors for sums
$loss$	Losses reference
$wall$	Wall reference
∞	Not perturbed fluid
n	Cursor for layer of the wall

Dimensionless Numbers

Nu	Nusselt Number
Pr	Prandtl Number
Re	Reynolds Number

Abbreviations

$Corr$	Corrective
$e.v.$	Expected Value
htc	Heat Transfer Coefficient
Ins	Insulation
$m.s.$	Measurement Section
$m.v.$	Measured Value
PT, RTD	Resistance temperature detector
TC	Thermocouple
tot	Total

List of Figures

List of Tables

1 INTRODUCTION

The climate change is hot topics in nowadays both social and technical field. The European Union approved in December 2008 the “2020 climate and energy package”. This set of binding legislation has the target of: 20% reduction (from 1990 levels) of greenhouse gas emission in the EU, 20% rising of the share of EU energy consumption produced from renewable resources and 20% improvement in EU’s energy efficiency [1].

The European situation in terms of primary energy consumption, sees the natural gas as the second main energy resource with the $32{,}8\%$. In Italy natural gas plays an important role $(36{,}4\%)$, since the electricity production is based on this resource. Even in nations where the resource consumption share is more balanced, like in Germany, natural gas is the second resource used with the $(23{,}2\%$, all energy shares from BP statistical review 2014 [2]). Supply methods of natural gas can be standard, using gas-pipes or not standard through methane carriers. For the second option, the natural gas is liquefied and transported as liquid to the destination, where a regasification plant introduces it to the gas-net. Pro of this technology is the difference in specific volume between the gas and liquid state that allows to transport 600 time more natural gas in liquefied form (LNG). Con is the use of facilities capable of handle liquid at $-160°C$ (liquefy temperature of natural gas at $1\ bar$). The choice of using this technology is strictly bounded with geo-politics. In Italy, for instance, there are two regasification plant running, with the purpose of being less dependent on European gas market and because of Italy’s particular geographical position.

In order to liquefy the natural gas, specific cooling cycles are developed. In this case a two-cooling-level cycle is used, one for pre-cooling and the second for the actual liquefaction. An important issue for this step is the energy efficiency, because the deep temperatures are affecting both energy and exergy balance.

In the Thermodynamics faculty of Kassel University a test facility has been built with the purpose carrying out a research upon the efficiency during condensation of hydrocarbons. Normal plants with similar aim are composed by a unique path where the working fluid is flowing at the wanted conditions. The peculiarity of this facility is that it is run by a multiphase pump in order to use two different fluids as working fluids, one liquid and one gaseous, at the same time. Both liquid and gas phase are

flowing in two different paths before entering the test pipe. In this way it is possible to recreate an artificial two-phase flow which allows to perform tests in this particular conditions. The final goal of this test rig is to perform tests on an enhanced pipe with propane condensing inside it, but in order to perform the tests in the proper way the commissioning of the test facility has to be carried out.
After the end of the construction, tests carried out to compare the behavior of the facility with other facilities reported in literature. Hydraulic and Thermal commissioning using $3/4$" pipes, with isopropanol (liquid) and nitrogen (gas) are the first step. The second step is to run the plan with propane and perform the same test carried out before. The third step is to change the test pipe with a 1" pipe in order to check the consistency of the values recorded in this new configuration. The fourth one is to substitute the pipe with an internal enhanced pipe of 1", which is the final goal of the project. This work will handle the thermal commissioning of the test facility, explaining all the test made in order to understand the behavior of the test rig and in case to improve its performances.

The present work, with all the practical tests needed, is developed at the Institute of Technical Thermodynamics of the University of Kassel (Germany) within the Erasmus exchange program of the University of Padua (Italy).

2 THEORETICAL BASIS

2.1 Convective Heat Transfer

Thermal convection is one of the fundamental heat transfer mechanisms between two systems at different temperature. It takes place when the two systems are in relative motion upon each other. These can be two fluids or more commonly a fluid and a surface.

Convection involves two basic processes:

- Conduction: diffusion of heat at a microscopic scale depending on the temperature gradient and the thermal conductivity.
- Advection: heat transfer at a macroscopic scale due to the movement of the fluid particle, so dependent on the flux proprieties.

These two mechanisms act together in order to transfer heat from the hotter system to the colder one. Their contribution hangs on the flux behavior. In laminar flows conduction is predominant, due to the parallel movement of the fluid layers. In turbulent flow conduction acts in proximity of the wall and advection takes advantage of the chaotic flow of the bulk to transfer heat between particles with different thermal characteristics. Convection is therefore controlled by both fluid dynamics and thermodynamics.

An important classification of the convective heat transfer is made by the source of the fluid movement. Forced convection occurs when the fluid is in motion over the surface due to machines like pumps, stirrers, etc. When the fluid moves because of the density gradient (buoyancy forces), caused by thermal gradient, natural convection is happening. These phenomena are not always recognizable, since they can take place at the same moment but sometimes the effect of one is prevalent. In the actual applications forced convection is almost always used.

2.2 In Tube Convective Heat Transfer

2.2.1 Boundary Layer

When a fluid enters in a pipe with a certain velocity, its behavior is affected by the change of boundaries. When it flows in contact with a wall, shear stresses are generated due to viscous effects and so a velocity boundary layer will develop all

over the inner perimeter of the pipe. In this particular geometrical configuration this layer modifies the shape of the velocity profile. Since every infinitesimal part of perimeter has its own boundary layer between the wall and the center of the pipe, the general result is that all the layers will uniform due to mutual influences. The zone where these phenomena happen is called entry length.

In the fully developed zone, the final shape of the profile depends on the Reynolds number. With laminar flow the profile will be parabolic while with turbulent flow the profile will be flatter, as shown in Figure 2.1.

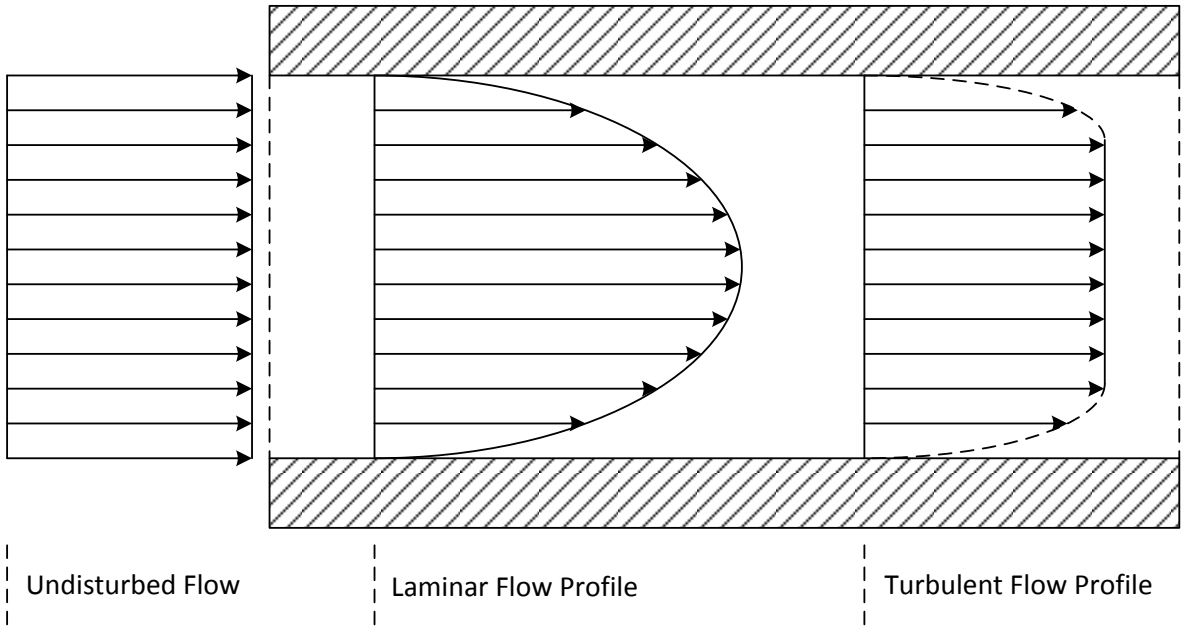

Figure 2.1: Representation of hydraulic and temperature profile

2.2.2 Heat Transfer Coefficient

When a fluid flows in a tube with a temperature difference between them, a heat flux is generated and a thermal boundary layer will develop just like in the hydrodynamic case. The shape of the thermal profile depends on the boundary condition of the heat transfer. Two possibilities are constant heat flux or constant wall temperature, both of them will lead to the same relative shape of temperature profile only involving a different development along the pipe. Considering the zone where both thermal and hydraulic boundary layers are fully developed, the hydro- thermal characteristics of the system can be considered as steady. So according to the similarity between electrical and thermal phenomena, the bodies at different thermal potential are

connected with a *thermal resistance* that is the proportionality between driving force for the flow of heat and the heat flux itself. Since the heat flux takes place through the interface between the two mediums, the resistance is directly linked to the extension of the surface.

The specific thermal conductance, reciprocal of the specific thermal resistance, represents the heat transfer coefficient $\alpha\ [W/m\text{^}2 * K]$, so the specific heat flux per area unit will be:

$$q = \frac{Q}{A} = \frac{t_{wall} - t_{fluid}}{R^*} = \alpha \cdot \left(t_w - t_f\right) \qquad 2.1$$

This equation was first stated by Newton and it is only based on experimental observation. In this way the convective heat transfer can be easily seen in the same way of the conductive heat transfer, only regulated by a different coefficient.

The htc coefficient Alpha is

$$\alpha = f\left\{\lambda;\ \rho;\ c_p;\ \mu;\ L;\ w_\infty\right\} \qquad 2.2$$

With:

- λ = Thermal Conductivity $[W/m \cdot K]$;
- ρ = Density $[kg/m^3]$;
- c_p = Isobaric specific heat $[kJ/kg \cdot K]$;
- μ = Dynamic Viscosity $[kg/m \cdot s]$;
- L = Characteristic Length $[m]$;
- w_∞ = Fluid Speed $[m/s]$.

It is difficult to estimate since is dependent on various parameters such as the fluid proprieties $\left(\lambda;\ \rho;\ c_p;\ \mu\right)$, the fluid speed (w_∞) and the characteristic length (L, referred on the geometrical configuration).

The characteristic length of the in-pipe flow cases is the hydraulic diameter D_h:

$$L = D_h = \frac{4 \cdot A}{P} \qquad 2.3$$

defined as four times the size of the cross-sectional area of the flow upon the perimeter of the cross-sectional area itself. Using the Buckingham theorem, with seven physical variables involving four units of measurements, a convective heat

transfer problem can be solved using a set of three non-dimensional parameters, which are:

- Nusselt number (Nu);
- Prandtl number (Pr);
- Reynolds number (Re).

The Nusselt number:

$$Nu = \frac{\alpha \cdot L}{\lambda} \tag{2.4}$$

is the ratio of heat transferred via convection upon the heat transferred via conduction. So being able to compute this number allows estimating the Alpha value of the examined problem.

The Prandtl number:

$$Pr = \frac{c_p \cdot \mu}{\lambda} \tag{2.5}$$

is the ratio between momentum diffusivity and thermal diffusivity and is directly bounded to the ratio between the velocity boundary layer and the thermal boundary layer which develops when a viscous fluid is moving among a wall.

This dimensionless Number is only composed by fluid characteristics, without accounting the influence of the boundary of the mass flux.

The Reynolds number

$$Re = \frac{\rho \cdot w_\infty \cdot L}{\mu} \tag{2.6}$$

defined as the ratio of inertial forces to viscous forces. The contribution of these two effects leads the mass flux to a laminar flow ($Re < 2100$ Viscous forces predominant) or to turbulent flow ($Re > 10^4$, inertial forces predominant

2.3 Correlation

The alpha value is estimable with empirical correlations which connects all the three dimensionless parameter. The usual form of a correlation is the following:

$$Nu = C \cdot Re^m \cdot Pr^n \tag{2.7}$$

Where *C*, *m* and *n* are specific parameters experimentally estimated for each heat transfer configuration. A Nusselt correlation has always to be used within its range of validity. Working in this range guarantees the accuracy of the calculation. To compare the experimental result with the literature are here presented four different correlations:

- Gnielinski (turbulent flow):

$$Nu_{Gn} = \frac{f/8 \cdot (Re - 1000) \cdot Pr}{1 + 12{,}7 \cdot (f/8)^{\frac{1}{2}} \left(Pr^{\frac{2}{3}} - 1\right)} \cdot \left[1 + \left(\frac{D_h}{L}\right)^{\frac{2}{3}}\right] \tag{2.8}$$

  With

$$f = (1{,}82 \cdot logRe - 1{,}64)^{-2} \tag{2.9}$$

  and valid for $2300 \leq Re < 5 \cdot 10^6$ and $0{,}5 \leq Pr < 10^6$

- Gnielinski (transition zone flow)

$$Nu_{Gn,trans} = (1 - \gamma) \cdot Nu_{Gn,lam,2300} + \gamma \cdot Nu_{Gn,turb,10^4} \tag{2.10}$$

  With

$$\gamma = \frac{Re - 2300}{10^4 - 2300} \tag{2.11}$$

  And

$$Nu_{Gn,lam,2300} = \left(Nu_{Gn,1} + Nu_{Gn,2,2300} + Nu_{Gn,2300}\right)^{\frac{1}{3}} \tag{2.12}$$

  Practically, the Gnielinksi correlation calculated at the limit of laminar and turbulent flow, modulated by the factor γ that places the calculated flow in the right spot of the transition zone.

- Petukhov & Popov:

$$Nu_{PP} = \frac{f/8 \cdot (Re - 1000) \cdot Pr}{C + 12{,}7 \cdot (f/8)^{\frac{1}{2}} \left(Pr^{\frac{2}{3}} - 1 \right)} \cdot \left[1 + \left(\frac{D_h}{L} \right)^{\frac{2}{3}} \right] \quad 2.13$$

With f like Gnielinski and

$$C = 1{,}07 + \frac{900}{Re} - \frac{0{,}63}{1 + 10 \cdot Pr} \quad 2.14$$

Valid for $4000 \leq Re < 5 \cdot 10^6$ and $0{,}5 \leq Pr < 10^6$.

- Dittus-Bölter:

$$Nu_{DB} = 0{,}026 \cdot Re^{0{,}8} \cdot Pr^{0{,}3} \quad 2.15$$

Valid for $2500 \leq Re < 125000$, $07 \leq Pr < 120$ and $L/D_h > 60$

- Hausen (for gas only):

$$Nu_{Ha,1} = 0{,}0214 \cdot (Re^{0{,}8} - 100) \cdot Pr^{0{,}4} \cdot \left[1 + \left(\frac{D_h}{L} \right)^{\frac{2}{3}} \right] \quad 2.16$$

for $0{,}5 \leq Pr < 1{,}5$

$$Nu_{Ha,2} = 0{,}012 \cdot (Re^{0{,}87} - 280) \cdot Pr^{0{,}4} \cdot \left[1 + \left(\frac{D_h}{L} \right)^{\frac{2}{3}} \right] \quad 2.17$$

for $1{,}5 \leq Pr < 500$

3 EXPERIMENTAL SETUP

This chapter will show how the test rig is built and show the entire main components in order to explain how the setup is prepared to measure the convective heat transfer coefficient.

3.1 Test facility

The KIIR test rig was built by the Thermodynamic department of the Kassel University to measure the convective heat transfer coefficient inside tubes during condensation. The test tube can be changed to analyze condensation in enhanced tubes. The working fluid may be changed to perform different tests.

The facility, represented in Figure 3.1, consists mainly of a primary cycle which includes the test section, a bypass cycle and three secondary cycles, one of them involved in the test section.

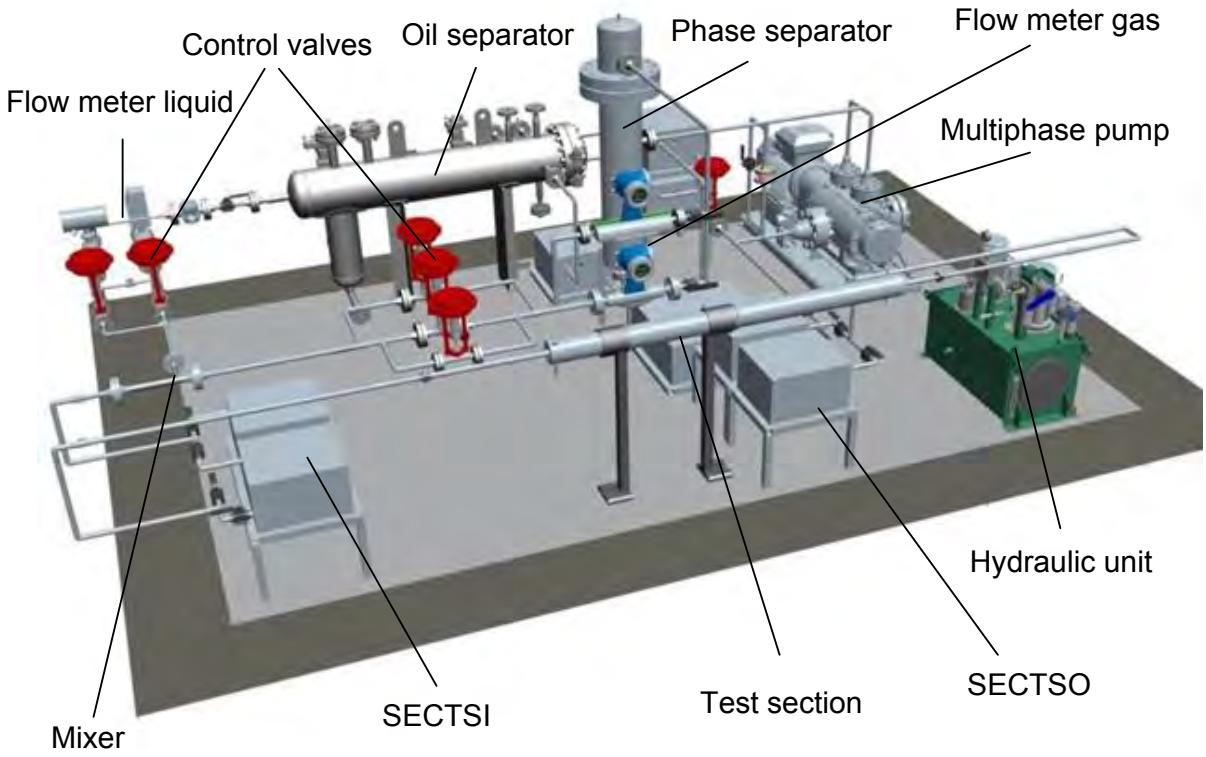

Figure 3.1: 3D representation of the main components of the test rig

3.1.1 Primary Cycle

According to Figure 8.1, following the path of the working fluid the first piece of equipment in this cycle is the multiphase pump (*MPP*). It overcomes the pressure drop and sets the pressure of the cycle. Here installed is a screw pump and to ensure that it works properly three conditions must be checked:

- Gas content (mass based) at suction greater than 94%, to avoid overheating due to compression
- Suction pressure greater than $0{,}5\ bar$, to avoid cavitation
- Pressure difference between suction and supply lower than $10\ bar$, to avoid too high mechanical stress

Two absolute pressure sensors are placed before (*AP1*) and after (*AP2*) the pump with the purpose of verify the previous conditions. The gas content is calculated using the flow meters installed in the whole primary cycle. The rotational speed of the multiphase pump can be set in the range of 400 to $1500\ rpm$ so as to change the volumetric flow in the primary cycle. Downstream the pump the flow enters in the droplet separator (*Gas/liquid separator*) where gravitational separation happens. The separator is equipped with a level controller.

The liquid flow forks in two branches, one side leads to the liquid bypass section which is provided with a flow meter (*Rotameter bypass*) and two heat exchangers that dissipate the heat injected by the pump. It has the duty to preserve the integrity of the multiphase pump and has the possibility to adjust the liquid mass flux in the test section with a remote controlled valve (*RV6*). It can also be used to set the pressure in the phase separator in order to control the inlet pressure of the test section.

The other side leads to the test section and takes the fluid to the Oil separator unit (*Oil separator*). This component extracts the oil from the liquid flow that is used as sealing and lubricant in the pump. This process takes place due to the coalescence phenomena and is important since oil presence in the working fluid can affect the heat transfer measurements [7].

After being purified, the liquid flows in two parallel pipes connected with two Coriolis flow meters (*Mass 2100-6 and Mass 2100-15*) able to measure mass flow in different but partially overlapped ranges. Further detail of the sensors will be discussed in a following section.

Next to this measurement station there are the two needle valves (*RV4* and *RV5*) to control the mass flow. Also the valves operate in different but overlapped ranges.
The gas section starts from the top of the droplet separator and its path is composed by the same measurement station (*Promass 83A04* and *Promass 83F25*) and by three needle valves in parallel (*RV1*, *RV2* and *RV3*) capable of setting the pressure loss like the previous one.
After the mass flow control site, the fluid path and the gas path converge to a static mixer that forms the desired fluid to the test section.

3.1.2 Secondary Cycles

Secondary cycles used in this test facility are auxiliary components placed to vary the thermal level of the working fluid. They are mainly composed of a heating machine, a pump, a heat exchanger and a thermostat that controls the temperature of the secondary working fluid. In total three Cycles are installed:

- Test Section Inlet Cycle (*SECTSI*), placed before the entrance of the test section, provides heat to the working fluid in order to rise the inlet temperature, especially to provide overheated gas for the test. In two phase applications it can be used to control the gas quality of the working fluid. It is equipped with five valves that allow the working fluid to bypass the heat exchanger or to flow in a smaller part of it so as to reduce the pressure drop for high mass flows.
- Test Section Cycle (*SECTS*), is the cycle connected to the test section and will be discussed in Section 3.1.3.
- Test Section Outlet Cycle (*SECTSO*) is connected to a heat exchanger downstream the test section used for the validation of the test rig and to complete the condensation in phase transition tests and is connected to one of the two heat exchangers in the bypass. So its duty is to extract heat from the working fluid.

3.1.3 Test Section

The test section is the main part of the test rig and it is composed of the test pipe coupled with the Test Section Cycle (*SECTS*).
The test section is a 3400 millimeter long straight tube-shell heat exchanger and it is positioned between an inlet and outlet straight stretch in order to avoid hydrodynamic influences that pipe bends may have in a such a built test rig.

In the test tube flows the primary cycle working fluid and before the entrance of this section, pressure and inlet temperature are measured by an absolute pressure sensor (*AP5,6*) and a temperature sensor (*RTD12*, *800* millimeters upstream the pipe inlet). In order not to disturb the in-pipe flow and consequently to have a better hydro-thermodynamic behavior of the working fluid, in the test pipe there are no sensors. The possibility was not taken into account also because of technical difficulties of such an installation. The outlet temperature and the pressure loss are then measured after the exit of the test section with a second temperature sensor and a differential pressure sensor (*RTD15*, 63 centimeters after the pipe outlet and *DP01* between inlet and outlet).

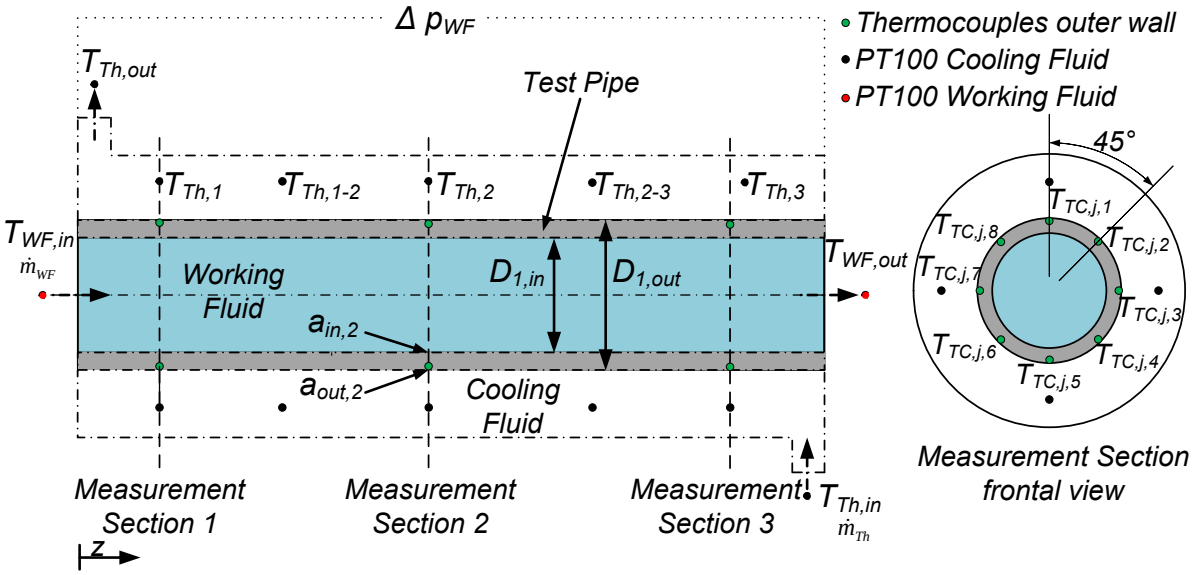

Figure 3.2: Schematic view of the test section

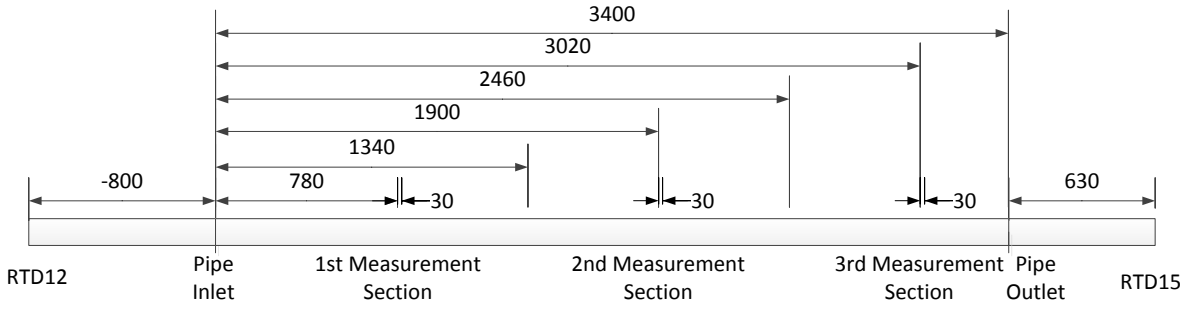

Figure 3.3: Position of the sensors in the test section [mm]

On the external surface of the test pipe there are three measurement sections, the first positioned after 780 millimeter from the inlet and the others at a distance of 1120 millimeters each. The actual length of the test section is therefore 2400 millimeters., Every section is composed of eight temperature sensors (*TC1-24*) glued in grooves, 0,5x0,5 millimeter large and 30 millimeter long, situated along the outer circumference of the pipe with a distance of 45 degrees one from the other as shown in Figure 3.4. So it is possible to measure the azimuthal and longitudinal outer wall temperature of the test section. Thanks to this the temperature variation of the working fluid in the tube can be analyzed.

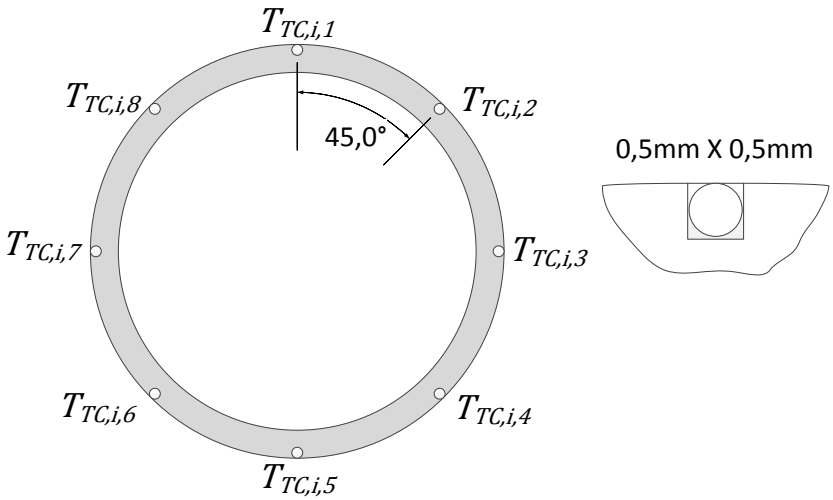

Figure 3.4: Cross-section of a measurement section

As mentioned in the previous section, the Test Section Cycle (*SECTS*) is the secondary cycle connected to the test section. It is equipped with a cooling machine (*Huber 635 W*) which provides the set temperature to its working fluid and conveys it towards the test section. It is also equipped with a bypass valve which can be used to regulate the mass flow to the test rig. The secondary working fluid flows through a flow meter (*Mass Flow Cooling B*) and then in the shell side, normally in counterflow to the primary working fluid. In fact it is possible to change the delivery and the return pipe so as to work in direct flow heat exchange. Before entering the heat exchanger, inlet temperature of the secondary working fluid is measured (*RTD14*) then three sub pipes, with a pitch angle of 45°, connect the delivery with the test section. The working fluid is led to flow homogeneously in the ring cross-section.

Along the outer pipe there are five measurement sections consisting of four temperature sensors (*RTD24(1-4) - 26(1-4)*) each at a distance of 90 degrees along the circumference. Beginning from the outlet, primary working fluid inlet, the first section is positioned after 780 millimeter and the others after 560 millimeter each. The sensors are threaded in the outer pipe and positioned in the center of the bulk flow. Having more measurement section allows to estimate with more accuracy the temperature trend of the secondary working fluid along the test section. This data set is important data to calculate the local heat transfer coefficient with the help of the specific heat flow.
The outlet temperature of the secondary fluid (*RTD13*) is measured after the regroup of the outlet sub pipes. A return pipe connects the outlet of the test section with the cooling machine closing the cycle.

3.2 Sensors

Several types of sensors are used in the test rig to measure the hydro- thermal proprieties of the fluids. All the sensors are connected to a multiplexer where all the signals coming from the test rig converge in order to be processed by the measurement computer. With this computer, thanks to the LabView software, it is possible to control the needle valves and all the cut off valves (*SDV1-7*) in the cycle but also to watch live the situation of the rig and to record data from it. All the needed sensors to calculate the htc are presented in this section, which are Temperature, Pressure and Flow sensors.

3.2.1 Temperature Sensors

As mentioned in the previous description there are two kinds of temperature sensors in the test rig called with different acronyms: TC for Thermocouple and RTD for Resistance Temperature Detector.

- The thermocouples installed are type K, so build with Chromel and Alumel alloys. Property of these sensors is that they are able to work in oxidant environment with a wide range of temperature. Each TC sensor is covered with two protective layers: the outer one is of Inconel while the inner one is of Magnesium oxide. For the calculation of the heat transfer coefficient, the outer surface temperature of the wall is needed but since the sensors are placed in

grooves like shown in Figure 4.3 a wall correction must be added. This correction takes into account also the fact that, due to technical problems the thermocouples are glued in the groves instead of being soldered. Effect of this variation will result in a reduction of thermal performance of the sensor caused by the lower conductivity of the glue layer. Since TC´s are active sensors, they do not need electrical alimentation and their output is a voltage difference. The cold junction used as reference to calculate the actual thermal output given by this sensor is placed in a box where the temperature is monitored by two temperature sensors (*RTD_TC1*, *RTD_TC2*).

- Resistance Temperature Detector RTD's installed in the rig are PT100, so a platinum electrical resistance that measures 100 Ohm at a temperature of 0 degree. These are passive sensors; the resistivity of the sensor is temperature dependent. This effect is used to record its changes, and so as to perform it the measurement circuit must provide electricity to the RTD. They work in a more limited range of temperature in comparison with Thermocouple but have a more linear behavior which allows them to be calibrated easily. The calibration of these elements has been made through a calibration bath (Julabo FK31SL). This instrument provides highest temperature stability to ±0.005 °C and temperature uniformity better than ±0.01 °C in order to perform a precise calibration (from datasheet). Recording the output data of the sensors put in this machine, for a mean time of one hour and thirty minutes, it was possible to build a polynomial curve that represent the behavior of the RTD:

$$T = f\{R\} = A + B_1 \cdot \sqrt{B_2 + B_3 \cdot R} \qquad 3.1$$

With A, B_1, B_2, B_3 different coefficient for every sensor. The calibration ended verifying the curve built by recording the output in degrees and comparing the value with the JuLabo temperature reference. An example of the results is shown in Figure 3.5. The calibration curve of the sensors RTD13 and RTD14 are often far from the expected values, because their curve has not been built in the same calibration campaign of the other sensors. This difference has in the end no big influence since it is always between $\pm 0{,}05℃$ from the expected value.

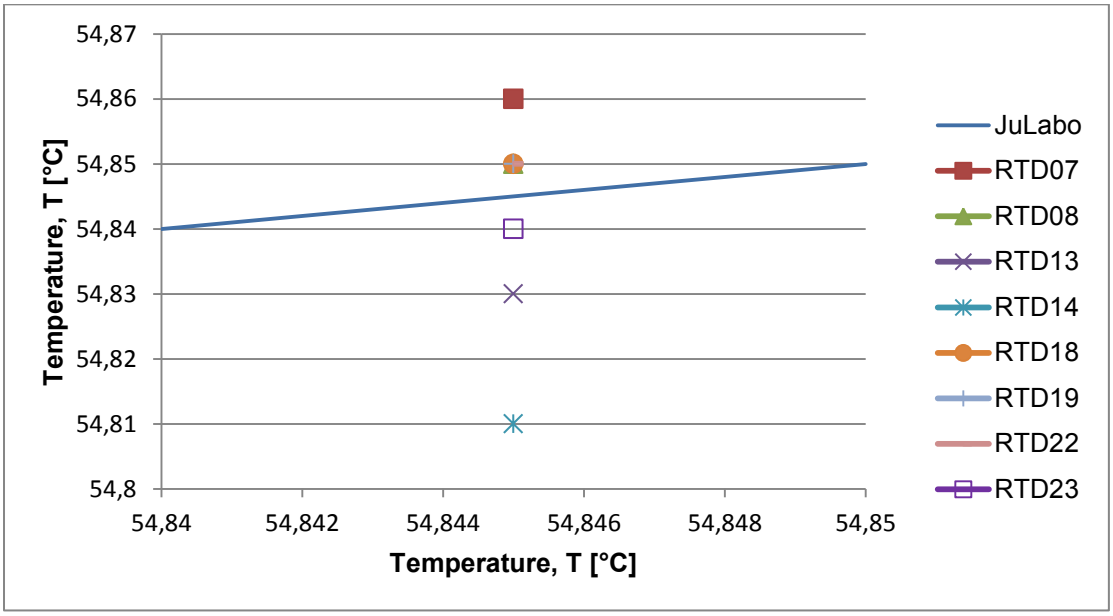

Figure 3.5: Calibration plot at $T = 55°C$

3.2.2 Pressure Sensors

Absolute and Differential Pressure transducers are used for the measurement of the pressure in the rig. Pressure measurements are used to calculate the fluid proprieties in the test section and to analyze the pressure drop while measuring the htc. Furthermore they are used to ensure the orderly functioning and integrity of the multiphase pump. Here installed are strain gauges pressure sensors, a diaphragm in contact with the fluid which is deformed by the pressure and the deformation can be measured by strain gauged element.

3.2.3 Flow Sensors

There are two types of flow meters in the test rig: Coriolis and Rotameter flow sensors.

- Coriolis sensors are inertial flow meter that measure directly mass flow through the variation of the angular momentum induced in the fluid by the sensor. These sensors are used to measure the gas and liquid mass flow in the divided phase segment of the rig.

- Rotameter sensors are variable area meter and are used here to measure the bypass flow, so a shaped weight inside the sensor is pushed up by the drag force of the flow and pulled down by gravity. The position at the equilibrium

defines the volumetric flow in the pipe. The output value is also noticeable by an analogic indicator outside the sensor.

3.2.4 Sensors Data Sheets

Table 3.1: Data sheets of the sensors involved in the measurement

Sensor	***Range***		***Unit***	***Accuracy***
	Minimum	*Maximum*		
TC			°C	$\pm$ 0,1 °C of m.v.
RTD			°C	$\pm$ 0,05 °C of m.v.
AP1	0	30	bar	$\pm$ 0,2 % of e. v
AP2	0	100	bar	$\pm$ 0,2 % of e. v
AP5,6	5	85	bar	$\pm$ 0,106 % of e. v.
DP01	0	1000	mbar	$\pm$ 0,040 % of e. v
Promass 83A04	0	90	kg/h	$\pm$ 0,1 % m.v. off 22,5 kg/h
Promass 83F25	0	3600	kg/h	$\pm$ 0,1 % m.v. off 540 kg/h
Mass2100-6	0	563,2	kg/h	$\pm$ 0,05 % m.v. off 30 kg/h
Mass2100-15	0	2914	kg/h	$\pm$ 0,05 % m.v off 80 kg/h
Mass Flux Coolin B	0	10000	kg/h	$\pm$ 0,1 % m.v. off 105 kg/h
Rotameter	0	5,5	m³ / h	$\pm$ 1,6 % m.v. off 3,065 m^3/h

3.3 Fluids of the Test Rig

All the fluids in the test rig can be categorized in primary and secondary working fluids.

As explained in Section 3.1.2 secondary fluids are used to set the temperatures of the cycle and to cool the test section. In order to quantify the intake or outtake of heat in the test rig, thermal proprieties of these fluids have to be established. There are two types of secondary fluids:

- Water: used directly only in the first heat exchanger of the bypass cycle and then as waste heat fluid in the cooling machine of the SECTSO and in all the Huber thermostats. It is not directly involved in the htc calculation, but if necessary its proprieties are simply retrievable from REFPROP software.
- Therminol D12: it is a heat transfer fluid specially developed for use in single fluid combined heating and cooling systems. It is based on halogen-free chemistry and has an operating temperature range of $-85℃$ to $190℃$. In the test rig it is used in all secondary cycles, so it exchanges heat directly with the working fluid. Furthermore, it is used also in the test section. For that reason its proprieties have to be evaluated precisely. In this purpose polynomial formulas taken from the Therminol producer are used and reported in Section 8.2. This test facility is built to test condensation of propane, but in the commissioning phase the working fluid is a two-phase mixture of isopropanol (2-propanol) and nitrogen at variable quality. Also, their thermal proprieties acquirable in software like REFPROP or EES and if necessary, polynomial correlations are present in HEATATLAS [3]

4 DATA REDUCTION

After showing the setup of the test rig, this chapter explains how the data collected from the test section are used to evaluate the thermo-hydraulic behavior of the working fluid and to calculate the heat transfer coefficient. With this configuration the htc can be calculated in three different ways: mean heat transfer coefficient of the whole pipe, α_{tot}; mean heat transfer coefficient referred to every measurement section, α_i; and heat transfer coefficient along the inner circumference of the pipe at every measurement section, $\alpha_{i,j}$.

4.1 Thermal Configuration

To understand the analytical approach of the problem, the actual heat flow situation in the test section is shown in Figure 4.1.

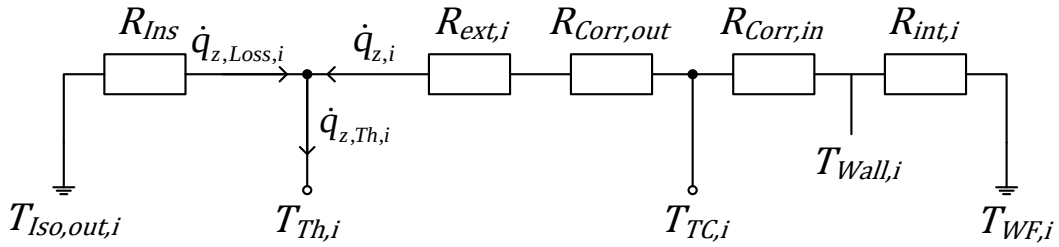

Figure 4.1: Thermal resistances involved in the data reduction

- Insulation Resistance, R_{ins}, is the resistance of the insulation layer of the outer tube. It occurs between the outer temperature of the isolation layer and the temperature of the cooling fluid. This temperature difference originates a heat flux towards the secondary working fluid considered like a loss in the energy balance. The resistance is composed by the layer of insulating matter and the wall of the outer pipe. Here used is a micro-cell structured insulant named Armaflex AF developed by Armacell. The considered sub-resistances are shown in Table 4.1. Since the thermal conductivity of the isolation layer is three orders of magnitude smaller than the expected htc between cooling fluid and outer tube wall, the insulation results in controlling the heat exchange

process so the unknown heat transfer coefficient between cooling fluid and inner wall of the outer part is negligible.

Table 4.1: Layers of the isolation resistance

$\boldsymbol{Pos.}$	$\boldsymbol{Material}$	$\boldsymbol{D_n}$ $[mm]$	$\boldsymbol{\lambda}$ $[W/m \cdot K]$
1	Outer Pipe Internal D.	48,000	
2	Outer Pipe External D.	52,000	57
3	Isolation Layer	152,000	0,033

- The external Resistance, $R_{out,}$ is the thermal resistance of the shell side of the test pipe. It is represented by the outer convective heat transfer coefficient α_{out}. It occurs between the temperature sensed by the thermocouples on the outer wall of the test pipe and the temperature of the cooling fluid. Its value could be estimated by one of the correlation presented before but since there are components like flanges needed for the construction and RTDs and supports of the TCs the flow of the cooling fluid is disturbed and thus the actual flow behavior is not easily predictable. So this alpha value is supposed to be calculated from the energy balance or with other experimental methods.

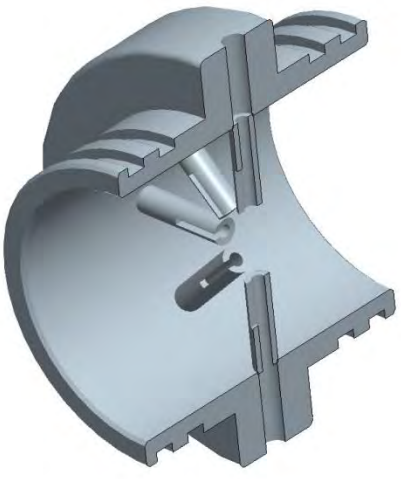

Figure 4.2: Shell side longitudinal section of the shell side mid measurement section

- Corrective Resistance, $R_{Corr,ext}$, $R_{Corr,int}$. Like explained in Section 3.2.1, in order to consider the right position of the sensing part, the evaluation of the layers composing the thermocouple is needed. The effects of these layers are calculated building a cylindrical thermal resistance, which dimensions are shown in Table 4.2 and composed like in equation 4.1 and 4.2

Table 4.2: Layers of the Test Pipe

Pos.	***Material***	D_n $[mm]$	λ $[W/m \cdot K]$
1	Pipe	14,650	57
2	Glue	18,400	1
3	TC Inconel – Inc, Internal	18,500	15
4	TC Magnesium oxide - MgO, Internal	18,680	50
5	TC	18,750	50
6	TC Magnesium oxide - MgO, external	18,820	15
7	TC Inconel – Inc, external	19,000	

$$R_{Corr,in} = \sum_{n=1}^{4} \frac{\ln \frac{D_{n+1}}{D_n} \cdot D_{int}}{2 \cdot \lambda_n} = 7{,}43 \cdot 10^{-5} \ \frac{m^2 \cdot K}{W} \qquad 4.1$$

$$R_{Corr,out} = \sum_{n=5}^{6} \frac{\ln \frac{D_{n+1}}{D_n} \cdot D_{int}}{2 \cdot \lambda_n} = 6{,}74 \cdot 10^{-6} \ \frac{m^2 \cdot K}{W} \qquad 4.2$$

In case that the TC sensor are not used for the calculation, these two resistance will be replaced by a unique resistance consisting of the entire thickness of the pipe made by only one layer of steel alloy:

$$R_{Wall} = \frac{\ln \frac{D_{ext}}{D_{int}} \cdot D_{int}}{2 \cdot \lambda_1} = 3{,}81 \cdot 10^{-5} \ \frac{m^2 \cdot K}{W} \qquad 4.3$$

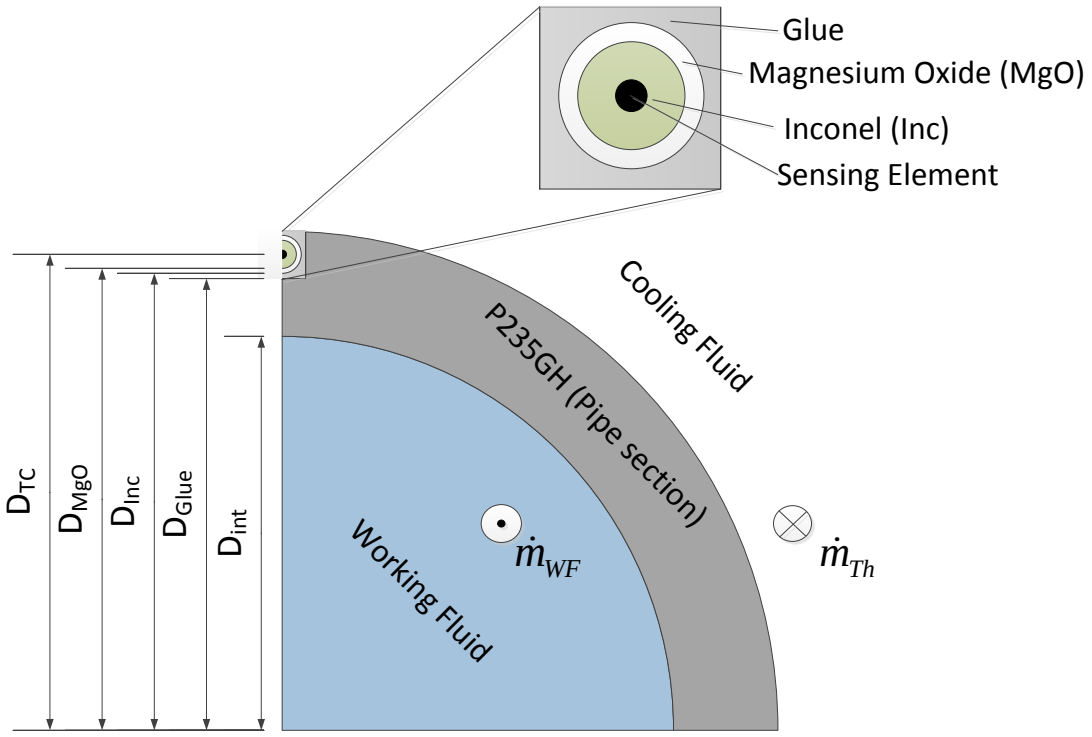

Figure 4.3: Composition of the layers in the wall of the test pipe

- The internal Resistance, $R_{int,}$ is the resistance of the convective heat transfer coefficient and its calculation is - as stated before - the purpose of this test rig. It occurs between the inner wall temperature and the working fluid temperature. Both of them are unknown but in the first case, the problem can be overcome considering the TC´s temperature and the relative additional resistance. In the second case, it can be indirectly estimated using an energy balance that involves the heat exchanged at every measurement section. The alpha value itself is here calculable in both experimental and analytical way.

4.2 Temperatures of the test section

4.2.1 Outer wall temperature

The position of the Thermocouples along the outer perimeter of the test pipe can be seen in Figure 3.2. That configuration allows evaluating the wall temperature profile and indirectly the working fluid temperature profile. If as simplification or as assumption of constant temperature profile due to turbulent flow, the mean value of a

measurement section can be sufficient, then the temperature can be calculated in this way:

$$T_{TC,i} = \sum_{J=1}^{8} \frac{T_{TC,i,j}}{8} \qquad 4.4$$

Due to several reasons like bad electric connection or actual malfunction, some sensor may record wrong data which can affect the result of the data reduction. To avoid this problem it is possible to disconnect the sensor from the multiplexer or to ignore their records and substitute them with the mean value of the adjacent TC´s. The ignored sensors are reported in Table 5.3.

4.2.2 Working Fluid Temperature

As mentioned before, to ensure an undisturbed flow in the tube, inside the test pipe there are no sensors. Nevertheless, the temperature of the working fluid is a very important unknown in the purpose of this test rig since it is needed in the htc calculations. The temperature inside the tube is calculated indirectly, involving the heat exchanged with the cooling fluid at each measurement section. Considering the energy balance in the cooling fluid as visible in Figure 4.1, the heat flux of the working fluid in the *i-th* measuring section is:

$$\dot{Q}_i = \dot{Q}_{Th,i} - \dot{Q}_{Loss,i} \qquad 4.5$$

With therminol balance

$$\dot{Q}_{Th,i} = \dot{m}_{Th} \cdot c_{p,Th} \cdot \left(T_{Th,out} - T_{Th,i}\right) \qquad 4.6$$

And heat losses balance

$$\dot{Q}_{Loss,i} = \frac{\lambda_{Iso} \cdot 2\pi \cdot z_i}{\ln\left(\frac{D_{Iso,out}}{D_{Iso,in}}\right)} \cdot \Delta T_{iso,i} \qquad 4.7$$

Between the thermal potential

$$\Delta T_{iso,i} = T_{Iso,out,i} - T_{Iso,in,i} \qquad 4.8$$

Heat loss are not easy to estimate since the thickness of the insulating layer and the temperature at each side are not known. A simplification option is to ignore those losses since the isolation conductivity controls the heat exchange with the external ambient.

The temperature of the working fluid in each measurement section is:

$$T_{WF,i} = T_{WF,in} - \frac{\dot{Q}_i}{\dot{m}_{WF} \cdot c_{p,WF}} \quad 4.9$$

The flow values and temperatures are measured directly in the test rig, so the heat can be balanced. The mean temperature between inlet and outlet of both sides is used to calculate the thermal proprieties of fluids in the test section. ($T_{WF,in}$ and $T_{Th,in}$) and outlet ($T_{WF,out}$ and $T_{Th,out}$). A way to validate this calculation is to perform it considering the outlet temperature and proceeding backwards.

4.3 Heat Transfer Coefficient

Like stated in the introduction of this chapter, the sensors in this rig are placed to calculate the htc in different ways. Since now all the needed temperature in the test section are known, the following sections will explain the calculation of heat transfer coefficient.

4.3.1 Mean heat transfer coefficient

First it is important to define the boundaries of the problem. The heat exchange process can be handled in two different ways: one solution is to consider the entire test section from inlet to outlet of the two fluids. The energy balance of the heat exchanger results:

$$\dot{Q}_{i-o} = \dot{Q}_{th,i-o} - \dot{Q}_{loss} \quad 4.10$$

With heat balance therminol side

$$\dot{Q}_{th,i-o} = \dot{m}_{th} \cdot c_{p,th} \cdot \left(T_{th,out} - T_{th,in}\right) \quad 4.11$$

And heat losses balance

$$\dot{Q}_{Loss,i-o} = \frac{\lambda_{Iso} \cdot 2\pi \cdot L_{i-o}}{\ln\left(\frac{D_{Iso,ext}}{D_{Iso,int}}\right)} \cdot \Delta T_{iso} \quad 4.12$$

Also in this case the losses can be neglected due to their little influence. A way to validate this balance is to directly calculate the heat taking into account the working fluid side only:

$$\dot{Q}_{i-o} = \dot{m}_{WF} \cdot c_{p,WF} \cdot \left(T_{WF,out} - T_{WF,in}\right) \quad 4.13$$

Both working fluid and therminol proprieties are calculated at mean temperature between inlet and outlet. Since the heat is balanced, the total heat exchanged can be calculated with the heat exchanger correlation:

$$\dot{Q}_{i-o} = K_{int,i-o} \cdot A_{int} \cdot \Delta T_{ln,i-o} \quad 4.14$$

With the heat transferring surface

$$A_{int} = \pi \cdot L_{i-o} \cdot D_{int} \quad 4.15$$

And the logarithmic temperature difference

$$\Delta T_{ln,i-o} = \frac{\left(T_{WF,in} - T_{th,out}\right) - \left(T_{WF,out} - T_{th,in}\right)}{ln\frac{\left(T_{WF,in} - T_{th,out}\right)}{\left(T_{WF,out} - T_{th,in}\right)}} \quad 4.16$$

Out of the global heat transfer coefficient

$$K_{int,i-o} = \frac{1}{R_{int} + R_{wall} + R_{ext}} = \frac{1}{\frac{1}{\bar{\alpha}_{int,i-o}} + R_{wall} + \frac{D_{int}}{\alpha_{ext} \cdot D_{ext}}} \quad 4.17$$

The value of the htc inside the tube

$$\bar{\alpha}_{int,i-o} = \left(\frac{A_{int} \cdot \Delta T_{ln,i-o}}{\dot{Q}_{i-o}} - R_{wall} - \frac{D_{int}}{\alpha_{ext} \cdot D_{ext}}\right)^{-1} \quad 4.18$$

is finally calculated.

As visible in the overall heat transfer coefficient formula, two unknowns are present: α_{int} and α_{ext}. The first one is the purpose of this calculation and will be isolated in order to be estimated, the second one has to be established in order to complete the calculations.

One way to do it is using a correlation. Like e.g. the one Gnielinski [4] has published for annulus heat transfer. As explained before, the shell side flow is not easily predictable, but considering the whole transit of the cooling fluid in the shell side, the effect of the disturbing elements may not be influent.

Second option of calculating the heat transfer coefficient shell side is to use the Wilson plot method that will be handled in Section 5.5.2.

To avoid the external alpha calculation, it is possible to change the boundaries of the problem, so considering the heat exchange that happens between the first and the third measurement section. In this case it is possible to evaluate the overall heat transfer coefficient not taking into account the resistance from the shell side to the test tube, since the outer wall temperature is known. The heat balance of this region of the working fluid side results:

$$\dot{Q}_{1-3} = \dot{m}_{WF} \cdot c_{p,WF} \cdot \left(T_{WF,1} - T_{WF,3}\right) \quad 4.19$$

Considering the whole heat exchange:

$$\dot{Q}_{1-3} = K_{int,1-3} \cdot A_{1-3} \cdot \Delta T_{ln,1-3} \quad 4.20$$

With the heat transferring surface

$$A_{1-3} = \pi \cdot L_{1-3} \cdot D_{int} \quad 4.21$$

And the logarithmic temperature difference

$$\Delta T_{ln,1-3} = \frac{\left(T_{WF,3} - T_{TC,3}\right) - \left(T_{WF,1} - T_{TC,1}\right)}{ln\frac{\left(T_{WF,3} - T_{TC,3}\right)}{\left(T_{WF,1} - T_{TC,1}\right)}} \quad 4.22$$

From of the global heat transfer coefficient

$$K_{int,1-3} = \frac{1}{R_{int} + R_{corr,in}} = \frac{1}{\frac{1}{\alpha_{int}} + R_{corr,in}} \quad 4.23$$

the heat transfer coefficient of this case is calculated as:

$$\alpha_{int,1-3} = \left(\frac{A_{1-3} \cdot \Delta T_{ln,1-3}}{\dot{Q}_{1-3}} - R_{corr,in}\right)^{-1} \quad 4.24$$

In the same way it is possible to calculate the internal heat transfer coefficient taking into account the outer alpha, so with restricted boundary physical boundary but enlarged thermal boundary:

$$\dot{Q}_{1-3} = K_{int,\overline{1-3}} \cdot A_{1-3} \cdot \Delta T_{ln,\overline{1-3}} \quad 4.25$$

With logarithmic mean temperature difference

$$\Delta T_{ln,1-3} = \frac{\left(T_{WF,3} - T_{th,3}\right) - \left(T_{WF,1} - T_{th,1}\right)}{ln\frac{\left(T_{WF,3} - T_{th,3}\right)}{\left(T_{WF,1} - T_{th,1}\right)}} \quad 4.26$$

And global heat transfer coefficient

$$K_{int,\overline{1-3}} = \frac{1}{\frac{1}{\bar{\alpha}_{int,1-3}} + R_{wall} + \frac{D_{int}}{\alpha_{ext} \cdot D_{ext}}} \quad 4.27$$

And so the heat transfer coefficient can be expressed as:

$$\bar{\alpha}_{int,1-3} = \left(\frac{A_{int} \cdot \Delta T_{ln,\overline{1-3}}}{\dot{Q}_{1-3}} - R_{wall} - \frac{D_{int}}{\alpha_{ext} \cdot D_{ext}}\right)^{-1} \quad 4.28$$

A way to calculate the external mean heat transfer coefficient needed in this calculation, is to calculate the heat balance between cooling fluid and external surface of the pipe with the restricted boundaries like in 4.24:

$$\alpha_{ext,1-3} = \left(\frac{A_{1-3} \cdot \Delta T_{ln,1-3}}{\dot{Q}_{1-3}} - R_{corr,out}\right)^{-1} \quad 4.29$$

With logarithmic temperature difference:

$$\Delta T_{ln,1-3} = \frac{\left(T_{TC,3} - T_{th,3}\right) - \left(T_{TC,1} - T_{th,1}\right)}{ln\frac{\left(T_{TC,3} - T_{th,3}\right)}{\left(T_{TC,1} - T_{th,1}\right)}} \quad 4.30$$

4.3.2 Local heat transfer coefficient

Thanks to the configuration of the RTDs in the shell side of the heat exchanger a heat transfer coefficient can be calculated locally. Having five measurement sections in the cooling fluid side allows building a more accurate polynomial curve that interpolates the trend of temperature of Therminol. The curve has been calculated with the Excel fitting tool, as a second degree polynomial. Its slope is involved in the calculation of the specific heat flux originated in the cooling fluid:

$$\dot{q}_{z,th,i} = \dot{q}_{z,i} + \dot{q}_{z,loss,i} \quad 4.31$$

With specific heat loss in the i-th section

$$\dot{q}_{z,i} = \frac{\delta\dot{Q}}{\delta\varphi\delta z} = \frac{\dot{m}_{th} \cdot c_{p,th}}{\pi \cdot D_{int}} \cdot \frac{\delta T_{th,i}}{\delta z} - \dot{q}_{loss,i} \quad 4.32$$

Defined by the temperature polynomial

$$T_{th,i}(z) = A \cdot z^2 + B \cdot z + C \quad 4.33$$

Derived as

$$\frac{\delta T_{th,i}(z)}{\delta z} = 2 \cdot A \cdot z + B \quad 4.34$$

And with specific heat losses

$$\dot{q}_{loss,i} = \frac{\lambda_{Iso} \cdot 2\pi}{D_{Iso,int} \cdot ln\frac{D_{Iso,ext}}{D_{Iso,int}}} \cdot \Delta T_{Iso,i} \quad 4.35$$

Specific heat flux is now dependent on the position z along the test pipe, so it is possible to calculate it for every measurement section. This calculation is based on the hypothesis that in shell tube heat exchanger with turbulent flow the radial heat gradient of every infinitesimal section is equal to zero. The boundaries of the problem are also important here, since it is possible not to involve the external heat transfer coefficient from the shell side to tube in order to minimize calculation errors.

Considering as thermal potential the temperature difference between outer wall and bulk flow:

$$\Delta T_i = T_{WF,i} - T_{TC,i} \quad 4.36$$

It is now possible to calculate the local htc with:

$$\dot{q}_{z,i} = \frac{\Delta T_i}{\frac{1}{\alpha_{int,i}} + R_{corr,in}} \tag{4.37}$$

The local heat transfer coefficient of the i-th measurement station is:

$$\alpha_{int,i} = \left(\frac{\Delta T_i}{\dot{q}_{z,i}} - R_{corr,in}\right)^{-1} \tag{4.38}$$

In the same way it is possible to calculate the external heat transfer coefficient, but in this case different thermal potential is considered:

$$\Delta T_i = T_{TC,i} - T_{th,i} \tag{4.39}$$

And so the alpha value is

$$\alpha_{ext,i} = \left(\frac{\Delta T_i}{\dot{q}_{z,i}} - R_{corr,out}\right)^{-1} \tag{4.40}$$

The local external heat transfer coefficient can be used as test for the annulus correlations, found in literature. With this value is it also possible to build a global heat transfer coefficient but referred to a single section.

5 EXPERIMENTAL RESULTS

In this chapter the procedure of the data acquisition for the experimental investigation is described. Afterwards, the results of the measurements are shown in chronological sequence in order to explain how the commissioning phase of the rig was carried out.

5.1 Measuring with the KIIR test facility

The components of the facility that have to be activated before starting the measurements are: the LabView software where it is possible to control the rig and to save the measured values collected from it, the multiphase pump conveying the process fluid in the primary cycle and all the secondary cycles to set the temperatures of the working fluid.

As explained in Section 3.1.2, the inlet secondary cycle heats the working fluid in order to set the inlet temperature of the test rig. Downstream the test section, the outlet secondary cycle has to lower the temperature of the working fluid to a level suitable for the functioning of the pump. Since the *SECTSO* is not yet available due to technical reasons, the only way to perform its duty is to use the *Cooling D* heat exchanger. This equipment runs with water as cooling fluid and the position of *SDV3* determines if the working fluid flows through the heat exchanger.

When the LabView software is booting and the pump is on, all the valves are set to 100% open and the rotational speed of the pump is set to 400 rpm, the minimum value that allows the pump to run. This is the starting configuration of every measurement session and during this time it is important to pay attention to the flow condition in the pump since all the valve, gas and liquid side, are fully open. Afterwards, the *SECTS* and *SECTSI* are turned on with a specific temperature set in the thermostat. Once the wanted mass flow of the working fluid is set, it is important to wait for the inlet temperature of the working fluid to become stable.

During the measurements it turned out, that the electrical heater of the *SECTSI* is regulated by a second degree under-dumped controller that follows the changes of the heat balance in a faster way but introducing oscillation in the resulting test section inlet temperature. After a while, this oscillation damps but it never disappears completely. Every time the control valves are set to a new mass flow, before recording a new measurement it was checked, that this oscillation is smaller then $1°C$. The temperature of the thermal oil in the test section is not affected by this

problem since it is highly accurately controlled with the Huber thermostat, whose oscillation varies in a range of $\pm 0{,}1°C$. So with a recording time of at least five minutes, is it possible to mean the effect of this oscillations.

As explained in Section 3.1.1, the mass flow can be regulated by the needle valve situated in the primary cycle, by *RV6* installed in the bypass or by the rotational speed of the pump. With a combination of the valve of both liquid (*RV4* and *RV5*) and gas side (*RV1*, *RV2* and *RV3*) it is also possible to set the wanted vapor quality. These possibilities, contribute to vary the pressure lost in the rig, and so it is always important to check the working condition of the pump. In this way is it possible to set the wanted fluid characteristic before the recording.

After a measuring session, the facility has to be stopped. The proper way of doing that is to shut down the heater of the SECTSI and let run the whole plant for five minutes, in order to cool the fluids in it. Afterward it is possible to shut off the entire components and at last to close the LabView software.

5.2 Preliminary Measurements

In the early phase of the commissioning the entire rig was not insulated and so prone to the room condition. At this time it was important to establish the performance of the test facility. This session of measurement was conducted although the test rig was not entirely insulated. In this way it was possible to collect some first result so as to proceed with a proper sequence of tests. The heat exchanger was running in counter flow. The five measurement points that have been recorded are listed in Table 5.1. Two of them have been made with isopropanol as working fluid ($x = 0$), two with nitrogen only ($x = 1$) and the fifth was a multiphase flow. The purpose of the one phase points was to test the maximum specific mass flow acquirable in these conditions. The working fluid specific mass flux is limited by the operating conditions of the multiphase pump, reaching a higher mass flow rate *G* was not possible due to the high pressure drop in liquid measurements, and due to high gas content in the pump during gas measurements. The upper limits of liquid and gaseous flow of process side are underlined in Table 5.1. The multiphase measurement point had the purpose of verify the prepared data reduction spread sheet.

Table 5.1: List of the preliminary measurements

$\boldsymbol{Test\ Nr}$	$\boldsymbol{G}$ $kg/(s \cdot m\text{^}2)$	$\boldsymbol{x}$	$\boldsymbol{t_{WF,in}}$ $°C$	$\boldsymbol{t_{th,in}}$ $°C$
1	3960	0	36,86	10,65
2	2550	0	32,59	5,60
3	275	1	44,19	5,65
4	90	1	46,19	5,66
5	150	0,49	24,91	10,50

Analyzing the output excel file, the first important thing notable is that *RTD25-3* gives NaN (not a number) as output, *TC3* gave strange results and *TC15´*s output was negative and four orders of magnitude bigger than the expected value. Also some other thermocouples show not credible values; therefore, it was decided to perform a temperature sensor test. This test is described in Section 5.3.1.
Considering the reliable TC it is possible to notice that the outer wall temperature of the test pipe has a particular trend as can be seen in Figure 5.1.

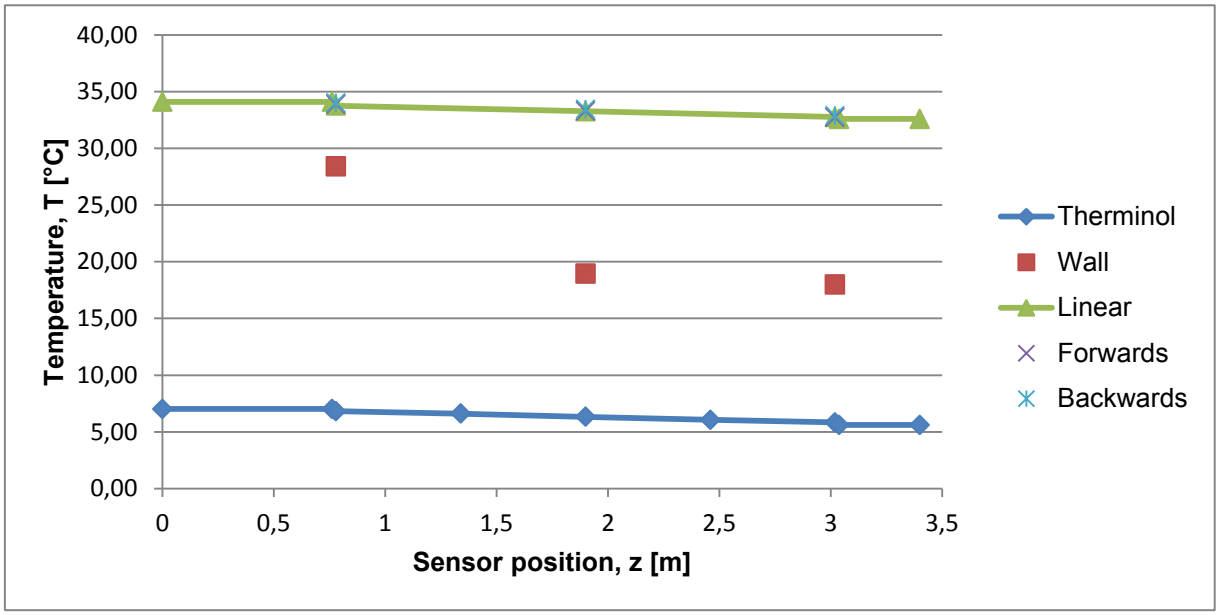

Figure 5.1: Temperature trend in the preliminary measurement nr.2

In these conditions, where no latent heat is exchanged the wall temperature should follow the temperature trend of the fluids involved. This does not happen in the

performed tests. Test nr. 2 is characterized by process media and coolant with the same thermal flow capacity, in this condition the slope of both fluids is the same along the heat exchanger, and so should be the slope of the wall temperature. It is obvious that this is not the case since the wall temperature in the first section is far higher than the remaining two. This may be explained with a problem in the measurement technique, for that purpose further tests on the thermocouple are planned.

The data reduction showed that apart from this phenomenon, also the resulting heat transfer coefficients are implausible. The Dittus Bölter correlation in liquid only tests shows always lower values (-40% compared with Gnielisnki and Petukhov) and in Gas only test shows always higher values (10% higher than Gnielisnki, Petukhov and Hausen). And these values compared to the internal htc from Section 4.3.1 are around 45% higher in liquid only test and circa 20% higher in gas only test. The only consistency that can be found is between the experimental mean heat transfer coefficient and the local one measured in the first section, with deviations from 1% to 20%, proportional to the working fluid mass flow.

Table 5.2: Heat transfer coefficient of the preliminary measurement

$\boldsymbol{Test\ Nr.}$	$\boldsymbol{x}$	$\boldsymbol{G}$ $\frac{kg}{s \cdot m^2}$	$\boldsymbol{Re}$	$\boldsymbol{\alpha_{DB}}$ $\frac{W}{m^2 \cdot K}$	$\boldsymbol{\alpha_{Gn}}$ $\frac{W}{m^2 \cdot K}$	$\boldsymbol{\alpha_{PP}}$ $\frac{W}{m^2 \cdot K}$	$\boldsymbol{\alpha_{Ha}}$ $\frac{W}{m^2 \cdot K}$	$\boldsymbol{\alpha_{1-3}}$ $\frac{W}{m^2 \cdot K}$
1	0	3954	40521	2795	4426	4368		2442
2	0	2548	23554	1867	2818	2778		1560
3	1	89	815	291	258	256	266	202
4	0,49	151	1340	823	767	753	693	972

As expected, without insulation of the test section the heat losses are not negligible and this leads to a discrepancy between the heat balance of the therminol side and the heat balance of the working fluid of up to -70% in the measurement nr.3. Because of this error the third measurement will not be taken in account in this paragraph. The remaining measurements are between -30% and -10%. This leads to a difference of the working fluid temperature up to $5°C$ depending on the choice of the “forward-” or “backward calculation method” of the process media temperature

(explained in Section 4.2.2). These errors are too high to calculate the htc properly, in fact all the calculations where the working fluid temperatures are involved are affected by this problem. For example considering one specific measurement section, in the worst case the local heat transfer coefficient varies from 2% to 20%. The heat balance is an important issue for the reliability of the measurements, so after the insulation of the test rig, a heat balance test will be carried out. Test reported in Section 5.3.3.

Tests with gas showed that even though the needle valves of the liquid streak were closed the liquid flow meters are sometimes giving output different from zero. To investigate this issue flow meter test are carried out and showed in Section 5.3.2.

The therminol flow can be regulated setting a bypass valve that connects deliver and supply of the Huber machine. The idea of changing the therminol mass flow has the purpose to diminish its thermal flow capacity in order to to see a greater temperature difference in the coolant side. This fact helps the energy balance to be more accurate. Therminol minimum flow is defined by the uncertainty of the flow meter in the *SECTS*, while maximum flow is set by the complete closure of the bypass in the *SECTS* (considering that the pump of the cooling machine cannot be regulated).

Tests made with the highest therminol flow show a more uniform temperature trend in every section as visible in Figure 5.2. The low therminol flow in the other tests allows the development of free convection that leads to a higher temperature sensed by the RTD placed at the top of the shell side as in Figure 5.3. To have a more stable temperature trend in the ring cross section and so a more uniform thermal behavior of the cooling fluid, the further measurement will be carried out with the highest flow therminol possible, so with bypass valve completely closed.

A high therminol flow guarantees also a sufficient heat transfer coefficient in the shell side and in this leads to more consistent values of the $\alpha_{int,i-o}$ and $\alpha_{int,1-3}$ calculated from therminol side to working fluid side. In fact, like showed in equations 4.18 and 4.28, it is possible to enlarge the boundaries of the heat balance considering also the outer htc. This method increases the uncertainty of the results but gives another result for comparisons. This is one more reason work under those conditions.

The following test and measures will be recorded using liquid isopropanol. In this way it is possible to work in a wider range of mass flows and the thermal proprieties of the working fluid will not be remarkably affected by the temperature changes. In addition,

at the end of this test, the test section has been insulated in order to improve the thermal performance of the rig.

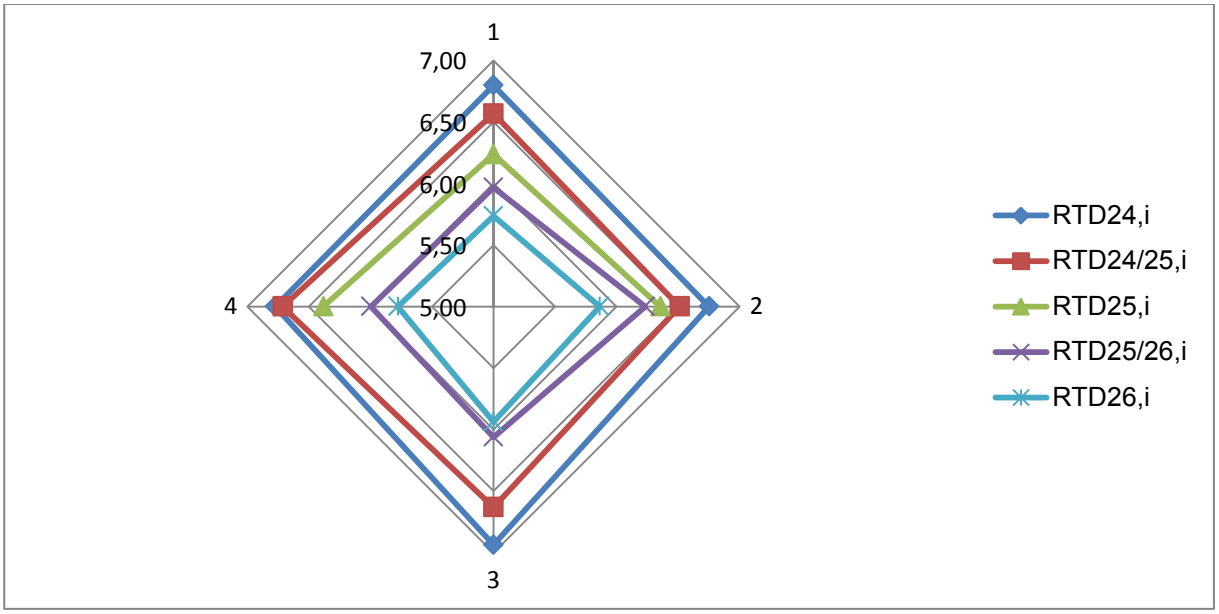

Figure 5.2: Therminol temperature trends in every m.s. with high therminol flow [°C]

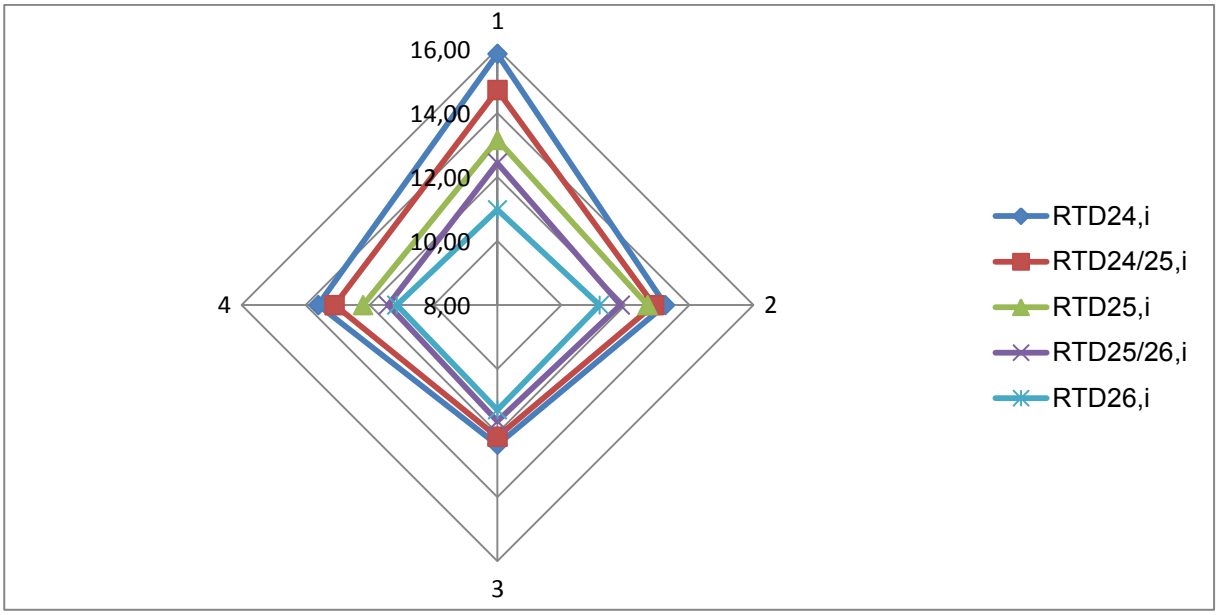

Figure 5.3: Therminol temperature trends in every m.s. with low therminol flow [°C]

5.3 Validation Tests

Preliminary tests showed that the main data collected have some particular, unexpected behavior. Because of that, further tests have been carried out and this section explains their results.

5.3.1 Temperature sensors Tests

To understand the behavior of the temperature sensors involved in the htc calculation, several tests have been carried out. The first was about the right positioning of the sensors in the multiplexer and in the cold junction for the thermocouples. Thanks to the help of the LabView software it was possible to check the connection between the measured value, the label in the software and the label in the output file. It was possible to notice that *RTD13* and *RTD14* were plugged in the wrong socket, so they gave inverted values. *RTD25-3* gave NaN (Not a Number) because it was not plugged in the right way. These issues were easily to solve, by plugging the sensors properly. Since the TC´s are glued on the surface of the core pipe, only a test with a substitute TC was possible. This TC was plugged in the electric connection and then turned into ice water. The LabView program shows the response of the temperature change and the connection between sensor and label. No issues were found in this test.

Afterwards consistency test have been carried out. By running the test facility with only the SECTS working and with only the primary cycle working, the behavior of the sensors during steady and unsteady measurement has been checked.

In the steady test all the RTD sensors behave in a consistent way. This happened even though the effect of the free convection in the shell side was dominant. In fact the two tests were carried out running alternatively just one pump delivering the media in the test section. The same result occurred also in the unsteady measurement, where the Huber machine is set to a different temperature imposing a temperature step. The transient regime resulted consistent for every sensor. These sorts of tests have been carried out also in direct flow conditions confirming the good behavior of the RTD´s (Figure 5.4).

The TC sensors had more issues. The results of these tests show that *TC3* and *TC15* are faulty, because like stated before they give not reliable values. The unsteady tests revealed furthermore a strange behavior of *TC11* and *TC22*.

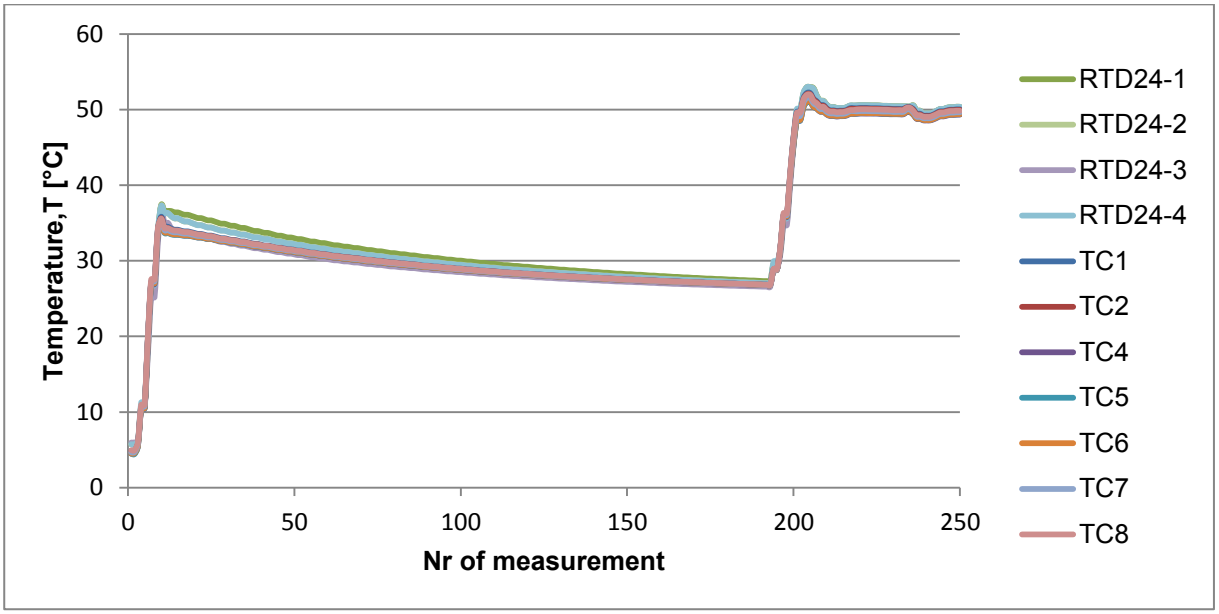

Figure 5.4: Results of unsteady test in the first section

TC11 mostly behaves like the others in its measurement section, but suddenly its values move in an inconsistent way. This may be caused by a fake contact, so in order to solve this problem it has been put in a short circuit. That did not lead to an improvement of the output, so it has been decided to take in account its values case to case according to the shown reliability.

TC22 was showing a mirrored behavior, in comparison to the other sensors of its measurement section. After checking a sign issue in the polynomial of this sensor in the software, the plug has been checked with the result that the poles are twisted. Correcting this plug issue this temperature sensor test ended. The sensors that will not be taken in account during the calculation made in this work are listed in Table 5.3 Unreliable temperature sensors .

Table 5.3 Unreliable temperature sensors

Sensor	***Used***	***Reason***
TC3	No	Fault
TC15	No	Fault
TC11	Case to Case	Not always reliable

5.3.2 Flow meters test

The described underestimation of htc compared to the one of the correlations may result from a wrong mass balance, which is a crucial data of the calculation of this work. The idea to check if the sensors work properly was to set a specific mass flow in each of them and then to check if the same pressure drops and htc appear in the test section. The result of this test is shown in Table 5.4.

Like introduced in Section 3.2.3, the flow meters installed in the primary cycle are Coriolis sensors. The issue was noticed in the liquid path, where in such a built rig these sensors may work in problematic conditions. In fact, the phase separation process acts macroscopically, but at the work pressure of the facility a certain quantity of gas remains in solution with the liquid phase. Like stated in Section 3.2.3, the sensors have partially overlapped ranges in order to perform measurement in a wider range of mass flow. This means that when measuring, only one sensor is actually working and the other is cut out by a valve. Due to the pressure loss along the test rig, it is possible that this gas degases and remains in the liquid sensor disturbing its measurement. This disturb may cause the sensor to show an output even if the is no actual flow through it.

Table 5.4: Result of flow meter test

	$\dot{m}_{wf}$	$AP5,6$	$DP01$
	kg/s	bar	$mbar$
Mass 2100-6	0,1566	6,856	70,913
Mass 2100-15	0,1555	6,813	69,772

As can be seen in Table 5.4, there is no difference in the pressure drop, so the measured mass flow seems reliable. If no liquid mass flows is occurring, the sensors values should be ignored.

Other possibility is that the needle valves do not completely close their passage, letting a little flow to pass. The valves have been tested and re-adjusted but the problem was persisting. Since it was not possible to change the equipment new steps to the measurement routine have been added. When measuring gas only flows, the ball valve *SDV6* has to be closed in order to avoid flow in the liquid streak.

5.3.3 Heat balance test

Tests made without insulation, showed that the effect of heat losses are remarkably influencing the measurements, worsening the heat balance. For that purpose it has been decided to proceed with the insulation of the test section. Since the efficiency of the insulation was unknown, a heat balance test has been carried out with cooling fluid at room temperature. In this conditions the heat losses are minimized (ideally no losses) and without thermal potential between the shell side of the test section and the environment, only the actual thermal process inside the heat exchanger is observable. The measurements have been taken in the conditions showed in Table 5.5.

Table 5.5 Heat balance test measurement points

	T_{SECTS}	T_{SECTSI}	G	%
	$°C$	$°C$	$kg/(s \cdot m\text{^}2)$	$WF\ over\ Th$
1	21	60	1000	-1,42
2	21	60	1150	-2,14
3	21	60	1955	-0,68
4	21	60	2740	-3,17
5	21	60	3220	-5,13
6	21	60	3316	-4,83

With minimized heat losses now the heat balance difference between therminol side and working fluid side has reliable results with its maximum value in the fifth measurement with the $5{,}13\%$ difference. Resulting from this the working fluid calculation difference (forward versus backward, Section 4.2.2) is now between $0{,}02\ °C$ and $0{,}09\ °C$. Thus the heat transfer coefficient in every measurement section has little variations.

The heat transfer coefficient measured in the test section has the same trend like in the preliminary measurements. A higher value in the first measurement section, according to Figure 3.2, and both second and third sections characterized by too low heat transfer coefficients. From this it can be conducted, that this effect does not seem to be correlated with the heat losses in the rig.

The first section, the most consistent one, is characterized by local alpha between 3% and 19% less than the Gnielinski value. Considering the global measured htc, with restricted boundaries and the logarithmic mean temperature difference between wall temperature and working fluid, the values are 33% to 50% smaller than the Gnielinski correlation. If the physical boundaries are extended to the inlet and outlet of the heat exchanger, the outer htc has to be taken in account, here calculated with the Petukhov correlation. The internal alpha results now 19% to 27% smaller. If the physical boundaries are the first and last measurement section, alpha results 7% smaller in measurement nr.1 to 49% smaller in measurement nr.6, showing proportionality with the flow density.

The calculation of the external heat transfer coefficient remains quite constant since all the measurement have been made in the same condition of the shell side. The external measured htc shows the opposite trend in comparison to the internal one, so smaller in the first section and higher in the second and third one

The temperature trend in the shell side shows that in every section the sensors are measuring homogeneous temperatures. But that does not happened in the third section, where the values are spreading with a range of up to $0{,}3°C$ in the worst case, the measurement nr.6 (reported in Figure 5.5).

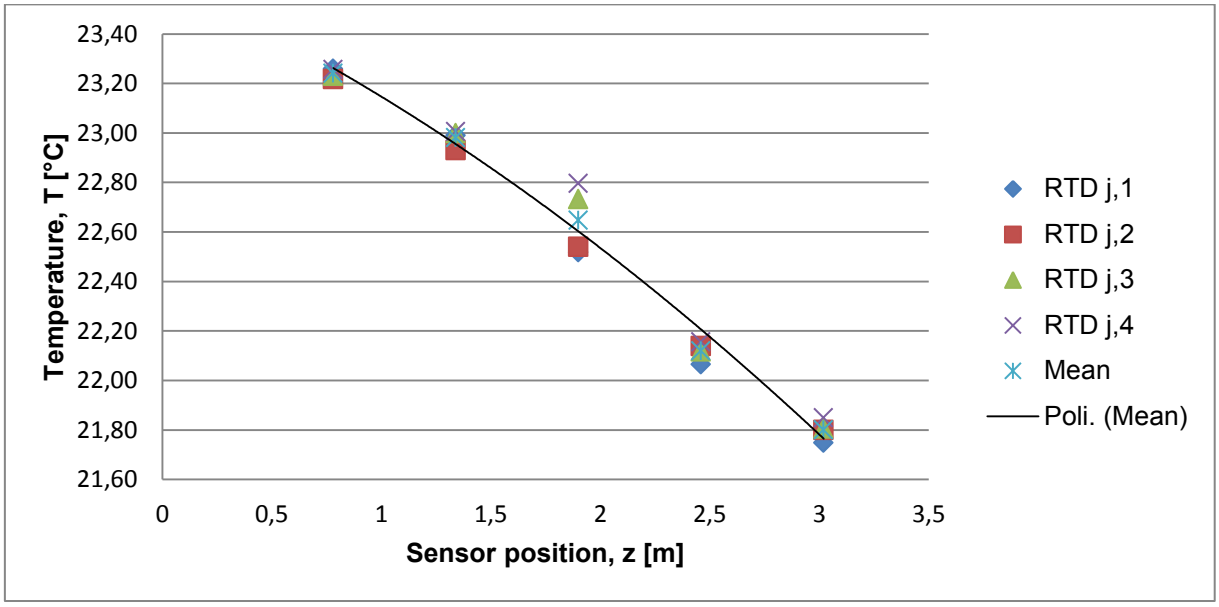

Figure 5.5: Therminol temperature trend in measurement nr. 6

The fourth section always shows values under the expected trend and this leads the interpolating polynomial to have a significant concavity, especially in measurement

nr.4. This leads to bad htc results, compared to the others measurement. Therefore it will be shown but ignored in the future interpretation.

Considering the temperature difference between every section in therminol side, the trend is the same for every measurement. As visible in Figure 5.6, only the fourth measurement has a strange behavior between the first section and the outlet of the cooling side. What is important is to notice that the fourth temperature difference, the one between the mid and the second intermediate section is way higher than the other. This means that in that stretch more heat is exchanged.

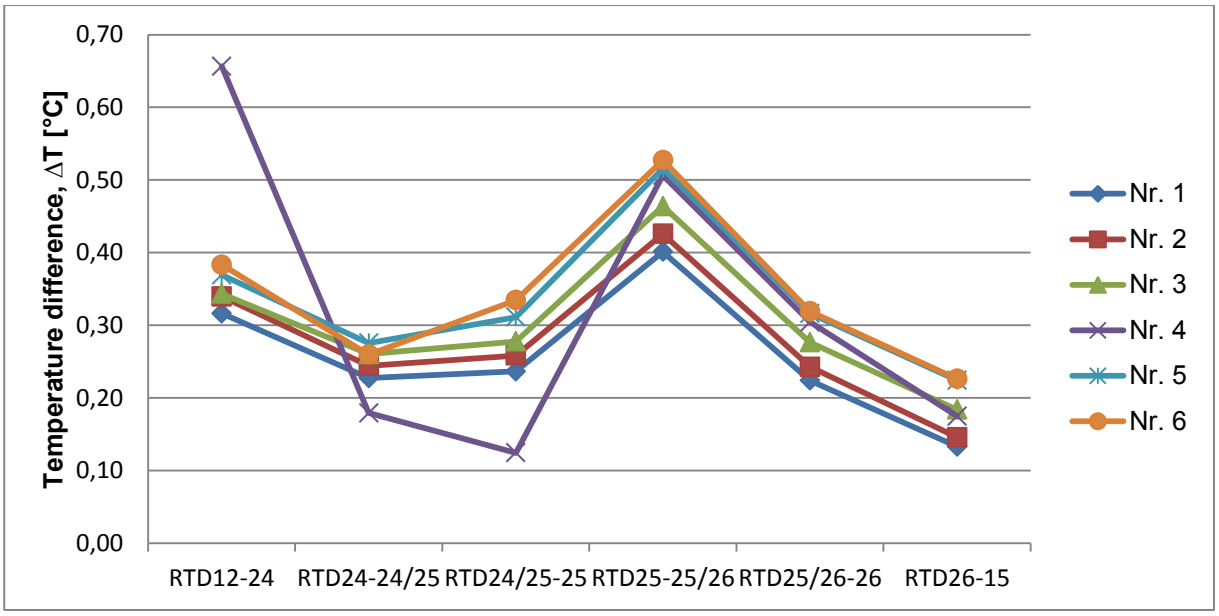

Figure 5.6: Temperature difference between every section of the shell side

An explanation for this fact can be found in the configuration of the mid measurement section. Figure 5.7 shows the configuration of this section. The mid m.s. has this particular construction in order to reach in an easier way the wanted location for the TC. The test pipe is so divided in two parts connected by an O-ring. This component contains the guide for the sensors and leads to capillary pipes that protect and sustain the Thermocouple from the shell side flow. Considering the position of the sensor as in Figure 3.2, the four *RTD25* are positioned at the black line, so for counter flow conditions this means that therminol flows before through the capillary pipes and then its temperature is recorded. The presence of the capillary pipes is a huge obstacle for the flow, and it introduce turbulence in the therminol right before the sensors. More turbulence, leads to a better local heat transfer coefficient which

results in more heat exchanged in this portion of the pipe and so to the peak visible in Figure 5.6. More tests will be carried out to understand this behavior since it is changing the heat transfer process.

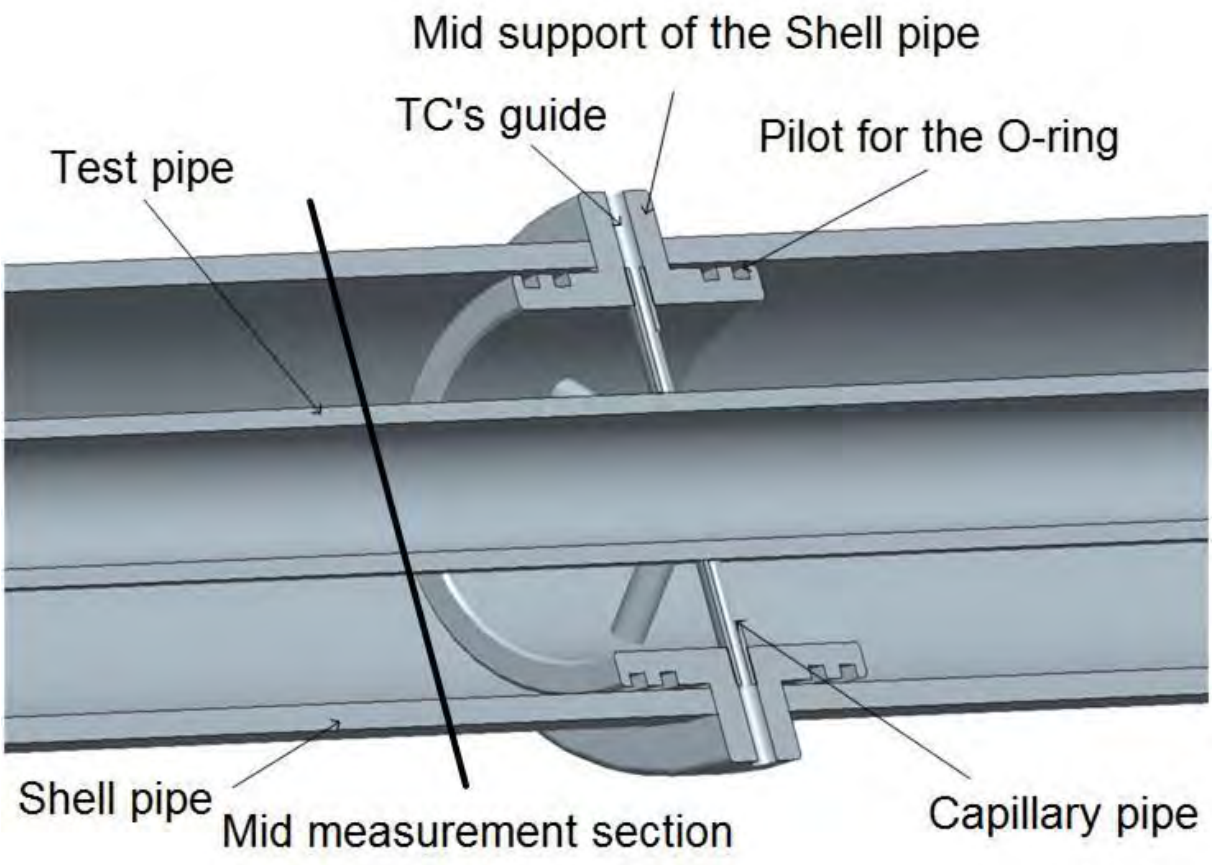

Figure 5.7: Configuration of the mid measurement section

Heat balance tests showed that the first measurement section (related to Figure 3.2) results reliable values in both working fluid and therminol side. For this reason it will be taken as reference of the heat transfer coefficient calculation. Further tests have been planned to figure out the behavior of the second and third section, and to understand why more heat is exchanged in that particular stretch.

5.3.4 Reproducibility of results

After testing the reliability of the rig and the effect of measurement uncertainty, an important step is to observe the reproducibility of the tests. The accuracy of how the test section is capable to be set in particular and predefined condition, and in this situation the consistency of the results.

In the early phase of the commissioning, several random points were recorded. These points have been recorded again subsequently paying attention to the parameters involved in the heat balance: working fluid and therminol mass flow, working fluid and therminol inlet temperature. Since the inlet therminol temperature is set by the purchased thermostat, the inlet therminol temperature is practically constant. Therefore the temperature difference in the cooling fluid assumes more importance than the inlet temperature. Setting these values, thanks to the LabView software, the test section should work in the same conditions and showing the same results. The points recorded are listed in Table 5.6. The table shows that some tests have been carried out with lower therminol flow in order to observe the reproducibility also in the type of test that normally do not show good results.

Table 5.6: Reproducibility tests

	G_{WF} $kg/(s \cdot m\text{^}2)$	$T_{in,WF}$ $°C$	G_{th} $kg/(s \cdot m\text{^}2)$	$T_{in,th}$ $°C$	$Nr.$ $Test$
1	3040	47,92	147	5,66	2
2	3500	40,44	143	10,60	2
3	3750	39,74	148	5,65	2
4	1000	50,75	438	5,63	4
5	1120	46,71	439	5,64	2
6	2000	45,69	438	5,61	4
7	2250	40,39	437	10,59	2
8	3500	40,16	437	10,59	2
9	3750	39,24	438	5,63	2

The reproducibility of the results is observed using the coefficient of variation, also known as relative standard deviation, defined as

$$Coefficient\ of\ Variation = CoV = \frac{Standard\ Deviation}{Mean\ Value} \quad 5.1$$

It allows to compare the standard deviation of non-homogeneous measurements and is consequently an efficient way to evaluate these test.

The purpose of this plant is the calculation of the heat transfer coefficient but since the calculations are dependent on the parameters set, also the reproducibility of them

is important. Tests have been made using two different cooling fluid mass flow values without acting on the valve that regulates it, for this reason the maximum coefficient of variation of therminol specific mass flow is $0{,}21\%$. The specific mass flow of the working fluid shows good reproducibility, even if the greater value of CoV $(1{,}55\%)$ is in the $G = 1000$ test, where a higher number of test should diminish the deviation. The working fluid flow is connected to the Reynolds number which shows more variation than expected with a maximum CoV of $3{,}01\%$. Even if characterized by small deviation, the inlet temperature of the working fluid has the greater relative deviation ($4{,}25\%$ in the worst case, and also the minimum value is greater than other with the $0{,}45\%$) probably because of the influence of the *SECTSI* controller that is unable to maintain a specific temperature during the measurement. Nevertheless, due to the stability of the cooling fluid condition at the inlet of the test rig, even if the other components of the heat balance show a greater relative standard deviation, the temperature difference of therminol has $0{,}82\%$ as maximum. Considering the calculated inside heat transfer coefficient all tests show good result with a maximum relative deviation of $1{,}99\%$ occurred in test number 1, between the high therminol flow tests the maximum is $1{,}26\%$.

In the measured inside alpha the fifth test shows the worst results with deviation between $10{,}01\%$ and $16{,}76\%$. Out of this, the rest of the tests have $5{,}31\%$ as maximum CoV, with the exception of the first section of first test where the CoV is $11{,}52\%$, but generally it is possible to say that the first section has always shown a worse behavior in relative deviation.

The calculated heat transfer coefficient in the shell side results always reproducible since conditions in the therminol cycle are not changing. When observing the htc per measurement section, in the worst case the relative deviation is $4{,}78\%$.

In light of the above, it is possible to state that the plant works with a good reproducibility. The mean value of all the CoV calculated before is lower than 2%, so working conditions are not influencing the accuracy of the system. Another important result is that in this configuration, only the first measurement section works as expected, but no reason have been found yet for the non-reliability of the other sections.

These tests have also given another support to the idea to not work with low therminol flow, since all the calculation made in this way gave completely wrong results.
Since the reproducibility of the point $G = 2000$ with maximum therminol flow showed better results in terms of CoV and since this mass flow is an average between the limiting values, from now on the conditions reported in Table 5.7 have been taken as reference for the future tests

Table 5.7: Reference conditions for comparison's tests

G	T_{SECTS}	T_{SECTSI}
$kg/(s \cdot m\text{^}2)$	$°C$	$°C$
2000	5	60

5.3.5 Adiabatic tests

As visible in Figure 5.8, with values taken from the repoducibility tests, the temperature trend is still the same as in the preliminary tests. Trusting the values occurring in the first measurement section, the second and third sections are measuring values leading to this unexpected trend. This could be the effect of actual variations of heat transfer coefficient in the shell side that reflects in the temperature sensed, o just thermocouples malfunctioning. Therefore, more tests are needed to prove the performance of the thermocouples.
An hypotesis about this strange behavior is that the second and the third section or just the first section have an offset issue. In fact considering the slope between the temperature of 2nd ant 3rd sections, if an offset is applied to it, a continuous temperature trend with the first section is obtainable and vice versa. Calculation showed that in the reproducibility test, in order to have a constant inside heat transfer coefficient along the pipe the offset to be applied is between $5{,}3°C$ and $10{,}5°C$. Tests are made and now explained to figure out this issue.
One possibility was the presence of additional parassite thermocouple present in the measurement chain, since all the TC´s of the third section are connected to the cold

junction with a cable extension. After some plug/unplug tests this configuration showed no influence in the measurement chain.

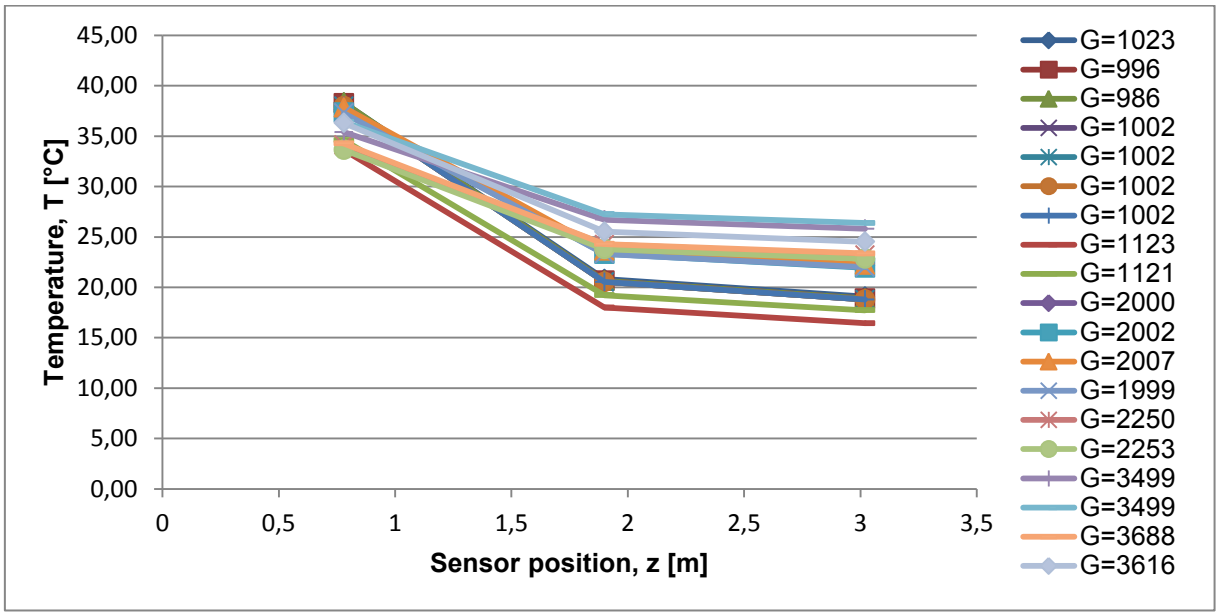

Figure 5.8: Outer wall temperature trend in reproducibility tests

Other tests are carried out in adiabatic condition. The rig has been run with working fluid temperature as close as possible to coolant temperature. In this way, the heat exchanged between the two fluids is minimized and so it is possible to see the behavior of the thermocouple when working in almost absence of thermal potential. Due to the unsteady behavior of the *SECTSI* temperature controller, this condition was difficult to achieve, that´s why one test resulted in therminol being warmer than working fluid and the second one with working fluid warmer than therminol. Anyway this test has shown the behavior of the TC´s in both heat exchange directions. Since the temperature difference between the two media is smaller than $1°C$ in the worst case, the heat balance results with high discrepance, but that was not the purpose of this test.

The result of the first test are shown in Figure 5.9. In this case therminol is warmer than working fluid so the heat direction is the opposite compared to the normal condition. It is possible to notice that the logarithmic mean temeprature difference between outlet and inlet of the heat exchanger is $0{,}13°C$. In this condition only $22\ W$ have been exchanged between the two fluids. The graphic shows the two method used to establish the workin media temperature, and as mentioned in Section 4.2.2,

the difference between the two procedure is now less than $0{,}5°C$. These value are compared to a linear temperature trend connecting the inlet and the outlet temperature of the working fluid. In a first sight appears that the measured wall temperature is not consistent since it should be between the two media, but if considering that the standard uncertainty of the TC´s is greater than that of the RTD´s the result is legit. In addition, errors in TC´s sensors can be caused by the cold junction, since it is sensible to the temperature in the rig and adapts itself slowly to an oscilating temperature condition (the temperature in the housing and in the lab changes along the day due to sun radiation and the hvac system). For the same reason, this strange wall temperature trend can be considered acceptable.

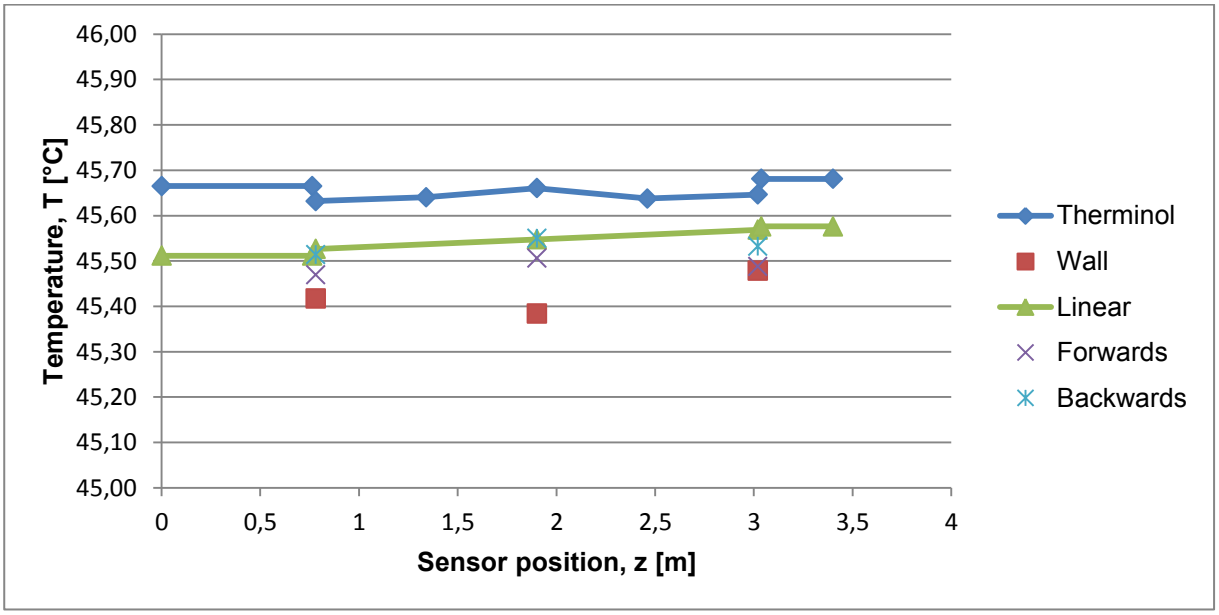

Figure 5.9: First adiabatic test

In the second test the fluid configuration is the same as in the normal condition, so with working medium warmer than therminol, like shown in Figure 5.10. The logarithmic mean temperature difference is now $1{,}01°C$, so in this case more heat is exchanged, $95\ W$. In this fluid configuration the wall temperature trend behaves like in the others tests.

Comparing the two tests, the relative temperature difference between therminol and outer wall seems that the TC´s of the second section are somehow better coupled with the cooling fluid. The therminol temperature trend is quite constant, but shows in every test a peak in the mid measurement section, like visible in Figure 5.11. Even

with little heat exchanged, the temperature difference between every section of the shell side has the same trend as in Figure 5.6, this means that the cause of this trend may be of hydrodynamic nature.

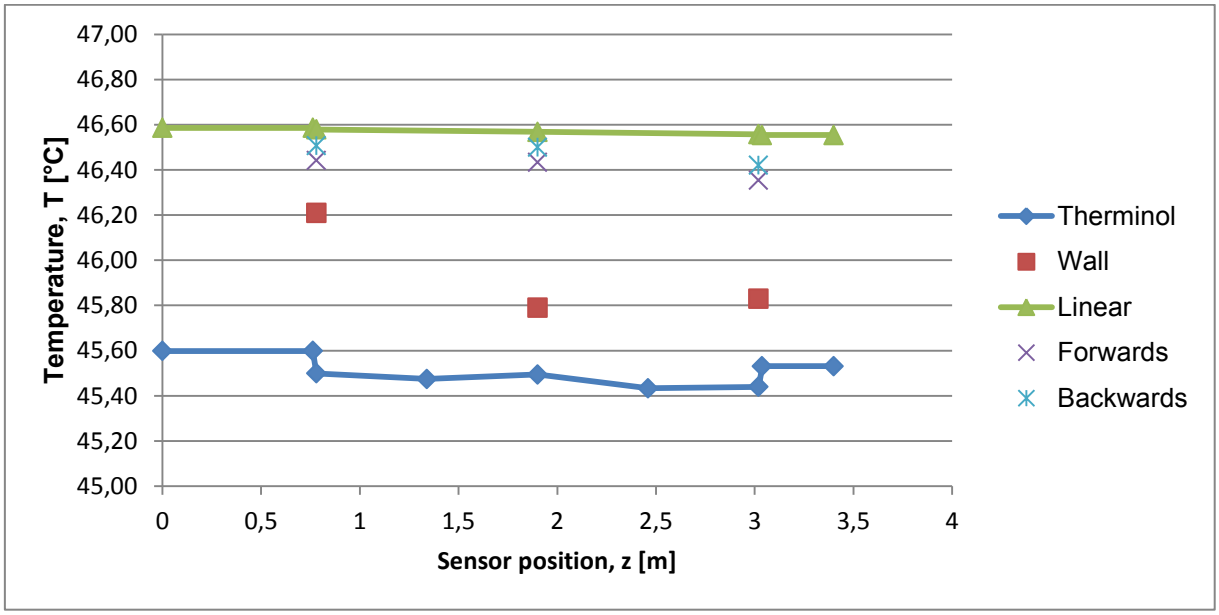

Figure 5.10: Second adiabatic test

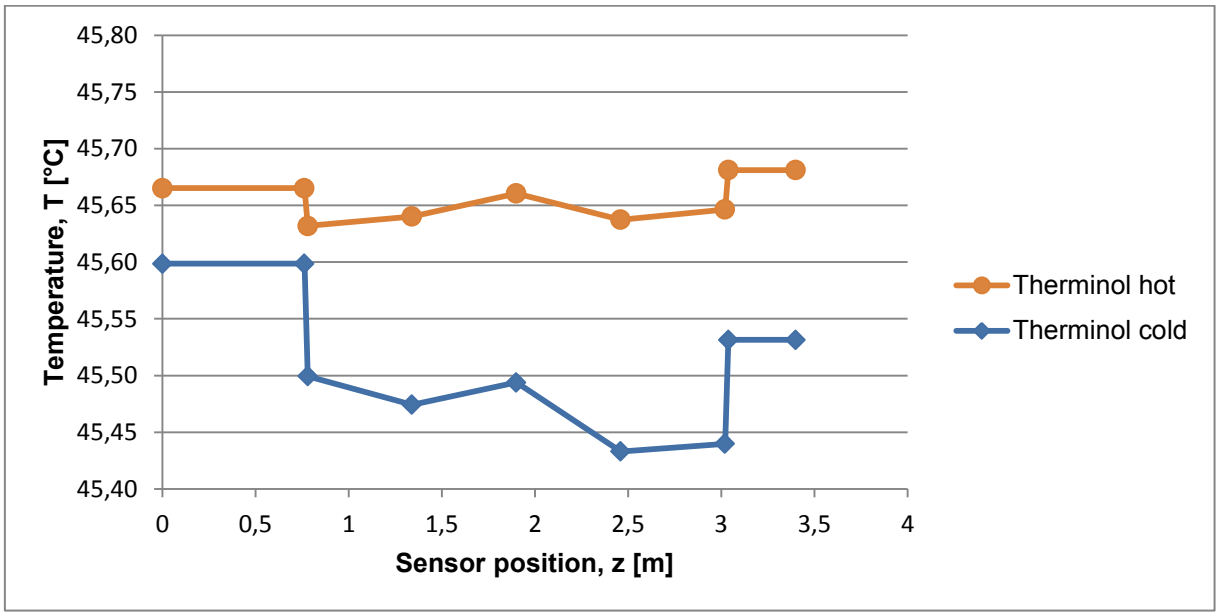

Figure 5.11: Therminol temperature trend in adiabatic tests

5.4 Internal heat transfer coefficient

The entire tests carried out to validate the rig have brought significant data about the internal heat transfer coefficient. Since this is the purpose of the test facility, these results are shown in this chapter.

As noticed in the preliminary measurement, the Dittus Bölter correlation always gives smaller values then Gnielinski and Petukhov, between $-36{,}25\%$ and $-56{,}24\%$.The discrepancy rises with higher Reynolds numbers. This occurs also in measurements done with low therminol flow. The Petukhov correlation is used for the calculations in this project. To obtain a good comparability with other project partners this correlation is used in following to validate the obtained experimental results.

Like stated in Section 5.3.4, tests with low therminol flow have to be ignored because the results are not consistent. In fact observing the alpha values measured in the whole campaign, they are far away from the expected value.

The htc in the first section gives quite acceptable results like visible in Figure 5.12. The values have a mean discrepancy of $-7{,}79\%$, with a peak of $-24{,}25\%$ like shown in Figure 5.13. This graphic shows also the behavior of the other sections. It is obvious that both 2nd and 3rd sections are inconsistent, since the discrepancy from the expected value is between -52% and -73%.

The mean heat transfer coefficient measured using smaller boundaries (equation 4.24) results not comparable with the correlation used as reference since it has discrepancy between -34% and -48%. Nevertheless this value is similar to the one obtained through the Dittus Bölter correlation. This fact may be just a coincidence.

The htc calculated with equation 4.18 and 4.28 has always given bad results, sometimes negative, sometimes hundred times more than Petukov's value. Including the external htc in the calculation adds more uncertainty to the result leading to unreliable results. For this reason, those two calculation will never be taken into account in the rest of the work.

The internal alpha behavior discovered in the preliminary tests is so confirmed also by the other tests done, but an explication has not been found yet. In the theory of heat transfer it is well known that the internal and external htc's are independent of each other. So in this case, regarding the inner heat transfer coefficient, it should not be dependent on the shell side of the heat exchanger. As noticed in the tests with low therminol flow, the behavior of the fluid in the shell side is actually affecting the inner

heat transfer coefficient especially in the second and third section of the test pipe. It comes that the amount of heat exchanged may be caused by hydrodynamic phenomena influencing the heat balance which has not taken in account so far. In order to observe the influence of therminol flow in the inner alpha, tests on the shell side are carried out.

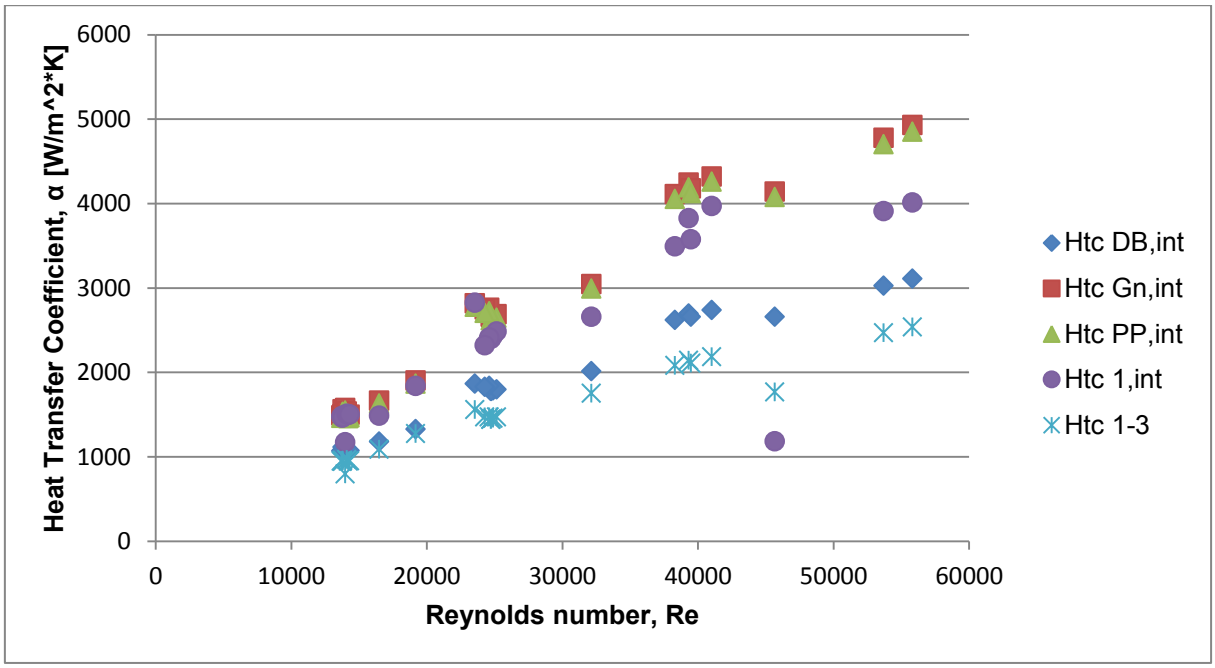

Figure 5.12: Comparison between calculated internal htc and measured htc

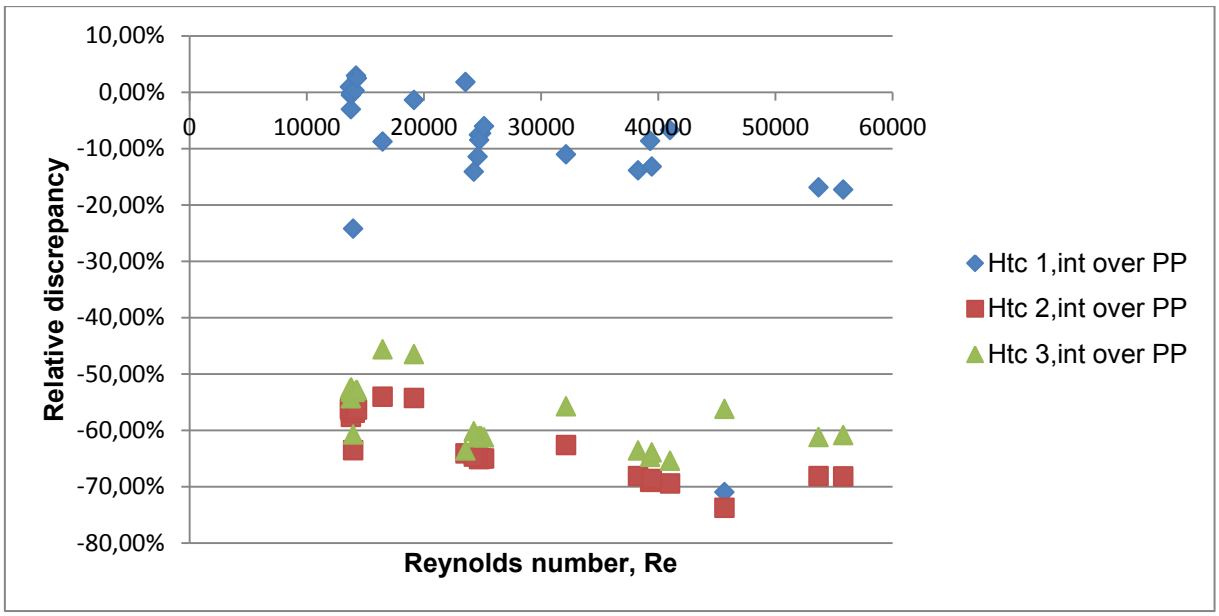

Figure 5.13: Relative discrepancy between local htc and Petukhov correlation

5.4.1 Sensibility of heat transfer coefficient calculations

In this section a simplified propagation of uncertainty is handled. This means that the result will be a unique mean uncertainty value for every quantity involved and those quantities are considered as not correlated. Since all the measurement points are different, there is no way to perform statistical calculations, the uncertainty chosen is therefore the type B.

Table 5.8: Uncertainty of the independent quantities

	Δ	u
$\dot{m}_{WF}$	$\pm$ 0,05 % $m.v.$	$\pm 0{,}0001\ kg/s$
λ_{WF}	$\pm$ 5,1% $m.v.$	$\pm 0{,}004\ W/m \cdot K$
$c_{p,WF}$	$\pm$ 5,1% $m.v.$	$\pm 0{,}06\ kJ/kg \cdot K$
μ_{WF}	$\pm$ 5,1% $m.v.$	$\pm 4 \cdot 10^{-5}\ Pa \cdot s$
$\dot{m}_{th}$	$\pm$ 0,1 % $m.v.$	$\pm 0{,}0004\ kg/s$
$c_{p,th}$	$\pm$ 5,1% $m.v.$	$\pm 0{,}06\ kJ/kg \cdot K$
D_n	$\pm$ 0,00001 m	$\pm 6 \cdot 10^{-6}\ m$
λ_n	$\pm$ 0,5 $W/m \cdot K$	$\pm 0{,}3\ W/m \cdot K$
D_{int}	$\pm$ 0,0001 m	$\pm 6 \cdot 10^{-5}\ m$
L, z	$\pm$ 0,005 m	$\pm 0{,}003\ m$
T_{TC}	$\pm$ 0,1 °C	$\pm 0{,}06$ °C
T_{RTD}	$\pm$ 0,05 °C	$\pm 0{,}03$ °C

The quantities taken in account in this section are the ones present in heat transfer coefficient formulas 2.8, 2.13, 2.15, 4.24 and 4.38. Among all this contributions some of them are independent, their uncertainty calculation is reported in Table 5.8. The values are considered as uniform (continuous) distribution, so the uncertainty is calculated through

$$u(X_i) = \frac{\Delta(X_i)}{\sqrt{3}} \qquad 5.1$$

If the delta value is given with a percentage of the measured value, in order to perform a calculation valid for every measurement point, it has been taken a mean

value among the recorded. The working fluid thermal proprieties are taken from Heat Atlas [3], but no information were reported about the uncertainty of this particular fluid. For this reason it has been decided to use a mean value among the ones suggested for the other substances reported in that book.

In order to calculate the composed uncertainty of the needed formula, the first step is to perform partial derivative of every formula for every quantity, obtaining the so called sensitivity indexes. Result of this operation is reported in the appendix (Section 8.3).

As reported in [5], the composed error for non-correlated quantities is calculated with equation 5.2, where the first multiplier is the sensitivity index and the second the uncertainty of the considered quantity.

$$u_c{}^2(Y) = \sum_1^N \left(\frac{\partial Y}{\partial X_i}\right)^2 \cdot u^2(X_i) \qquad 5.2$$

Table 5.9: Composed uncertainty of the quantities involved in htc calculations

	u_c			u_c	
Re	± 816		G_{WF}	± 15	$\frac{kg}{s \cdot m^2}$
Pr	± 1		A_{WF}	$\pm 1{,}3 \cdot 10^{-6}$	m^2
f	$\pm 7 \cdot 10^{-4}$		$Q_{WF,1-3}$	± 55	W
Nu_{Gn}	± 12		$Q_{Th,1-3}$	± 78	W
α_{Gn}	± 129	$\frac{W}{m^2 \cdot K}$	A_{tot}	$\pm 4{,}3 \cdot 10^{-4}$	m^2
C	$\pm 0{,}002$		ΔT_{ln}	$\pm 0{,}04$	°C
Nu_{PP}	± 11		α_{1-3}	± 51	$\frac{W}{m^2 \cdot K}$
α_{PP}	± 127	$\frac{W}{m^2 \cdot K}$	$q_{z,1}$	± 64	$\frac{W}{m^2}$
Nu_{DB}	± 6		$q_{z,2}$	± 73	$\frac{W}{m^2}$
α_{DB}	± 74	$\frac{W}{m^2 \cdot K}$	$q_{z,3}$	± 82	$\frac{W}{m^2}$
$T_{WF,1}$	$\pm 0{,}2$	°C	$\alpha_{int,1}$	± 59	$\frac{W}{m^2 \cdot K}$
$T_{WF,2}$	$\pm 0{,}07$	°C	$\alpha_{int,2}$	± 37	$\frac{W}{m^2 \cdot K}$
$T_{WF,3}$	$\pm 0{,}02$	°C	$\alpha_{int,3}$	± 44	$\frac{W}{m^2 \cdot K}$

Starting from the independent quantities, calculating the uncertainty of the chain of nested equations, it is finally possible to evaluate the composed uncertainty of the measured heat transfer coefficients. The result of the entire calculations is reported in Table 5.9

At first sight is possible to notice that the heat transfer coefficient calculated via correlation has a greater uncertainty than the measured one. That occurs because the uncertainty of the used sensors is way smaller than the adapted value of uncertainty used for the thermal proprieties.

The discrepancy between the measured and the expected value is however not comprehended within the uncertainty limits of both quantities, even if considering that the values here reported are mean values for all the measurement points.

5.5 Shell side tests

The tests carried out until now have brought some results also about the outer heat transfer coefficient.

First important thing is that the fluid in the shell side flows in transient condition. Low therminol measurement points have been recorded at the lower limit of the transient zone. The measurement taken in account have Reynolds results barely turbulent at the highest therminol flow, because of that a correlation for transition regime flow is needed. Heat atlas [3] advises a modified Gnielinski correlation (equation 2.10), furthermore also Dittus Bölter and Petukhov will be used in this work.

As in the inner side, the correlations show the same behavior between themselves, with Dittus Bölter giving always smaller values, between 29% and 35% compared to Pethukov.

Like in the inner side, the local heat transfer coefficient in the first section has an acceptable result, with a mean discrepancy of $-4{,}16\%$ like visible in **Errore. L'origine riferimento non è stata trovata.** and a peak of $-15{,}53\%$ in the worst case. The other two sections show in this case bigger values than the expected one, up to 180%.

As anticipated in Section 4.3.1, apart from the direct measurement, there is an experimental method to evaluate the heat transfer coefficient in condition of a steady flow. This is the Wilson plot method and will be discussed in Section 5.5.2. This test involves only the outlet and inlet temperature of the test section. In order to make

more accurate measurements of the therminol temperature, the sub-pipes have to be insulated. In fact, during the previous test it was possible to notice that the sub-pipes were covered in dew, that indicates that the outer surface of the sub-pipes is below the saturation temperature of water in the air (at the laboratory pressure, $1\ bar$). This leads to heat losses. These losses are difficult to take into account.

Before these parts were insulated, tests are carried out about the influence of the therminol flow entering and exiting the test section. The results of these tests are shown in Section 5.5.1.

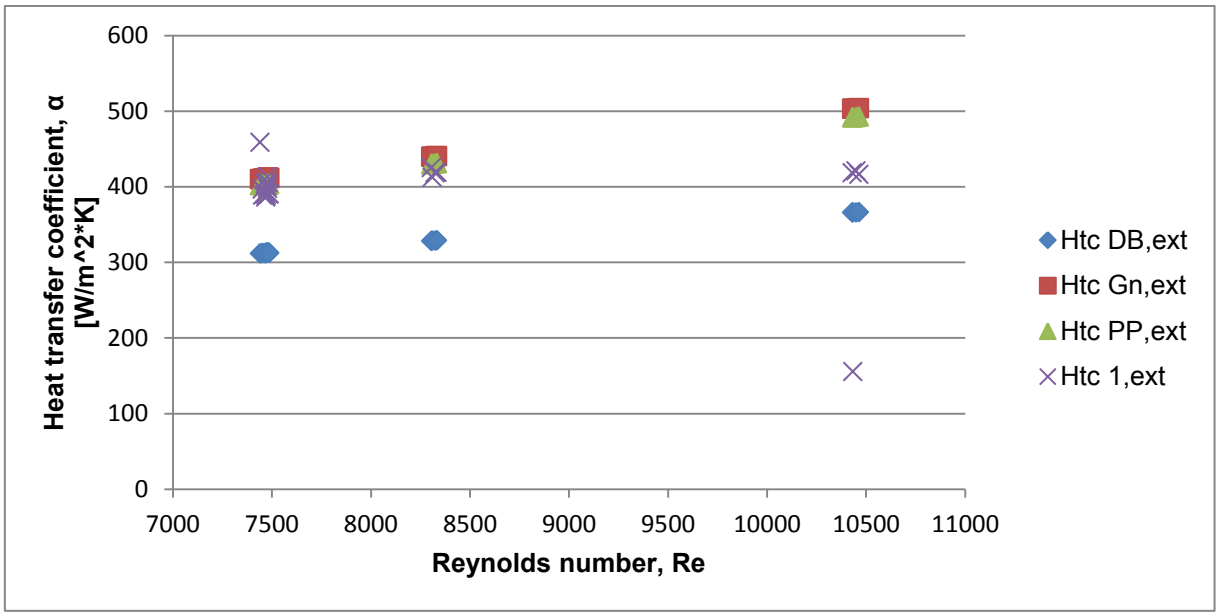

Figure 5.14: Comparison between calculated external htc and measured htc

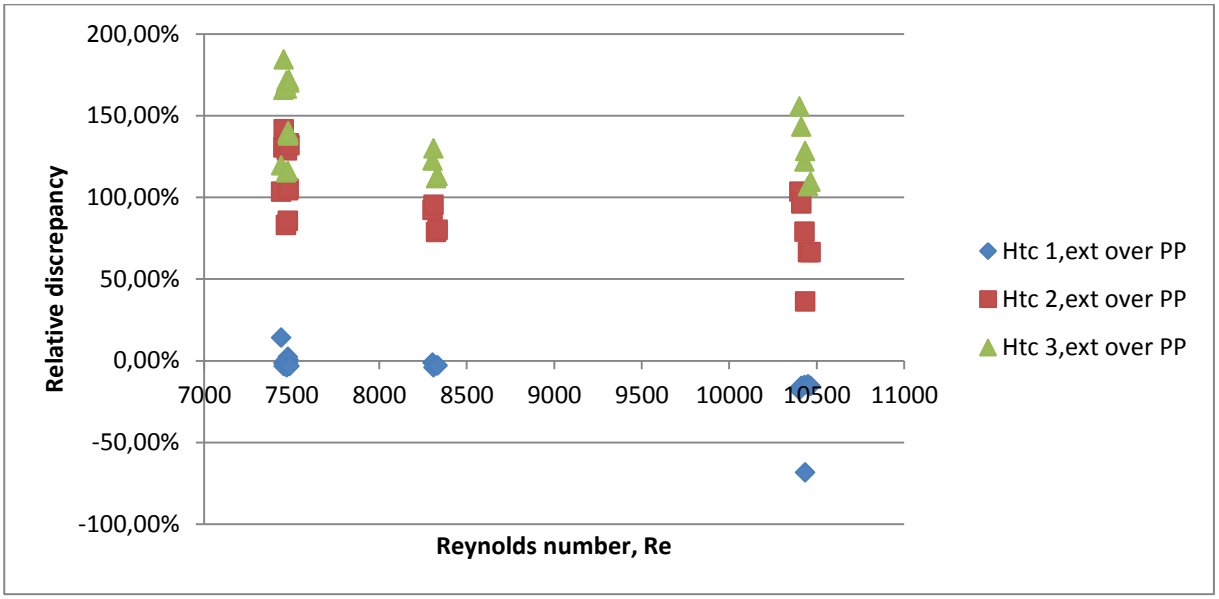

Figure 5.15: Relative discrepancy between Petukhov correlation and local htc

5.5.1 Sub Pipes Tests

Like stated in Section 3.1.3, sub pipes are connecting the *SECTS* with the test section in order to let the coolant flow in a more homogeneous way. Since these pipes feed the fluid in the heat exchanger in the proximity of the third and first section, they may have an influence on the sensors belonging to those sections. These tests have the purpose of investigate the effect of this influence on the internal heat transfer coefficient (equation 4.38). To change the behavior of the oil side, the sub-pipes are closed using a vise.

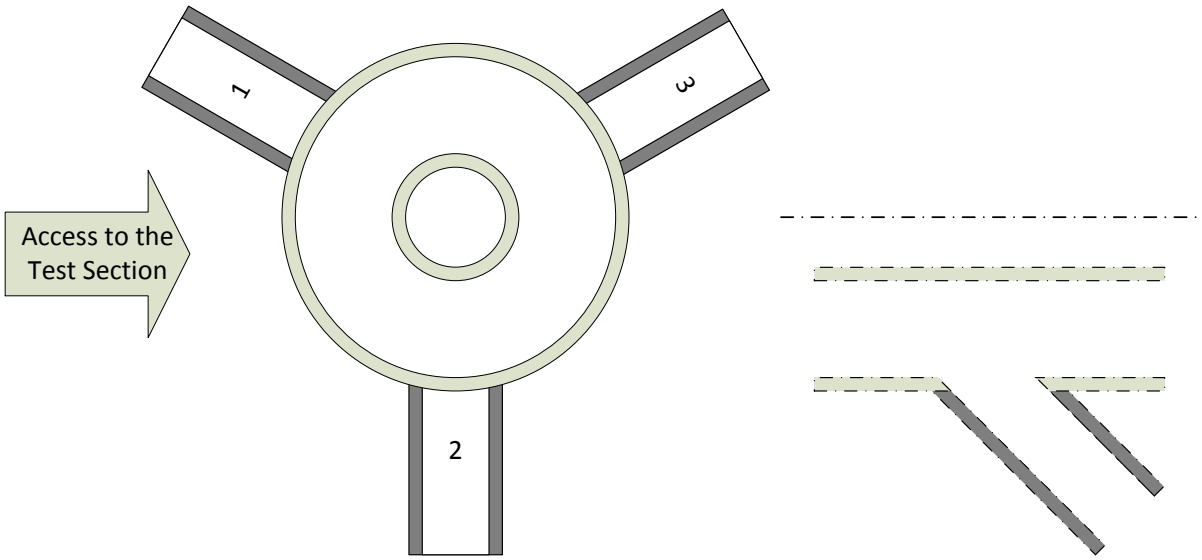

Figure 5.16: View of the connection between *SECTS* and heat exchanger

According to Figure 5.16, the sub-pipe closed in these tests are nr. 2 and 1. The first for single pipe test and the both of them for two closed pipes. The first tests are carried out closing the inlet sub-pipes and so since the heat exchanger runs in counter flow, some changes are awaited in the last measurement section. The last two tests are made closing the outlet, so affecting the first measurement section. These tests are recorded using as working fluid mass flow the assumed reference value ($G = 2000$). In this way is it possible to make comparisons between the different cases and the normal behavior taken as a mean value of the previous measurement.

The mass flow of both working fluid and cooling fluid is reported in Table 5.10. The working fluid shows obviously no variation, while the cooling fluid mass flow decreases as more sub-pipes are closed. As visible, the percentage of Reynolds number reduction is comparable in the case of two sub-pipes closed, but is important to say that this calculation refers to a mean value along the shell side. When only one sub-pipe is closed, the reduction results a bit different, but this may be caused by a bad positioning of the vise.

Table 5.10: Hydraulic effects of the sub-pipes tests

	G_{WF} $kg/(s \cdot m\text{^}2)$	Re_{WF}	G_{th} $kg/(s \cdot m\text{^}2)$	Re_{th}	% over Reference
Reference	2002	24879	438	7479	
1 inlet	1999	24857	422	7212	-3,58%
2 inlet	1994	24832	399	6817	-8,86%
1 outlet	1992	24828	427	7285	-2,60%
2 outlet	1998	24876	398	6815	-8,88%

Table 5.11 shows how the temperature upstream and downstream the heat exchanger are changing due to the variation of the therminol flow. The inlet temperature has no notable variation, because the cooling fluid temperature is set by the Huber machine whose temperature controller is very accurate.

The therminol outlet temperature depends on the heat exchanged in the test pipe and so since the mass flow is decreasing, in comparison with the reference case a greater temperature variation visible. Tests with two sub-pipes closed show a greater temperature increase caused by the reduced mass flow. This effect is more noticeable when the outlet sub-pipes are closed. The phenomena can be explained with a local increase of the heat transfer coefficient in the shell side caused by the rise of the coolant speed exiting the test section (due to the smaller cross section). This hypothesis is supported by the fact that the flux flowing out from the shell hits the *RTD13* with more pressure than in the normal case, causing the sensor to vibrate emitting some particular sounds.

Even if the decrease of mass flow is similar between the various tests, like shown in Table 5.10, the temperature increase is higher when closing the outlet sub-pipes. This happens because the increased temperature at the inlet it is just result of the decrease of mass flow, while in the outlet section also the effect of the entire heat exchange progress is considered.

Table 5.11: Thermal effects of the sub-pipes tests

	$T_{th,out}$	% over	$T_{th,in}$	% over

	℃	$\boldsymbol{Reference}$	℃	$\boldsymbol{Reference}$
Reference	7,489		5,619	
1 inlet	7,545	0,76%	5,624	0,08%
2 inlet	7,694	2,74%	5,628	0,15%
1 outlet	7,530	0,56%	5,626	0,13%
2 outlet	7,797	4,11%	5,638	0,34%

The effects on heat transfer coefficient are reported in analyzing the therminol inlet, when the correspondent sub-pipes are closed, the local heat transfer coefficient changes significantly. A slightly increase with one sub-pipe closed, and a way greater decrease (-14,17%) with two of them closed. The decrease can be explained with a bad distribution of the cooling fluid due to the fact that only one sub-pipe is opened. Since $\alpha_{int,i}$ are calculated from the therminol temperature trend and from the outer wall temperature this results to have a big influence.

The mid measurement section is showing that if the inlet sub-pipes are closed, the htc is lowering, while closing the outlet sub-pipes the htc is rising. In both cases, the relative variation is the same.

The first measurement section, shows always a similar decrease of the heat transfer coefficient. In the two outlet sub-pipes test, the htc is increasing probably due to the local condition in the shell side that are improving the heat exchange process.

Table 5.12. The first column is the Petukhov value, used as reference to compare the local htc measured, and since the conditions in the working fluid are the same in every measurement, no changes are notable. Like stated in the introduction of this chapter, this section should not bring some important results, since the two heat transfer coefficients are independent. But the particular hydraulic condition of the shell side is affecting the results. In fact analyzing the therminol inlet, when the correspondent sub-pipes are closed, the local heat transfer coefficient changes significantly. A slightly increase with one sub-pipe closed, and a way greater decrease (-14,17%) with two of them closed. The decrease can be explained with a bad distribution of the cooling fluid due to the fact that only one sub-pipe is opened. Since $\alpha_{int,i}$ are calculated from the therminol temperature trend and from the outer wall temperature this results to have a big influence.

The mid measurement section is showing that if the inlet sub-pipes are closed, the htc is lowering, while closing the outlet sub-pipes the htc is rising. In both cases, the relative variation is the same.
The first measurement section, shows always a similar decrease of the heat transfer coefficient. In the two outlet sub-pipes test, the htc is increasing probably due to the local condition in the shell side that are improving the heat exchange process.

Table 5.12: Thermodynamic effects of the sub-pipe tests

	α_{PP}	$\alpha_{int,1}$	% $over$	$\alpha_{int,2}$	% $over$	$\alpha_{int,3}$	% $over$
	$\frac{W}{m^2 \cdot K}$	$\frac{W}{m^2 \cdot K}$	$Ref.$	$\frac{W}{m^2 \cdot K}$	$Ref.$	$\frac{W}{m^2 \cdot K}$	$Ref.$
Reference	2769	2435		919		1021	
1 inlet	2767	2281	-6,35%	917	-0,17%	1034	1,25%
2 inlet	2763	2298	-5,65%	903	-1,75%	877	-14,17%
1 outlet	2762	2310	-5,13%	925	0,63%	1051	2,86%
2 outlet	2767	2552	4,81%	931	1,36%	1039	1,76%

The way the cooling fluid is fed in and extracted in the test section is actually affecting the measurement. To have a prove of this phenomena these tests will be carried out also in direct flow condition in order to understand the behavior of the shell side.

5.5.2 Wilson-Plot Tests

As visible in equation 4.18, and alternative method to estimate the internal heat transfer coefficient is to take in account also the external htc, enlarging the boundary of the needed heat balance. This factor is obtainable directly by the measurements through equation 4.29 or with correlations introduced in Section 2.3.
Another way to calculate it is the Wilson-plot method. A short description of the method will be given in this chapter followed by the results so obtained.
This experimental method is based on the independence between internal and external heat transfer coefficients of a heat exchanger. Considering the overall heat transfer coefficient in a shell pipe heat exchanger, as in equation 5.3, it is composed

by three terms: two referred to the heat transfer in fluids and one describing the heat transfer across the wall that separates the two fluids:

$$K \cdot A = \frac{1}{R_{tot}} = \frac{1}{R_{int} + R_{wall} + R_{ext}} \quad 5.3$$

With the aim to evaluate the external htc, several test points are measured with constant shell side conditions, and varying the pipe side behavior. This can be made, like in this case, by setting different mass flow of the working fluid. Starting from the hypothesis of this method, the wall and external resistance are not changing, therefore it is possible to group them in a constant

$$C_1 = R_{wall} + R_{ext} \quad 5.4$$

The internal resistance is varying due to the htc variations introduced in every measurement. It is possible to estimate it with correlation bounding the Reynolds and Prandtl numbers (equation 2.7) and so it comes that

$$\alpha_{int} \propto Nu^{-1} \propto w^n$$

with w speed of the working fluid and n subscript related to the used correlation ($n = 0{,}8$ for Dittus Bölter and $n = 1$ for Gnielinski and Petukhov). The internal resistance is defined by

$$R_{int} = \frac{1}{\alpha_{int} \cdot A_{int}} = C_2 \cdot \frac{1}{w^n} \quad 5.5$$

The series of thermal resistances is now represented by a straight line modulated by the working fluid speed powered n, as visible in equation 5.6

$$R_{tot} = C_1 + C_2 \cdot \frac{1}{w^n} \quad 5.6$$

If drawn in a R_{tot}/w^{-n} graph, in this case, it is possible to notice that the internal thermal resistance is responsible for the increasing overall resistance while the wall plus external resistance remain constant as the working fluid speed rises. Analyzing the equation of the straight, the known value C_1 is the y-intercept and since the wall contribution is known, it is possible to calculate the external resistance

$$R_{ext} = C_1 - R_{wall} \quad 5.7$$

and finally to isolate the external mean heat transfer coefficient

$$\alpha_{ext} = \frac{1}{R_{ext} \cdot A_{ext}} \quad 5.8$$

Technically, to perform this test the heat exchanger is considered as a black box, with boundaries consisting in the physical boundaries of the test pipe. With this hypothesis the main data to observe are the mass flows and the inlet and outlet

temperatures of both sides. Since these temperatures are not recorded in correspondence of the entrance and exit of the test pipe, the insulation plays a significant role in the accuracy of the results. Therefore, since the sub-pipes do not need to be manipulated for other tests, is it now necessary to insulate them.
The measurement points recorded for the calculation of the external alpha are shown in Table 5.13.

Table 5.13: Measurement point of the Wilson plot test for external htc

	$\dot{m}_{WF}$ kg/s	$T_{in,WF}$ $°C$	$T_{out,WF}$ $°C$	$\dot{m}_{th}$ kg/s	$T_{out,th}$ $°C$	$T_{in,th}$ $°C$
1	0,150	47,33	42,59	0,664	7,133	5,618
2	0,201	45,46	41,76	0,664	7,223	5,628
3	0,250	43,51	40,49	0,664	7,225	5,628
4	0,298	42,45	39,88	0,665	7,262	5,632
5	0,350	41,57	39,35	0,665	7,291	5,640
6	0,399	40,96	38,98	0,665	7,316	5,629
7	0,450	40,48	38,71	0,665	7,332	5,629
8	0,500	40,04	38,44	0,665	7,346	5,628

First result from the data reduction is that with the insulation of the sub-pipes, the heat balance discrepancy between shell side and pipe side is now obviously smaller, with a maximum error of $3{,}51\%$ in measurement number 8. This ensures that all the calculation bounded with this unit, will show better results in the further tests.
From the energy balance in equation 4.14 it comes that

$$R_{tot} = \frac{1}{K_{int,i-o} \cdot A_{int}} = \frac{\Delta T_{ln,i-o}}{\dot{Q}_{i-o}} = \frac{1}{\alpha_{int} \cdot A_{int}} + R_{wall} + \frac{1}{\alpha_{ext} \cdot A_{ext}} \qquad 5.9$$

Since the internal heat transfer coefficient is to be calculated with a correlation, it has been chosen not only to use the Petukhov correlation but also the one of Dittus Bölter in order to perform some comparison. The Wilson plot, with these two different internal htc is reported in Figure 5.17.

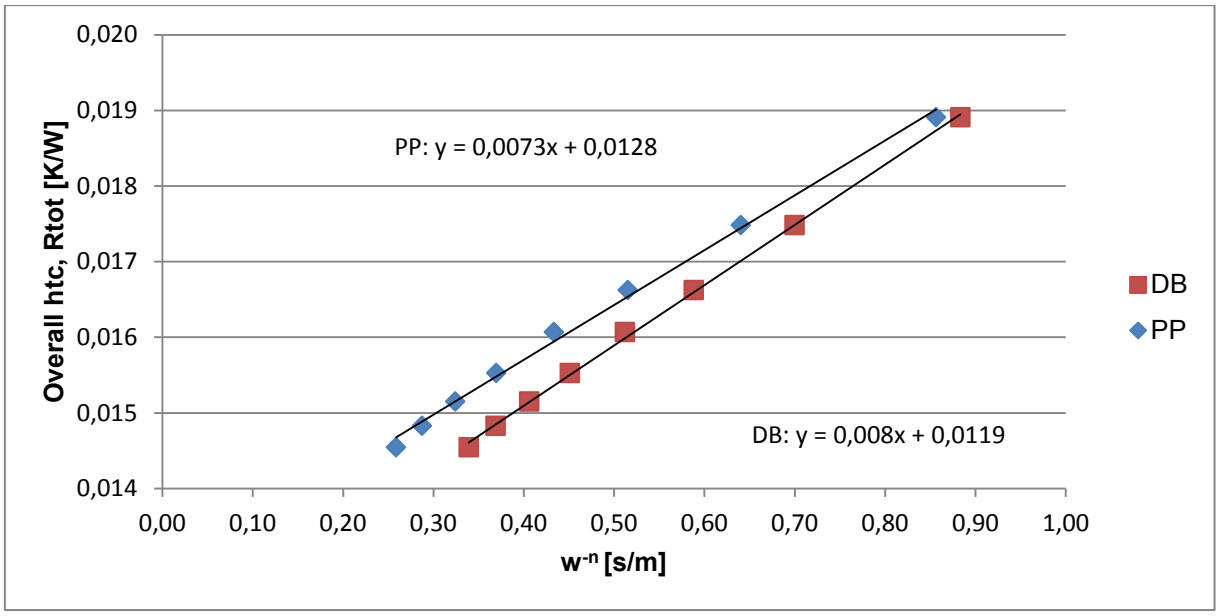

Figure 5.17: Wilson plot for shell side heat transfer coefficient

Thanks to the Wilson plot method, following the steps explained at the beginning of this section, is it possible to estimate the external heat transfer coefficient. The results are reported in Table 5.14.

Table 5.14: Results of the Wilson plot test for external htc

	C_1 $\frac{m^2 \cdot K}{W}$	C_2 $\frac{m^2 \cdot K}{W} \cdot w^n$	R_{ext} $\frac{K}{W}$	α_{ext} $\frac{W}{m^2 \cdot K}$	% **over expected**
Dittus ($n = 0{,}8$)	0,0119	0,008	0,0164	304	-1,9
Petukhov ($n = 1$)	0,0128	0,0073	0,0173	288	-29,3

The external htc calculated with this method, even using different correlations, are quite similar. This never happened with the direct calculation through correlation. The Petukhov correlation, that generally gives reliable results, in this case leads to a relative discrepancy of almost -30% over the expected value. The Dittus Bölter correlation, normally underestimates the htc and so in this case shows a relative discrepancy of only $-1{,}9\%$.

The same procedure has been applied in order to calculate the internal heat transfer coefficient, so varying the shell side flow with working fluid flow constant. This test has brought bad result since the relative discrepancy between calculated and expected htc is over -75%. In this test, the effect of the non-homogeneous temperature trend induced by the free convection may have influenced the results, leading to a bended R_{tot} function difficult to interpolate. For this reason the results of this test are not reported in this work.

5.6 Direct flow tests

The previous tests have shown a strange behavior of the test section. In fact a particular and unexpected temperature trend is characterizing the outer wall of the test pipe, as visible in Figure 5.8. This is connected directly to strange measurement of the heat transfer coefficient. In addition, the change of the therminol temperature difference in between the measurement sections (Figure 5.6), is also a prove that the hydrodynamic behavior of the shell side is somehow affecting the measurement. The last possibility to investigate this influence is to run the heat exchanger in direct flow conditions. In this way it is possible to prove the reliability of the measurement sections, in particular the first one since it is the one giving the best results. Otherwise change of the heat transfer behavior between the two configurations is comparable. Like this it might be possible to find an explanation to the data collected so far. For this purpose the main tests carried out in counter flow condition are repeated and the results are reported in the following sections.

5.6.1 Heat transfer coefficients measurement

Using the temperature reference conditions for the secondary cycles (Table 5.7), in the interval between $G_{WF} = 500$ and $3500\ kg/(s \cdot m\text{^}2)$, every 250 unities a measurement point is recorded. In this way the entire working conditions are spanned. As obviously expected, the new configuration of the test section changes the temperature trend of the cooling fluid, inverting the sign of its slope. In these conditions, the temperature difference between therminol and working fluid in the first measurement sections results greater than in the counter flow configuration. It becomes smaller along the heat exchanger, like visible in Figure 5.18.

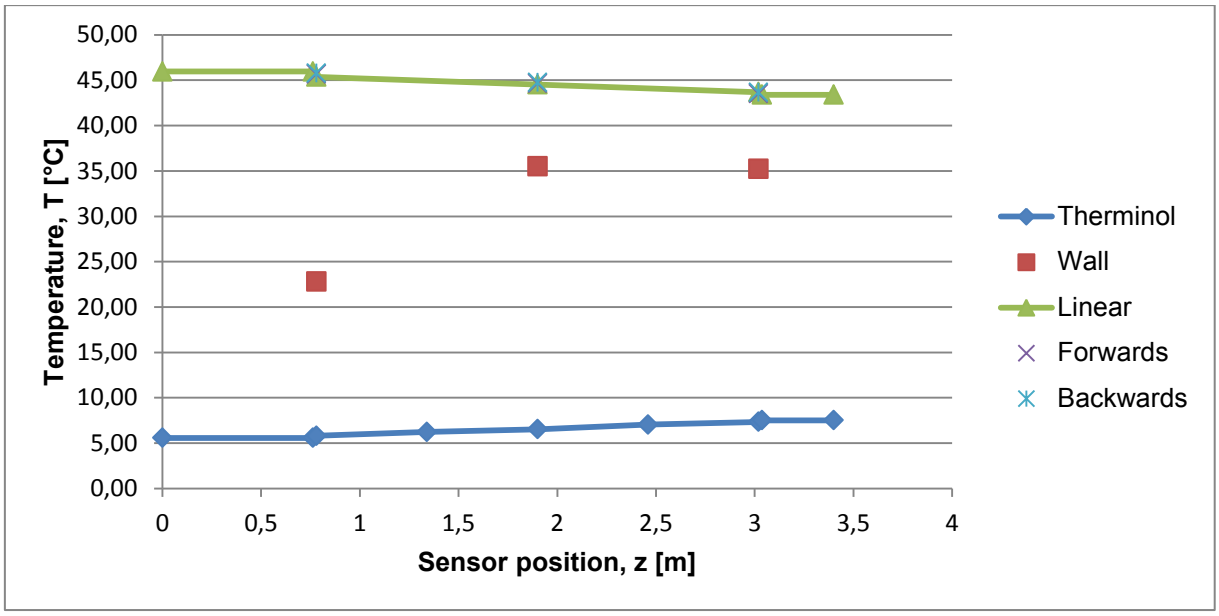

Figure 5.18: Temperature plot for reference conditions in direct flow

Not expected is the behavior of the wall temperature that normally showed a value nearer to the working fluid in the first sections, and nearer to the process in the other two. As in the counter flow tests, this tendency is observed in every direct flow measurement (Figure 5.19).

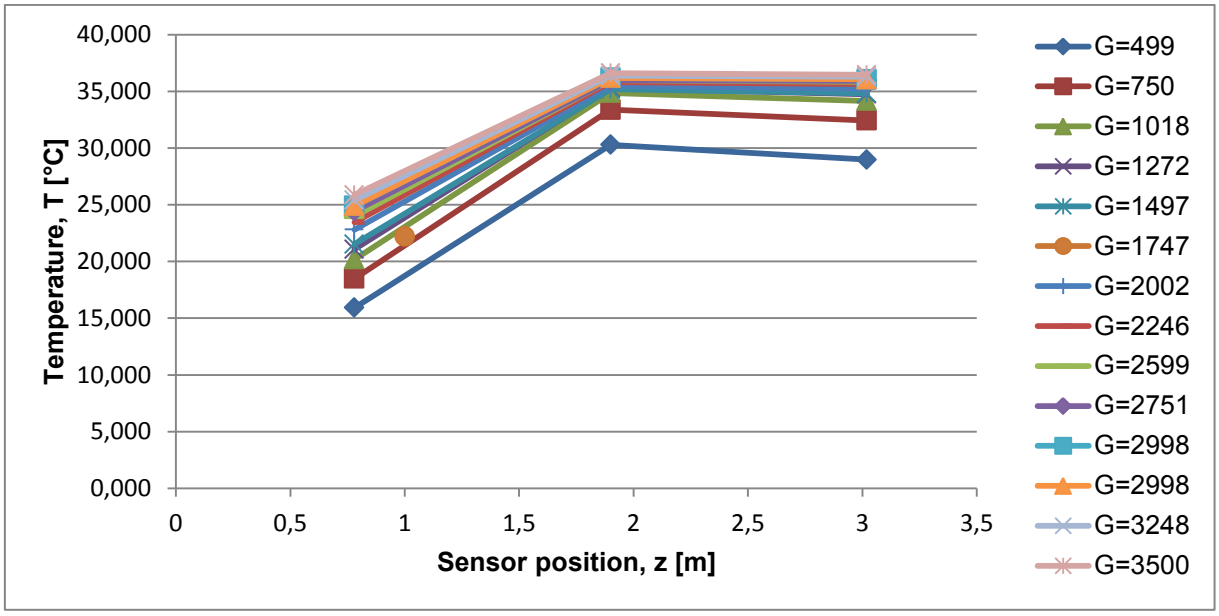

Figure 5.19: Wall temperature in direct flow tests

The outer wall temperature results always nearer to the therminol temperature in the first measurement section encountered (third m.s. for counter flow and first m.s. for direct flow, related to Figure 3.2) as noticeable in Figure 5.20. But in this case the data collected from the second measurement section remains unexplainable. Its behavior lead to the assumption that the hydrodynamic influence to be investigated in these tests is acting between the first and the mid measurement section.

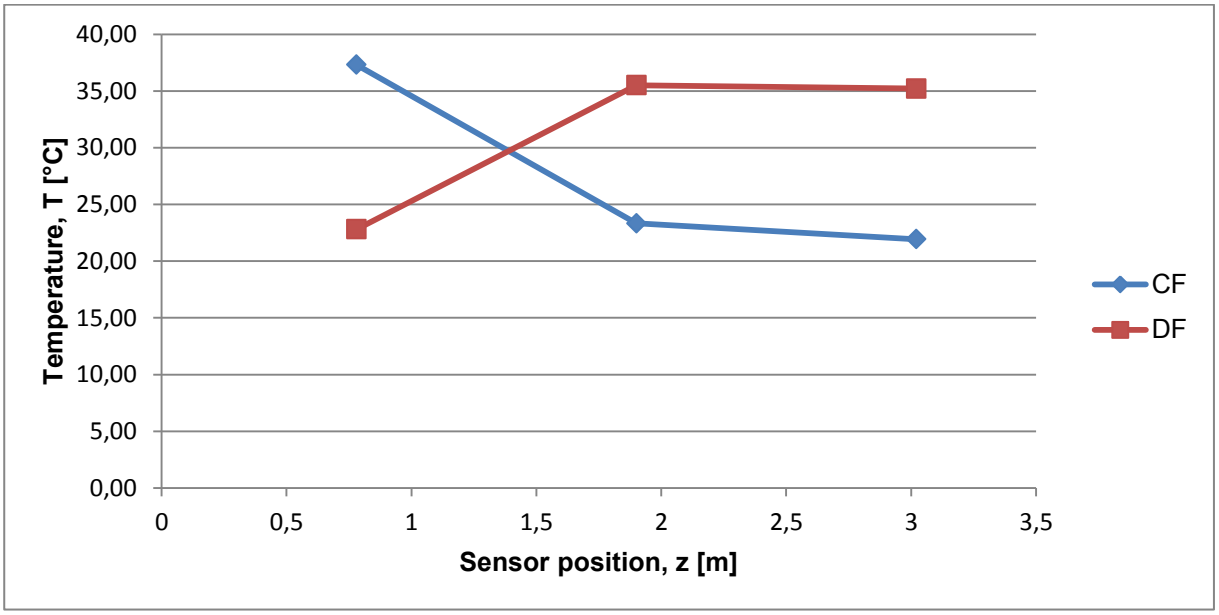

Figure 5.20: Wall temperature in counter and direct flow, for reference conditions

An important results is given by the trend of the temperature differences between each shell side sections, reported in Figure 5.21. In every measurement point recorded this difference acts in the same way, but showing a not regular heat exchange process. This occurred also in the counter flow tests, like shown in Figure 5.22, where the two operative conditions are compared. The irregularity of the process is different between the two cases. In counter flow tests, only an absolute peak in the fourth ΔT is visible. In direct flow tests, the same absolute peak is present, but with a greater value. In addition a secondary peak is present in the second ΔT, between the first and the first intermediate measurement section.

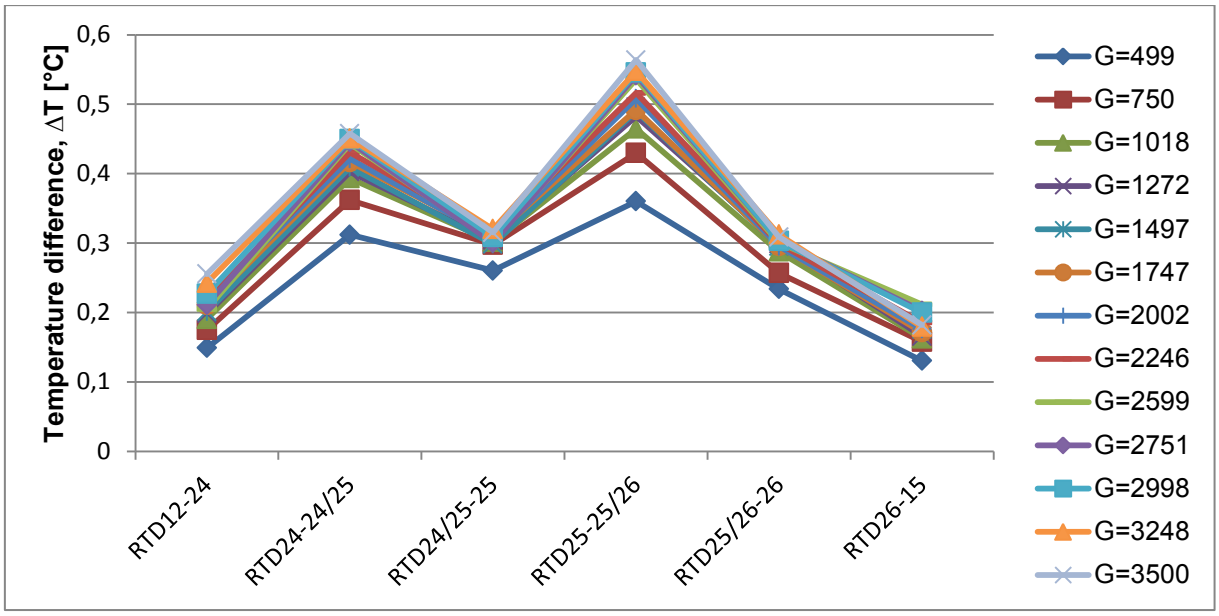

Figure 5.21: Temperature difference between every therminol measurement sections

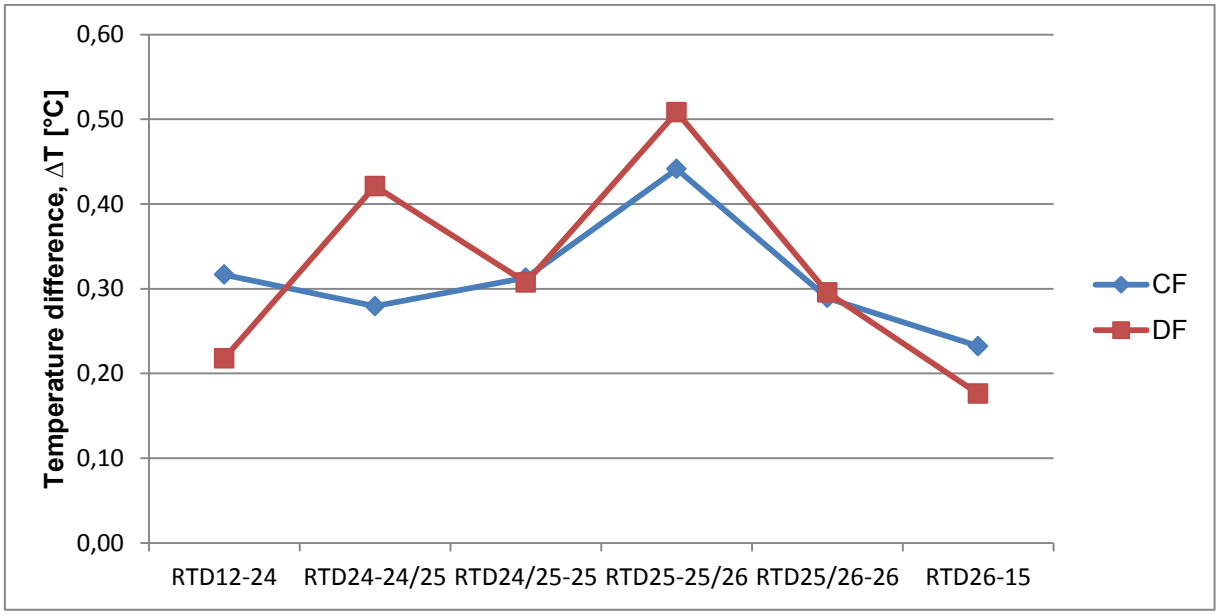

Figure 5.22: Coolant temperature difference in direct and counter flow for reference conditions

As explained in Section 5.2, even if the temperature trend of therminol is legit, the wall temperature has a strange behavior. Observing the way therminol warms up, an irregularity of the heat exchange process is noticed. The particular construction of the

shell side may be the cause of this effect. It causes turbulences in some streaks which leads to an irregular heat exchange.

To investigate this phenomenon, the project leader provided CFD simulation of the mid measurement section, reported in Figure 5.23. This simulation is carried out in direct flow configuration and in reference condition. Reminding Figure 5.7, the mid measurement section is actually placed on the left side of the capillary pipes. With this configuration, the temperature of both therminol and outer wall is measured before the turbulence site. In that portion of the shell side the flow is practically undisturbed and so the mean Reynolds number usually calculated (around 7500 in the transition flow regime) is properly describing the hydraulic behavior of therminol. The Reynolds number is half a way between laminar and turbulent behavior, so the heat transfer coefficient in the shell side before the capillary pipes is not good and this lead to high wall temperature.

After the measurement section, therminol flows through the capillary pipes where it gains turbulence. Locally the Reynolds number is rising, probably reaching the state of developed turbulence flow. In this condition, the heat transfer coefficient is way better than before decreasing the thermal resistance of the shell side fluid. For this reason a reduction of the wall temperature is visible, since in order to sustain the heat transfer process, a smaller temperature difference is needed. Downstream the capillary pipes, the gained turbulence fades away turning back to the initial flow conditions. The same phenomena occurs also in counter flow conditions, but in this situation therminol gains turbulence before the measurement section, resulting in a lower wall temperature.

This simulation helps understanding the reason behind the peak in therminol temperature difference between second and second intermediate measurement section. The reason why for the direct flow configuration the peak is higher is because the turbulence builds up and fades out between the two sections. In counter flow conditions, the turbulence develops between the two sections but the mid temperature is recorded immediately.

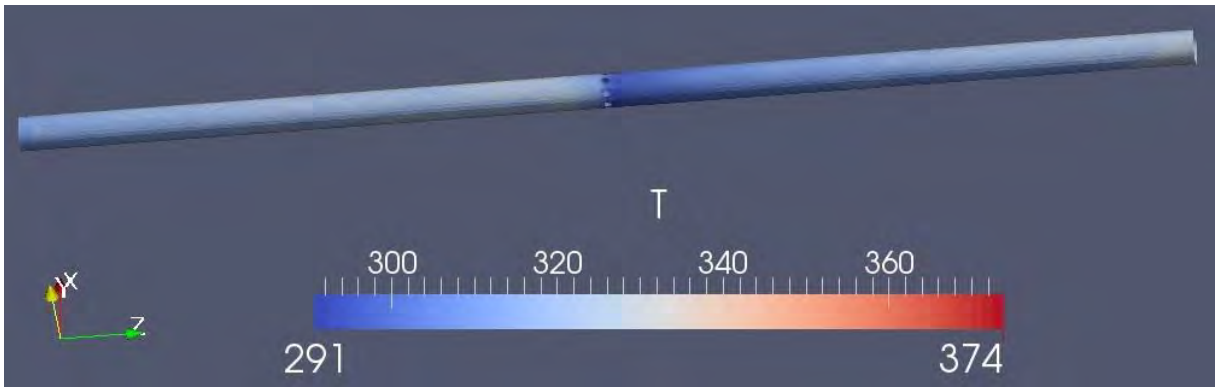

Figure 5.23: CFD simulation of wall temperature in the mid measurement section

In order to understand the reason behind the second peak present in direct flow tests, another CFD simulation made in the same condition of the first one, comes in help in **Errore. L'origine riferimento non è stata trovata.**.

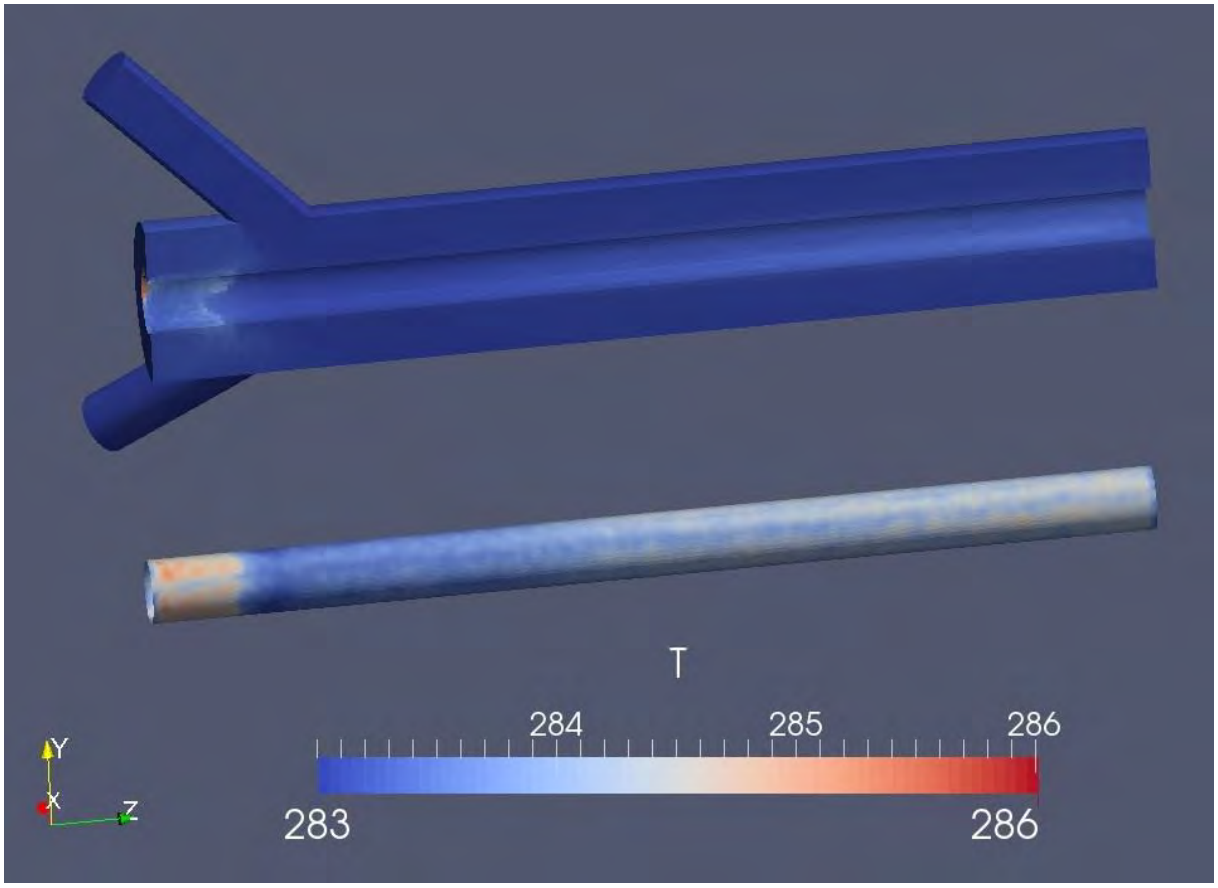

Figure 5.24: CFD simulation of the first measurement section in shell side

This time both wall temperature and therminol temperature are represented, so it is possible to see directly the influence between these two elements. The first part on

the left is placed before the sub-pipes that leads the coolant into the heat exchanger. It is possible to notice that fluid temperature so as the wall temperature are remarkably high, that because it is a dead end for the coolant and since it is not moving the heat transfer coefficient is bad. After this portion of pipe, there are the sub-pipes that lead the fluid with a pitch angle of $45°$ off the pipe axis. Important is to state that the first measurement section is placed in the proximity of the sub-pipes and so the coolant flows directly on it.
The effect of this is visible in the wall temperature which is very low here. The flow divided in the sub-pipes comes here in turbulent condition and streams towards the internal pipe, where the TC's are placed, increasing the heat transfer coefficient. Downstream the flow sets up homogeneously, turning back to the transition condition expected by the calculated Reynolds number. This inlet effect is also visible in the sub-pipe tests (Figure 5.20), where the internal alpha changes remarkably when the coolant flow is reducing, worsening the flow field in the shell side.
This behavior should occur also in counter flow condition, leading to a secondary peak also in its curve, but this is not the case. Considering Figure 5.22, since here, the first and last temperature difference were not taken in account due to the very short length involved. Nevertheless, in this case they bring some important information. In every configuration, the first temperature difference is generally bigger than the last one, even if they should be similar due to the same construction. In addition to that, considering the reference conditions, running the heat exchanger in direct flow allows the inlet temperature of both fluids to be 6% greater than in counter flow. These facts can be a contribution to this effect, but they do not explain a so huge temperature difference. This means that somehow more heat is exchanged before the first measurement section, that is why this secondary peak is still object of test by Thermodynamic Faculty of University of Kassel.

Temperatures measured in the test section reflects the thermodynamic conditions in the heat exchanger. They are the consequence of the heat transport effect between the two fluids and so of the heat transfer coefficients occurring in the process.
So as to change the wall temperature trend in the test section like showed in Figure 5.19, the heat transfer coefficient trend changed as well. Figure 5.25 represents a recap of the results obtained in direct flow tests. Gnielinski and Petukhov correlation are always taken as reference value leading to unexpected results. Opposite of the

counter flow tests, the second and third measurement section result reliable. The second measurement section shows a mean relative discrepancy of $2{,}9\%$, while the third one is behaving worse with the $10{,}8\%$. These values are surprisingly good also if compared to the ones of the first measurement section.

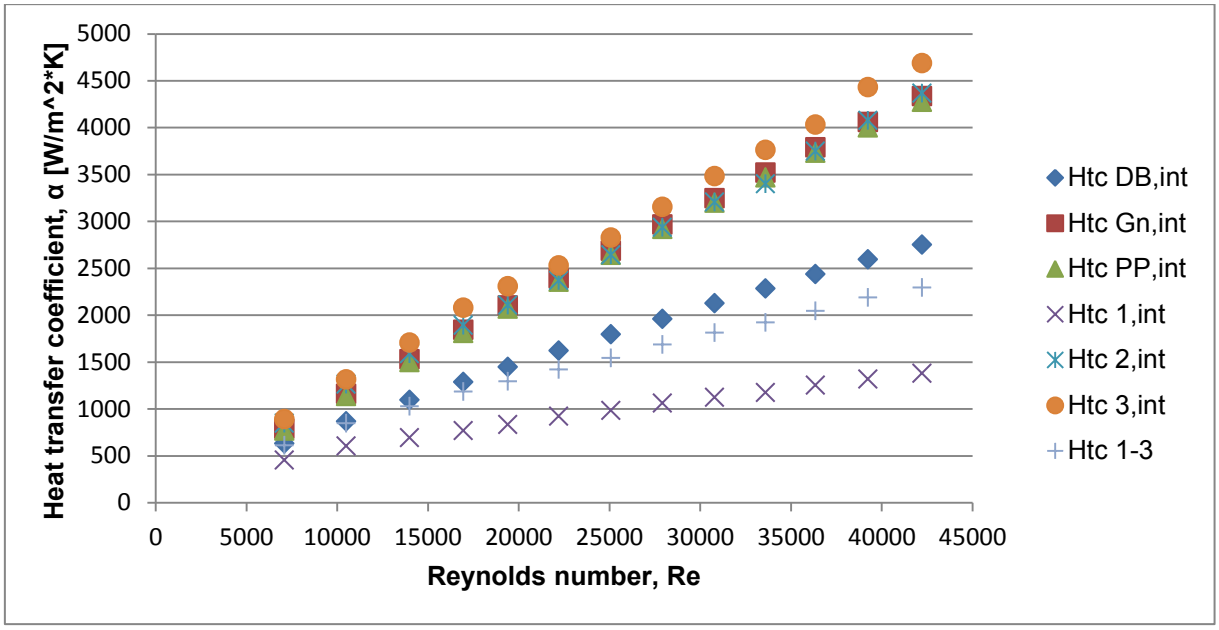

Figure 5.25: Internal heat transfer coefficients in direct flow tests

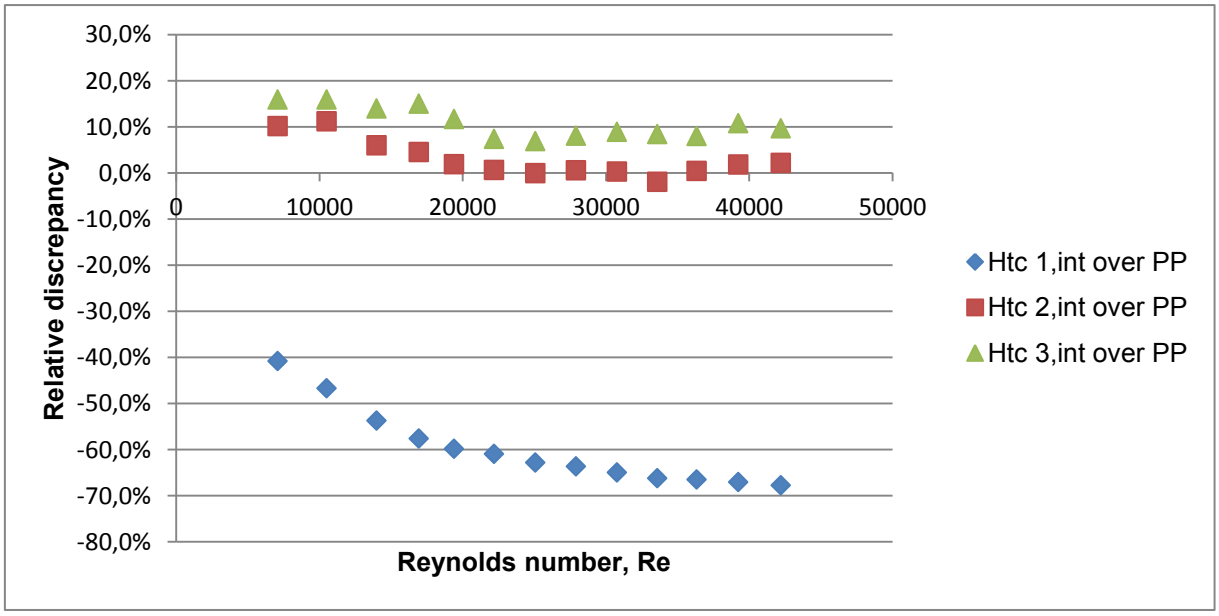

Figure 5.26: Relative discrepancy of local heat transfer coefficient in direct flow tests

In Figure 5.26 it is possible to see how its discrepancy is growing with the Reynolds number, reaching $-67{,}8\%$ in the worst case. Also if compared with the Dittus Bölter correlation, this measurement section results now totally not reliable. As in the counter flow tests the mean htc calculated measured through the wall temperature is giving lower results for the same reasons, and thus it results near the Dittus Bölter values.

The external heat transfer coefficient, as in counter flow tests, shows the opposite behavior of the internal one. Since now the second and third measurement section are giving higher values than the first one, now the external htc has higher values than in the other two sections as visible in Figure 5.27. Since these measurement points were recorded during a single measurement campaign, all the htc values should be in a flat straight with little variations caused by the little temperature variation influencing the thermal proprieties of therminol. This doesn't happen in the first measurement section, where the results are converging to better values as Reynolds increases. Is to notice that the entire data are represented in 100 units of Reynolds, this means that the measurement of external htc in the first section in this condition is affected by greater deviation. Since the data of the first measurement section are so distant from the expected value, in Figure 5.28 are not represented in order to let the graphic readable. This graph, shows the discrepancy between the second and third measurement section in comparison with the Pethukov correlation. It can be seen how the difference is growing with Reynolds even if it is not changing remarkably. The counter flow tests brought very little discrepancy with the expected value while in direct flow tests it results between 25% and 40%.
The heat transfer coefficient results in this configuration lead to the conclusion that if run in direct flow, this test rig gives good results on the second and third measurement section. Attention must be paid to the external htc since the values in the reliable section are deviating more than in counter flow condition.

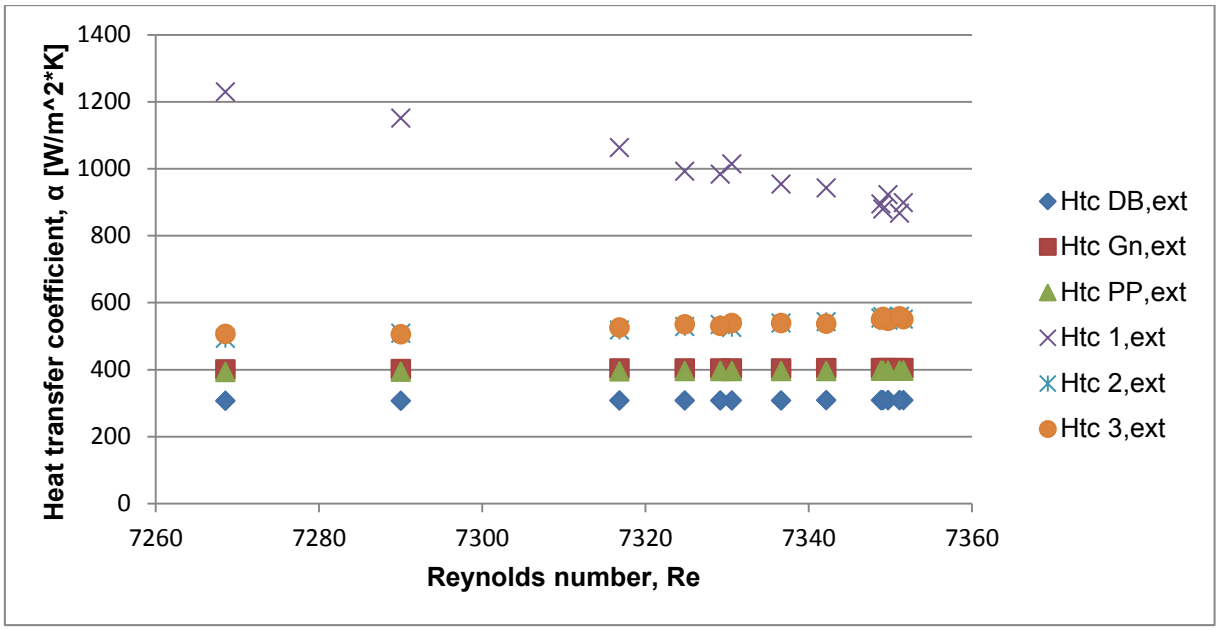

Figure 5.27: External heat transfer coefficient in direct flow tests

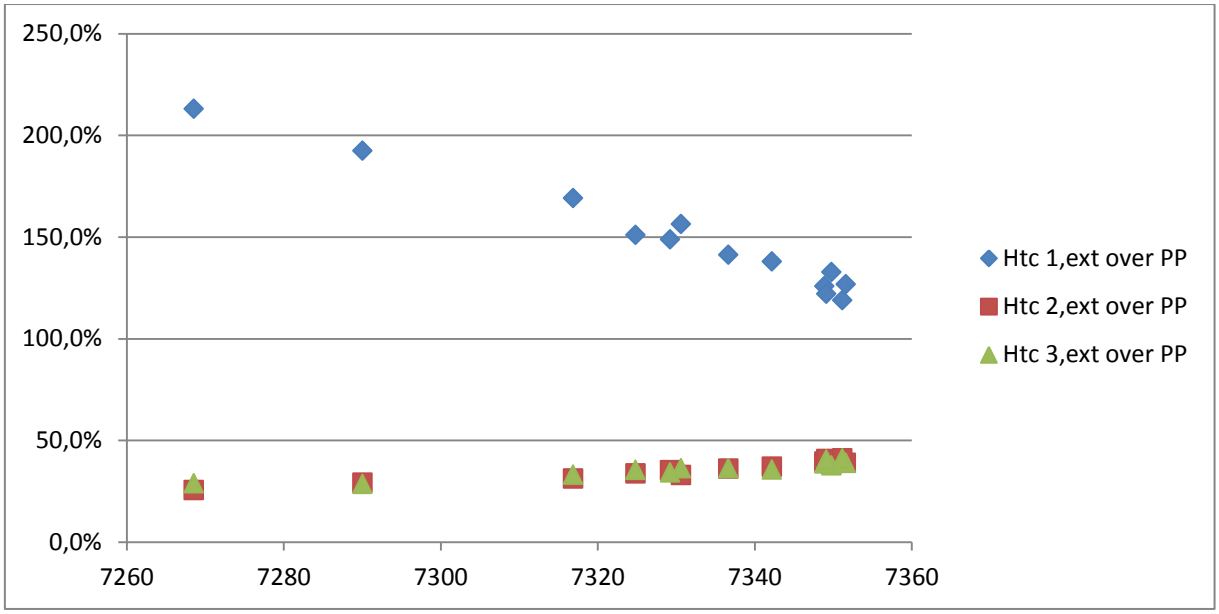

Figure 5.28: Relative discrepancy of external htc in direct flow tests

5.6.2 Wilson-plot test

As explained in the previous section, in direct flow conditions the external heat transfer coefficient measured locally results far from the expected value. This did not happen in the counter flow configuration where the discrepancy between the two

value was little. For this reason, and as validation of the external htc tests made before, Wilson plot test is carried out running the test rig in direct flow.

This test follows the same steps as the one presented in Section 5.5.2. The measurement point recorded are reported in Table 5.15 and the Wilson plot obtained is represented in Figure 5.29. At first sight it is possible to see that the behavior of the interpolating line of both test is following the trend seen in Figure 5.17, with the two interpolating straight diverging reaching the y-intercept. In fact as visible in Table 5.16, this behavior leads to similar results also for the calculated heat transfer coefficient. Pethukov correlation always far away from the expected value and dittus Bölter with very little discrepancy. So even with no good results, if comparing the reference correlation, it is possible to state that the tests made in both flow condition give consistent values.

Table 5.15: Measurement point of Wilson plot test in direct flow condition

	$\dot{m}_{WF}$	$T_{in,WF}$	$T_{out,WF}$	$\dot{m}_{th}$	$T_{in,th}$	$T_{out,th}$
	kg/s	$°C$	$°C$	kg/s	$°C$	$°C$
1	0,084	53,44	45,85	0,654	5,58	7,02
2	0,127	51,75	46,22	0,654	5,58	7,26
3	0,172	50,62	45,95	0,656	5,58	7,38
4	0,214	49,01	45,16	0,656	5,59	7,44
5	0,252	47,61	44,30	0,656	5,59	7,46
6	0,294	46,66	43,78	0,656	5,58	7,48
7	0,337	45,95	43,40	0,656	5,59	7,52
8	0,379	45,52	43,22	0,657	5,59	7,55
9	0,421	45,07	42,97	0,657	5,60	7,60
10	0,464	44,64	42,72	0,657	5,61	7,61
11	0,505	44,30	42,52	0,657	5,60	7,63
12	0,547	44,11	42,44	0,657	5,58	7,63
13	0,590	44,00	42,43	0,657	5,57	7,66

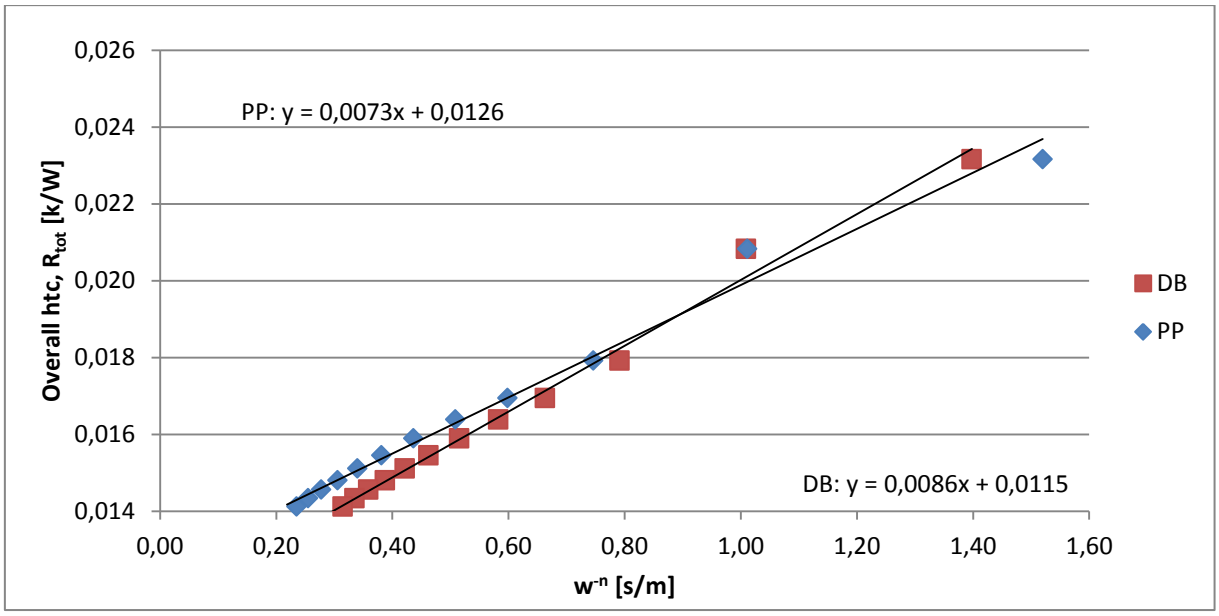

Figure 5.29: Wilson plot for external heat transfer coefficient in direct flow

Table 5.16: Result of the Wilson plot test in direct flow condition

	C_1 $\frac{m^2 \cdot K}{W}$	C_2 $\frac{m^2 \cdot K}{W} \cdot w^n$	R_{ext} $\frac{m^2 \cdot K}{W}$	α_{ext} $\frac{W}{m^2 \cdot K}$	% **over expected**
Dittus ($n = 0{,}8$)	0,0115	0,0086	0,0160	313	1,5
Petukhov ($n = 1$)	0,0126	0,0073	0,0171	292	-26,2

5.6.3 Sub-pipe test

These tests are carried out with the same procedure explained in Section 5.5.1. Table 5.17 shows the variation of mass flow, and so of mean Reynolds number due to the closure of the sub-pipes. In every case, the percentage in direct flow is 1% less than in the counter flow conditions. That can be caused by the different path of the fluid before reaching the test section. In fact, the check valve installed in order to avoid water hammer in the *SECTS*, in counter flow configuration is placed before the test section adding a pressure loss which allows therminol to enter the heat exchanger at a lower pressure. With one sub-pipe closed, it is possible to notice that the smaller loss of load is at the beginning of the test section (outlet for counter flow

and inlet for direct flow),that as in the same test made before, may be caused by practical difficulties in closing the sub-pipe.

Table 5.17: Hydraulic effects of the sub-pipe tests

	G_{WF} $kg/(s \cdot m\text{^}2)$	Re_{WF}	G_{th} $kg/(s \cdot m\text{^}2)$	Re_{th}	% **over Reference**
Reference	2001	24846	431	7346	
1 inlet	2002	24612	423	7209	-1,87%
2 inlet	1998	24568	397	6784	-7,65%
1 outlet	2002	24607	418	7129	-2,96%
2 outlet	2002	24625	400	6813	-7,25%

Temperature changes due to the closure of the sub-pipes are shown in Table 5.18. As in the counter flow test, inlet temperature is not affected by this change of conditions, since it is directly supplied by the thermostat of the Huber machine. Therefore tiny oscillation of this values are normale. The outlet temperature seems to be influenced by these tests only when two sub-pipes are closed even if in a smaller way than in counter flow. In fact, the increasing of the outlet temperature is compatible with the decreasing of the mass flow in the shell side, but the variation itself is not remarkable.

Table 5.18: Thermal effects of the sub-pipe tests

	$T_{th,in}$ ℃	% **over Reference**	$T_{th,out}$ ℃	% **over Reference**
Reference	5,589		7,501	
1 inlet	5,554	-0,63%	7,470	-0,41%
2 inlet	5,588	-0,02%	7,597	1,28%
1 outlet	5,579	-0,19%	7,492	-0,12%
2 outlet	5,555	-0,61%	7,532	0,41%

The heat exchange process in direct flow, as visible in Table 5.19, is affected almost in the same way as in counter flow. An “inlet effect” is noticed by a remarkable decrease of the heat transfer coefficient in the first measurement section, with the same percentage of the counter flow test. This inlet effect can be related also to the temperature difference trend in the shell side, since it is occurring in both conditions in the same way. The other section are behaving almost normally, without the notable variation at the outlet section recorded in the previous test.

Table 5.19: Thermodynamic effect of the sub-pipe tests

	$\boldsymbol{\alpha_{PP}}$ $\frac{W}{m^2 \cdot K}$	$\boldsymbol{\alpha_{int,1}}$ $\frac{W}{m^2 \cdot K}$	% $\boldsymbol{over\ Ref.}$	$\boldsymbol{\alpha_{int,2}}$ $\frac{W}{m^2 \cdot K}$	% $\boldsymbol{over\ Ref.}$	$\boldsymbol{\alpha_{int,3}}$ $\frac{W}{m^2 \cdot K}$	% $\boldsymbol{over\ Ref.}$
Reference	2627	1005		2701		2927	
1 inlet	2614	1018	1,29%	2763	2,27%	3012	2,89%
2 inlet	2610	843	-16,08%	2655	-1,70%	2933	0,20%
1 outlet	2614	1012	0,72%	2711	0,38%	2925	-0,06%
2 outlet	2615	1019	1,39%	2773	2,66%	2922	-0,18%

Since the change of operative conditions of the test section requires a significant amount of time, the choice is to perform the following tests only in direct flow configuration. For this reason, from now on only the actual result will be reported with comments but without comparison between the two stream directions. The project chief accepted this lack of information in change of a fast progression with the commissioning phase of the test facility.

5.7 Gas tests

After all the consideration about the behavior of the shell side, the tests are proceeded by changing the working fluid. In this section the main information and result about the measurements recorded with nitrogen as working medium are reported. In the preliminary measurement, Section 5.2, the upper limit in terms of mass flow for gaseous stream is tested. In those conditions, the heat exchanged between the two fluids is approximately $1{,}6\ kW$ and so even with an insulated test section, the magnitude of the heat losses becomes comparable with the exchanged

heat. This affects all the calculations depending from the heat balance like the working fluid temperature. In fact in this case, the difference between the working media temperature calculated with the forwards and backwards method of equation 4.9 results not negligible. This leads to not unique internal heat transfer values per measurement section. For this reason the local heat transfer coefficient for gaseous measurement is calculated using a nitrogen temperature, calculated as linear trend between inlet and outlet of the test section. A representation of this concept is given in Figure 5.30. The measurement point recorded with nitrogen as working fluid are reported in Table 5.20

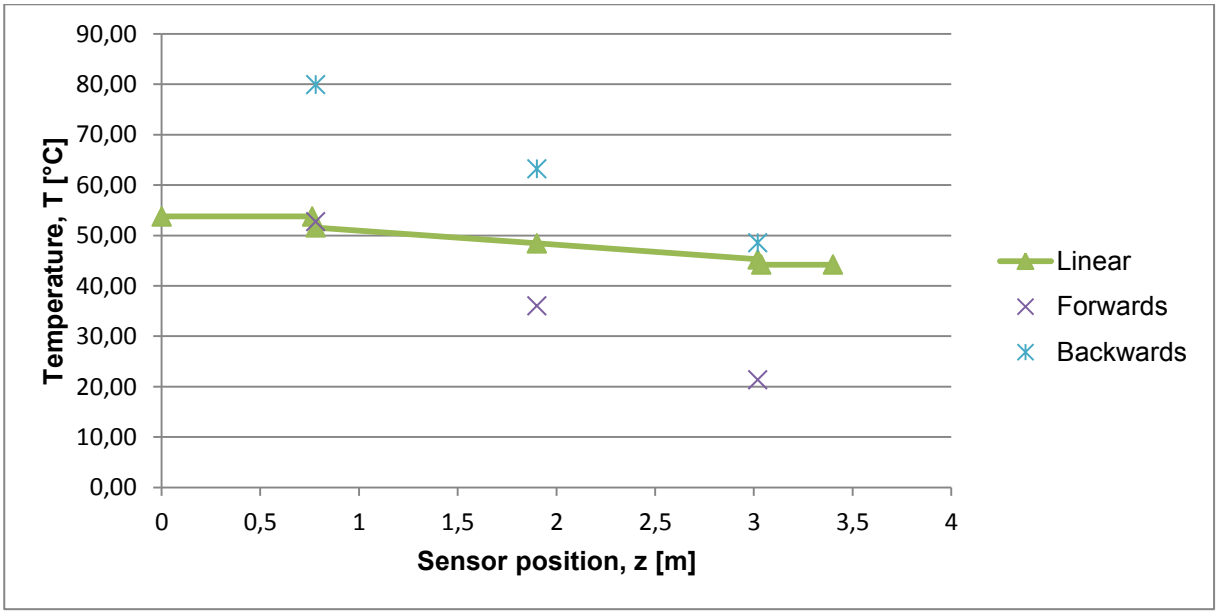

Figure 5.30: Typical working fluid temperature trends in gas measurement

Table 5.20: Measurement points of gas tests

		1	*2*	*3*	*4*	*5*	*6*	*7*	*8*	*9*
G_{WF}	$\frac{kg}{s \cdot m^2}$	10	30	50	70	80	100	120	140	160

The first measurement, $G = 10$ will not be taken in account when discussing the results, but since it is a result of the measurement session it will be shown in the graphs.

5.7.1 Heat transfer coefficients

With this calculation method, it is possible to analyze and compare the heat transfer coefficient value, using a unique temperature for each measurement section. Figure 5.31 reports the calculated heat transfer coefficients. As anticipated when discussing the preliminary measurement in Section 5.2, the behavior of the correlations is changing for gas only flow. The Petukhov correlation, always used as reference, is now giving the lowest result in comparison with the other correlations. Dittus values have a mean relative discrepancy with Petukhov reference of ca. 12% while Hausen's values are located always between the Dittus and Petukhov with a mean relative discrepancy of 3,7% from the reference.

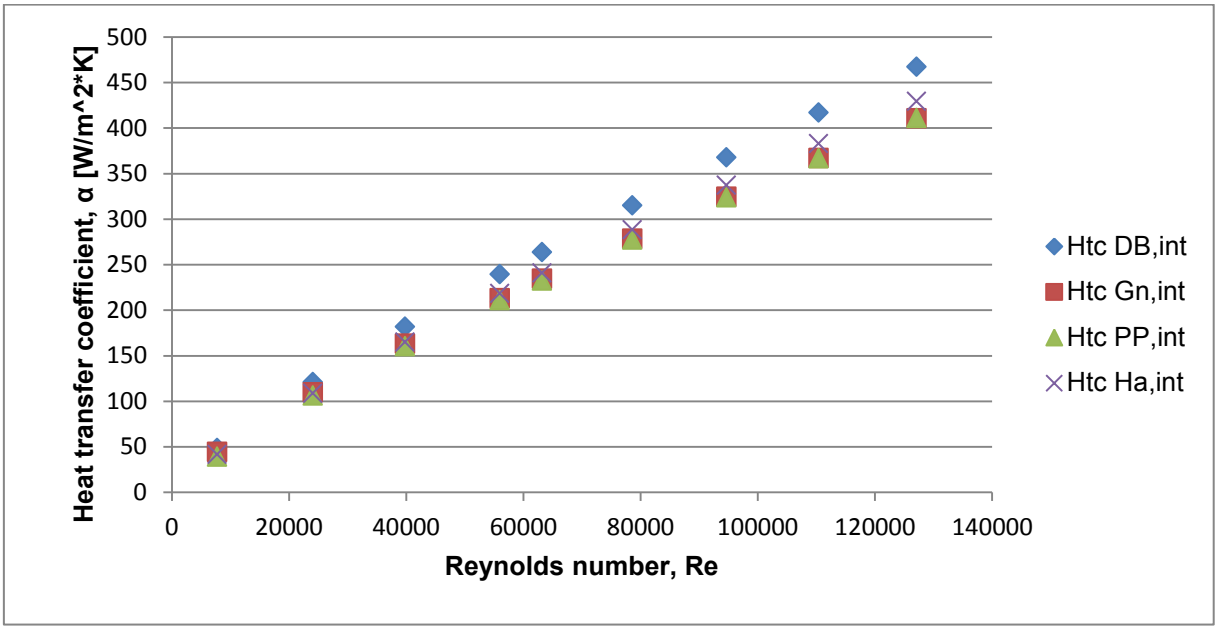

Figure 5.31: Heat transfer coefficient calculated through correlation in gas tests

Local heat transfer coefficients are reported in **Errore. L'origine riferimento non è stata trovata.**. Like in liquid-only measurement, if the test section is run in direct flow condition, the first measurement section is measuring a lower heat transfer coefficient with relative discrepancy between -17% and -33%. The second and third measurement section keep on resulting reliable and if considering also **Errore. L'origine riferimento non è stata trovata.** is it possible to notice that the second measurement section is measuring in the worst case with $-8{,}8\%$ discrepancy from

the expected value. The third section is behaving worse, with relative discrepancy starting from $13{,}6\%$ and decreasing as Reynolds number rises.

Figure 5.32: Local heat transfer coefficient measured in gas test

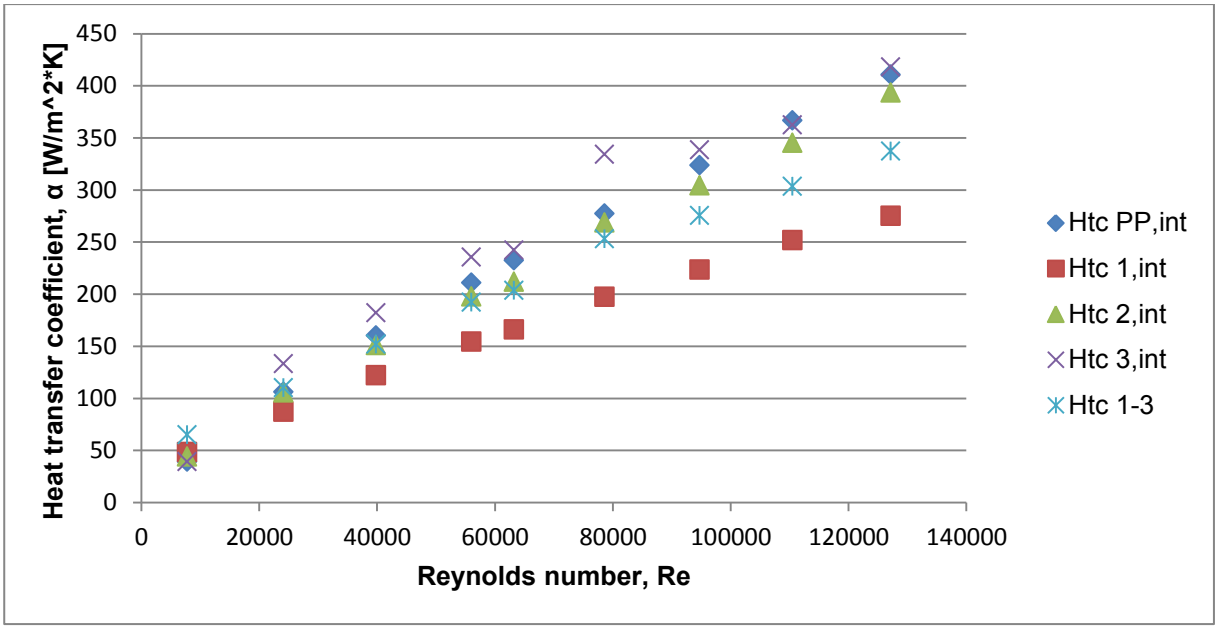

Figure 5.33: Relative discrepancy between local htc and reference

Considering the external heat transfer coefficient, since all the measurement point are recorded in a single session there should be no important differences in values between the measurement point. That's obviously happening in the calculated heat transfer coefficient, since its value is only depending by thermodynamic data of therminol. The results are shown in Table 5.21.

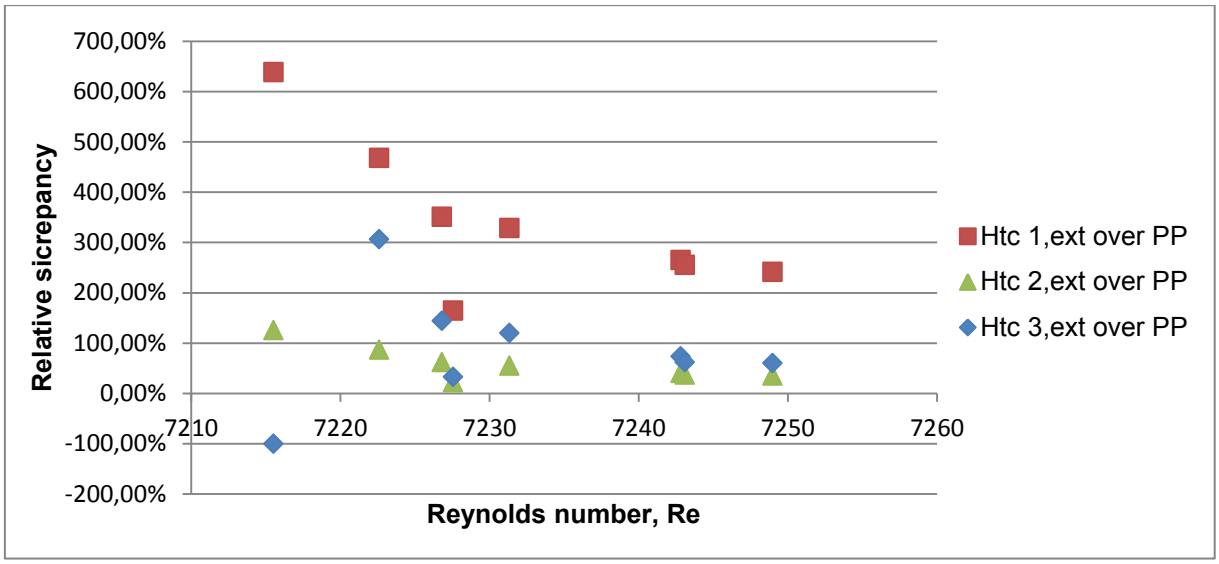

Figure 5.34: Relative discrepancy between external local htc and reference

Table 5.21: Calculated external heat transfer coefficient in gas tests

Re	α_{DB} $\frac{W}{m^2 \cdot K}$	α_{Gn} $\frac{W}{m^2 \cdot K}$	α_{PP} $\frac{W}{m^2 \cdot K}$
7232	306	400	392

The local external heat transfer coefficient, even in the reliable measurement section does not match the correlation values in any case. As evidence of this fact, **Errore. L'origine riferimento non è stata trovata.** shows that the best results are in the second measurement section and in this case the relative discrepancy is between 22% and 125%. The actual values are not reported for this reason.

5.7.2 Temperatures of the test section

Since now the test section runs in direct flow condition, even if the working fluid is different, the awaited behavior of the wall temperature is the same as Figure 5.19. Due to the different heat transfer condition, explained in the previous section, the heat exchanged in these tests is between $200\,W$ and $1000\,W$. In comparison with liquid measurements these values are between -90% and -64% smaller. Wall temperature trend are reported in **Errore. L'origine riferimento non è stata trovata.**. In this figure it is possible to notice that apart from the measurement $nr.1$,

where the working fluid flows in transition condition ($Re = 7760$), the other trends are quite similar between each other. These trends are therefore different from the awaited one, since the temperature of the third measurement section is colder than at the second. This may be caused by the smaller specific heat flow combined with the particular hydrodynamic shell side conditions.

Considering the heat balance, the main difference with the liquid measurement is in the heat flow capacity of the working fluid. The heat flow capacity of nitrogen is between 120 and 60 times smaller (if comparing the lower and upper mass flow limits) and this lead to greater temperature difference between inlet and outlet of the working fluid side. The heat flow capacity of the cooling media remains constant and this results in a decrease of the temperature difference between inlet and outlet. In this way the relative error of the therminol temperature becomes more important.

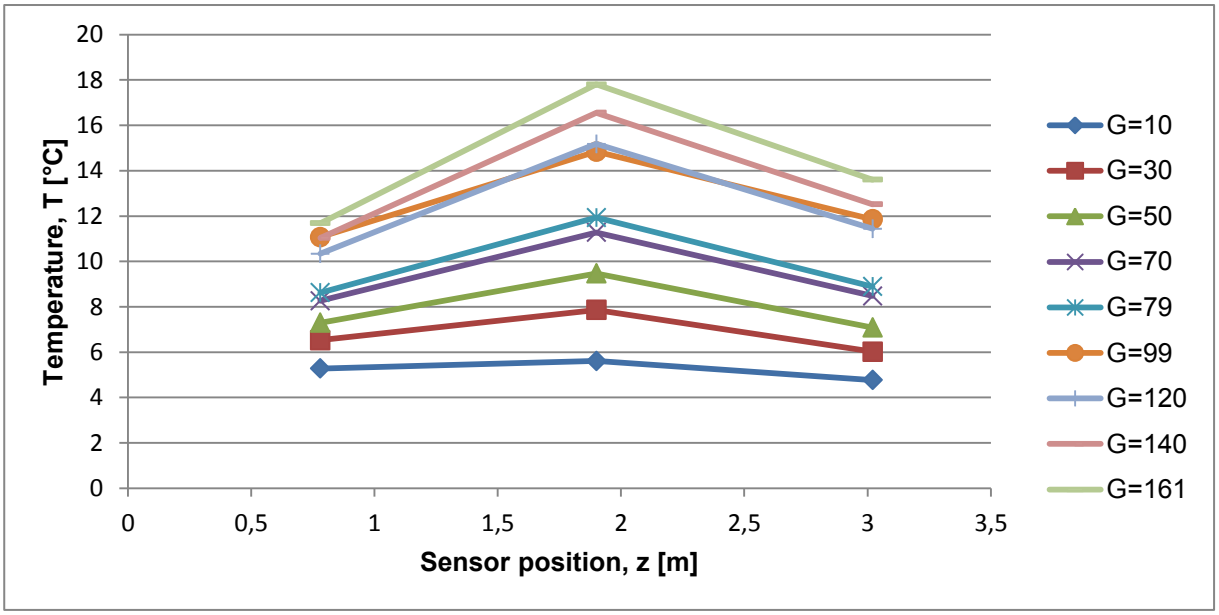

Figure 5.35: Wall temperature trend in gas measurement

Even though, apart from the first measurement, behaving differently because of the reason explained before, the other trends are quite similar. Temperature differences are increasing as Reynolds number grows, as visible in Figure 5.36.

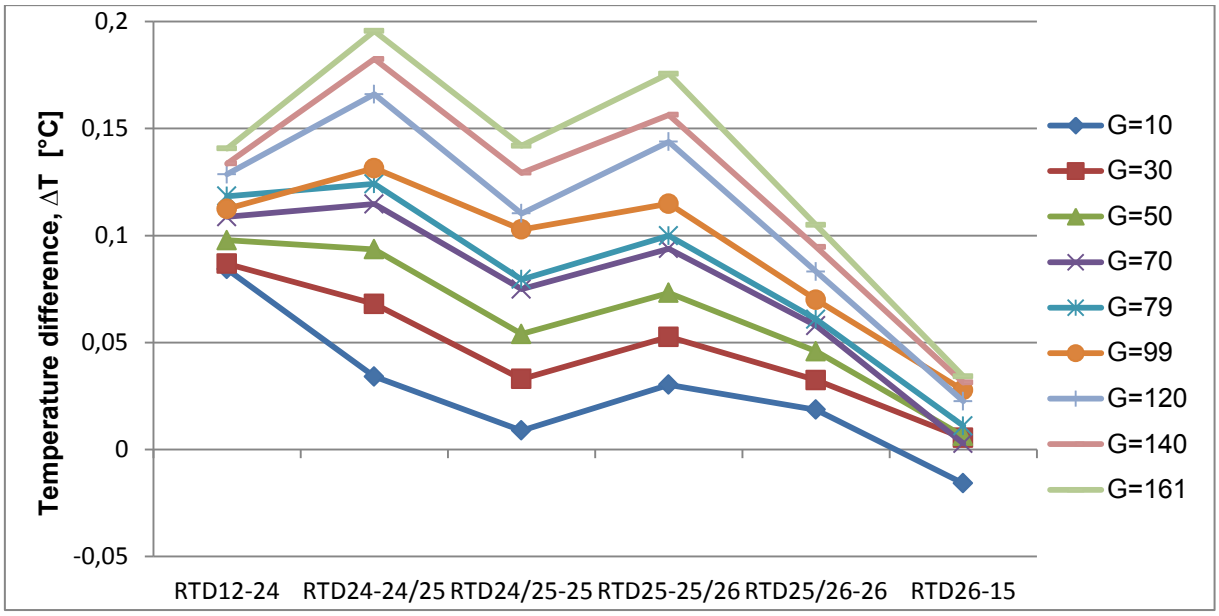

Figure 5.36: Temperature difference between every section of the shell side

It is possible to see how the curves are flatter at lower Reynolds number and the more it rises, the more a "V" trend between the second and fourth deltas is developing. As explained in Section 5.6.1, this trend is the result of the hydrodynamic conditions of the shell side, so with more exchanged heat these deltas become greater. The main difference between the liquid measurements is that the deltas are generally decreasing. This fact is strictly bounded with the outer wall temperature shown in **Errore. L'origine riferimento non è stata trovata.**.

5.8 Two-phase test

As explained in Section 3.1, the KIIR test facility is built in order to investigate the heat transfer coefficient during condensation of hydrocarbons. This means that during the experimental operation when testing actual condensation, in the test section will flow a two phase mixture with decreasing vapor quality along the heat exchanger. To simulate these conditions in the KIIR facility, nitrogen and isopropanol flow together in a non-condensing two phase mixture. Two phase tests are meant to verify the performance and behavior of the test rig when running in this particular condition. The collected data also allows to validate the data reduction spread sheet.

Furthermore heat transfer process of multiphase flow without phase transition is not yet sufficiently examined.

Some papers are already been published about this topic [6], but none of the reported cases fits to the fluid configuration of this plant. Even using the suggested correlation blindly, these lead to bad result not worth to be reported. For this reason the correlation used in this section are the same as in the whole commissioning phase. Mass flow and thermodynamic proprieties of the two phase mixture needed in the correlations are calculated with the homogeneous model, reported in Section 0. Because of this adjustment, the Petukhov correlation cannot be considered the reference anymore, but it will be used as term of comparison since it usually gave the best result. The Hausen's correlation has also been used but, since it is developed for gaseous flows, it loses accuracy as the vapor quality decreases. This lets the graphics to be unreadable, therefore its values are not reported in the figures.

Since it was not possible to perform lots of measurements in this phase of the commissioning, the two-phase test is carried out using a unique specific mass flow ($G = 110\ kg/(s \cdot m\text{^}2\ )$) with changing vapor quality. Six measurement points are recorded, starting from $x = 0$ with a step of $0{,}2$ unities. It was possible to set the rig in the needed flow condition thanks to the separated gas and liquid path. As explained in Section 5.1, every stretch is provided with needle valves capable to regulate the mass flow reaching the test section. Particular attention has been paid because of the pressure loss inducted, since they are significantly different for the two fluids.

5.8.1 Heat transfer coefficients

The calculated heat transfer coefficient is shown in Figure 5.37. The relative behavior of the results is the same as in gas measurement, where Dittus Bölter is giving a higher value than the reference (averagely 12% greater). The particularity is that the heat transfer coefficient of liquid ($x = 0$) is smaller than the one of gas ($x = 1$). This happens because normally, these two states are referred to the same fluid, but in this case gas and liquid are different, so with different thermodynamic proprieties.

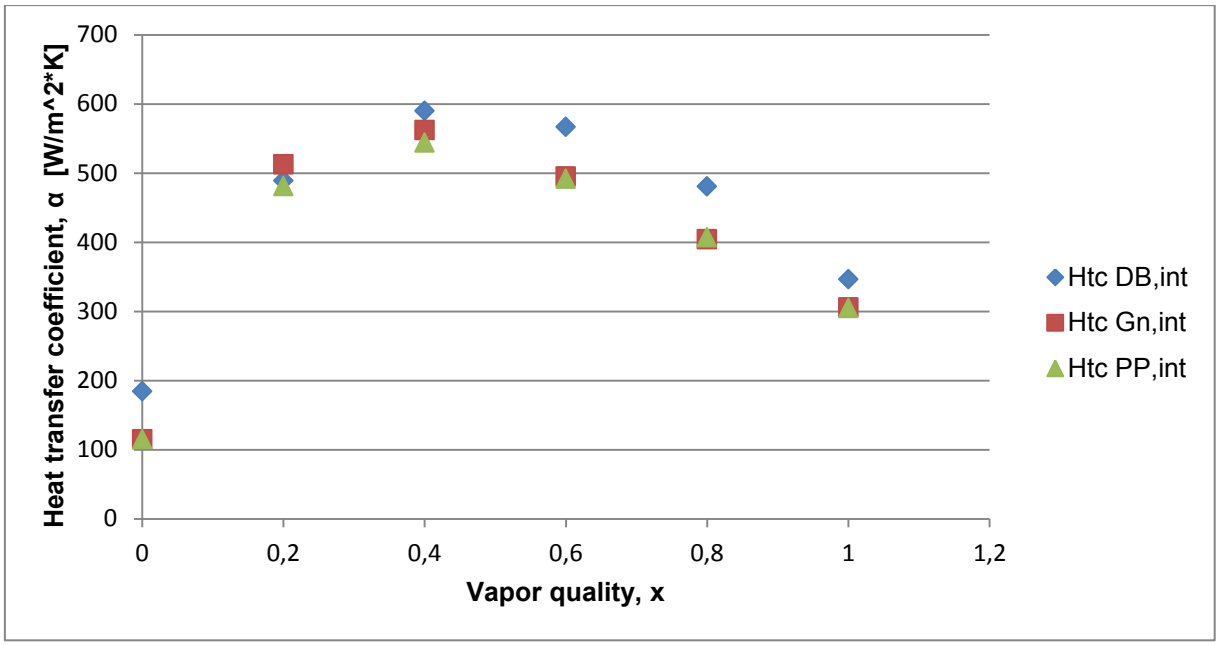

Figure 5.37: Calculated mean heat transfer coefficient in two-phase test

The measured heat transfer coefficients are reported in **Errore. L'origine riferimento non è stata trovata.**. It can be seen that apart the points with 80% of gas, where the values are spreading, all the data collected follow the trend of the reference correlation, so consistent with literature [8]. Particular is that the first and third measurement section are behaving in the same way, and just the second one is giving higher values. So the behavior is even different from the previous tests. In fact, Figure 5.39 shows how the relative discrepancy of first and third section are similar and never exceeding 30%, apart from $x = 0$ and $x = 0{,}8$. Also the calculated mean htc shows good results, according to the reference value with similar discrepancy as the first section. The bad behavior of the second section is here more visible, since the smaller discrepancy is of 32%.

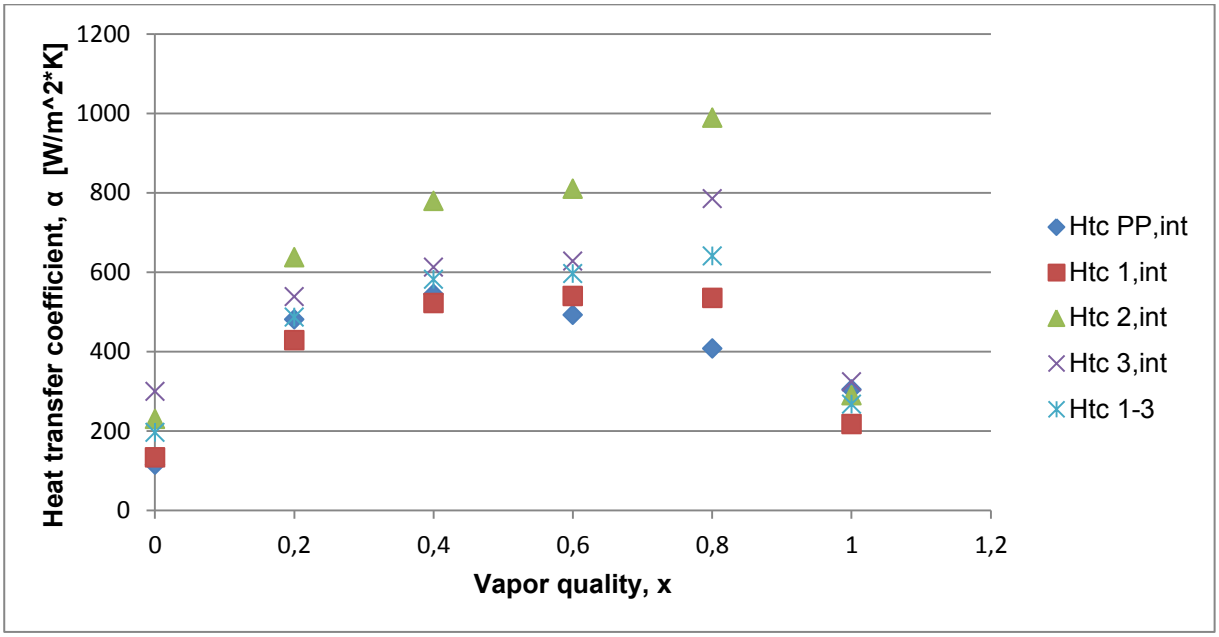

Figure 5.38: Local heat transfer coefficient in two phase test

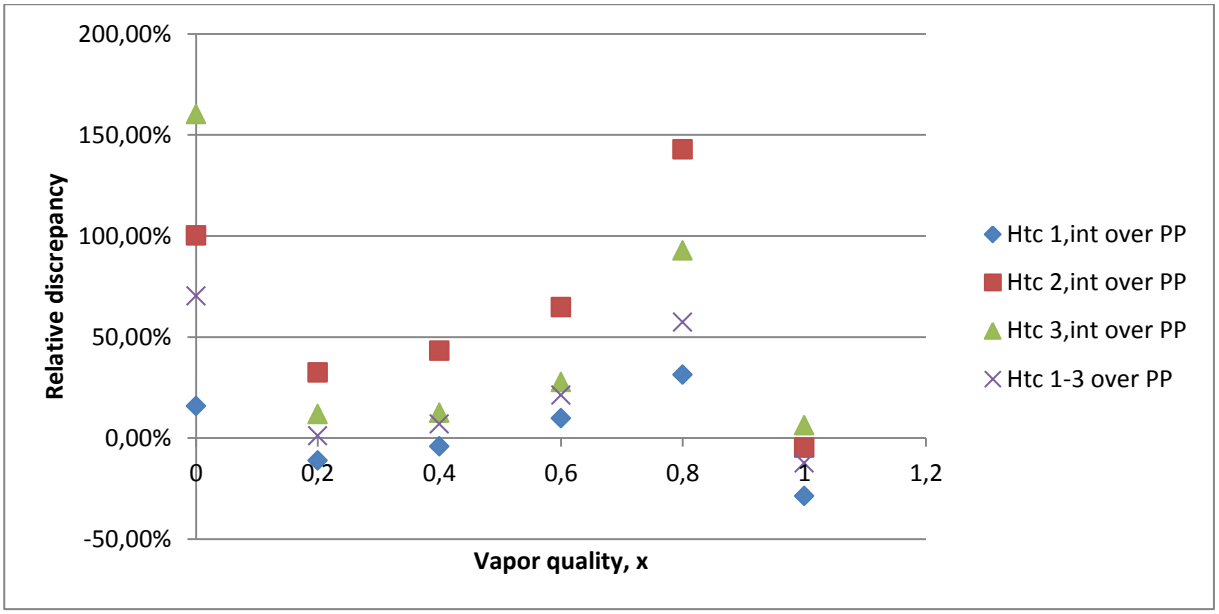

Figure 5.39: Relative discrepancy between local htc and the reference value

External heat transfer coefficient, like in Section 5.7.1, are constant when calculated through correlations as visible in Table 5.22. Actually the values are changed by just one unity.

Table 5.22: External calculated heat transfer coefficient in two phase test

Re	α_{DB} $\frac{W}{m^2 \cdot K}$	α_{Gn} $\frac{W}{m^2 \cdot K}$	α_{PP} $\frac{W}{m^2 \cdot K}$
7267	307	401	393

Measured heat transfer coefficient, in this case, shows interesting results. The first measurement section gives bad result with lesser discrepancy from reference of 162%, while second and third section are behaving good even if far from the expected value. The second section has a worse discrepancy of $37{,}38\%$ while the third has $69{,}18\%$, but with an average of 44%.

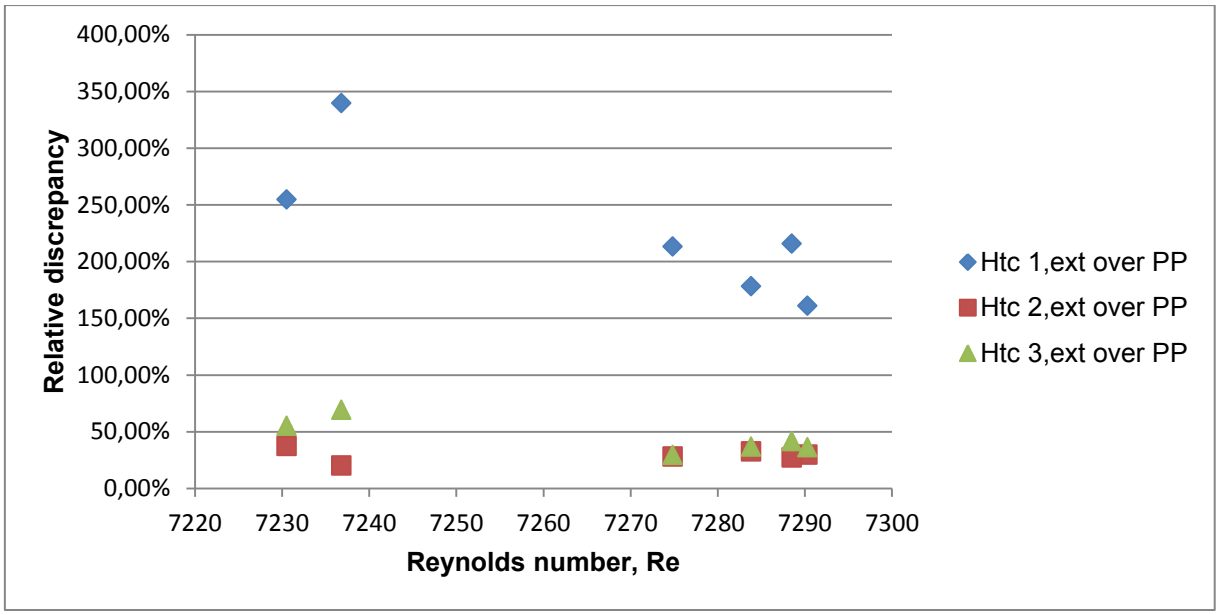

Figure 5.40: Relative discrepancy between local and expected htc in shell side

5.8.2 Temperature of the test section

At this point, where the behavior of gas and liquid measurement is known, the first ($x = 0$) and last ($x = 1$) measurement points behave in the expected way, as visible in Figure 5.41. The intermediate measurements show that the trend develops starting from liquid condition and modifying itself as vapor quality rises, reaching gas condition. The difference in temperature level between the "artificial" saturation condition and the two phase measurement, is caused by the higher heat transfer coefficient. In fact it allows the internal resistance to be smaller, rising the outer wall temperature.

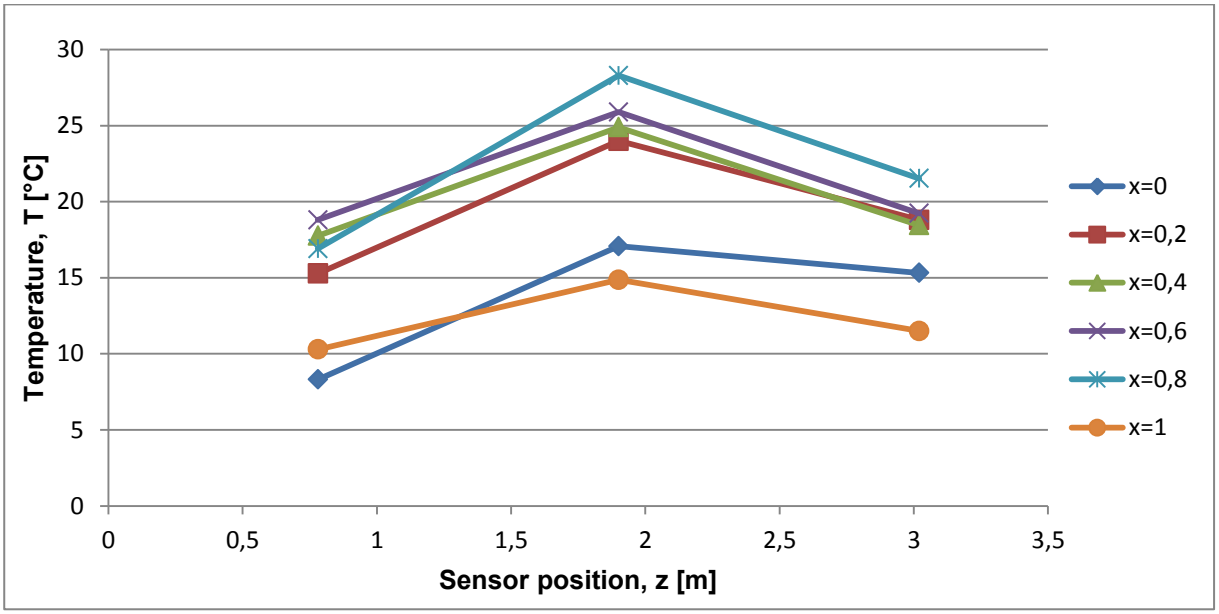

Figure 5.41: Outer wall temperature trend in two phase test

The difference in wall temperature profiles between a single phase (liquid) and a two-phase measurement point is visible in Figure 5.42 and Figure 5.43, is visible the difference in wall temperature profile. As said before, in order to perform a complete transition from liquid to gas flow, a very low mass flow has been chosen. In the first figure, it is possible to notice how the slow speed of the flow allows the development of free convection inside the test pipe. In fact the recorded temperatures of the sensors positioned in the upper side of the pipe are generally higher. Therefore attention must be paid when handling so small mass flows, especially when the working fluid is a liquid phase.

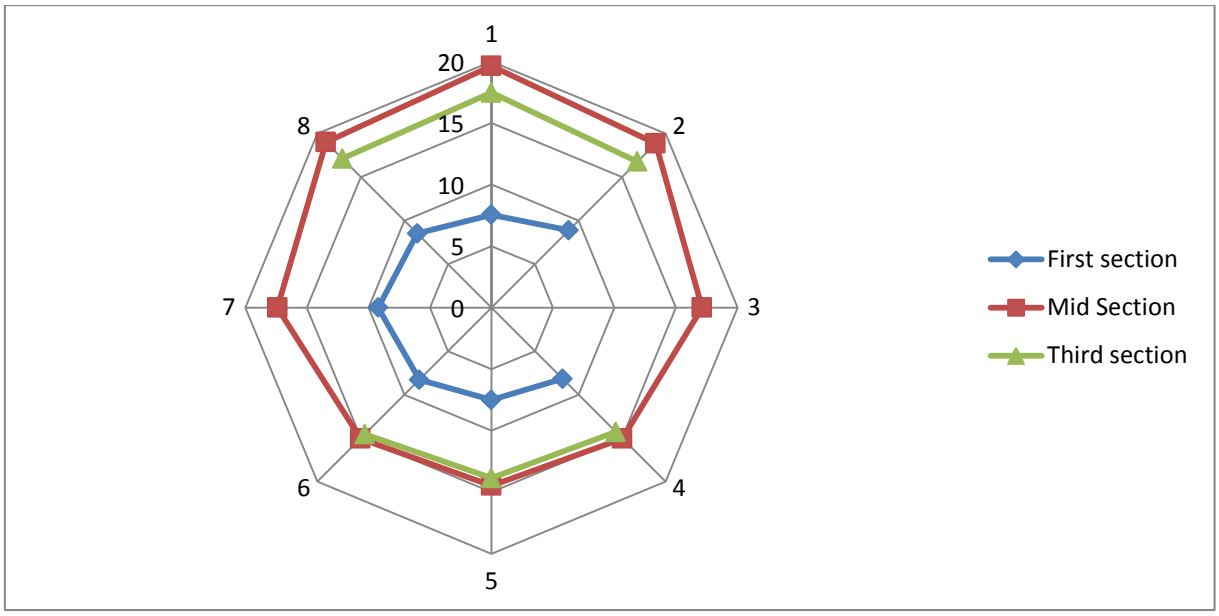

Figure 5.42: Outer wall temperature profile [°C] for $x = 0$

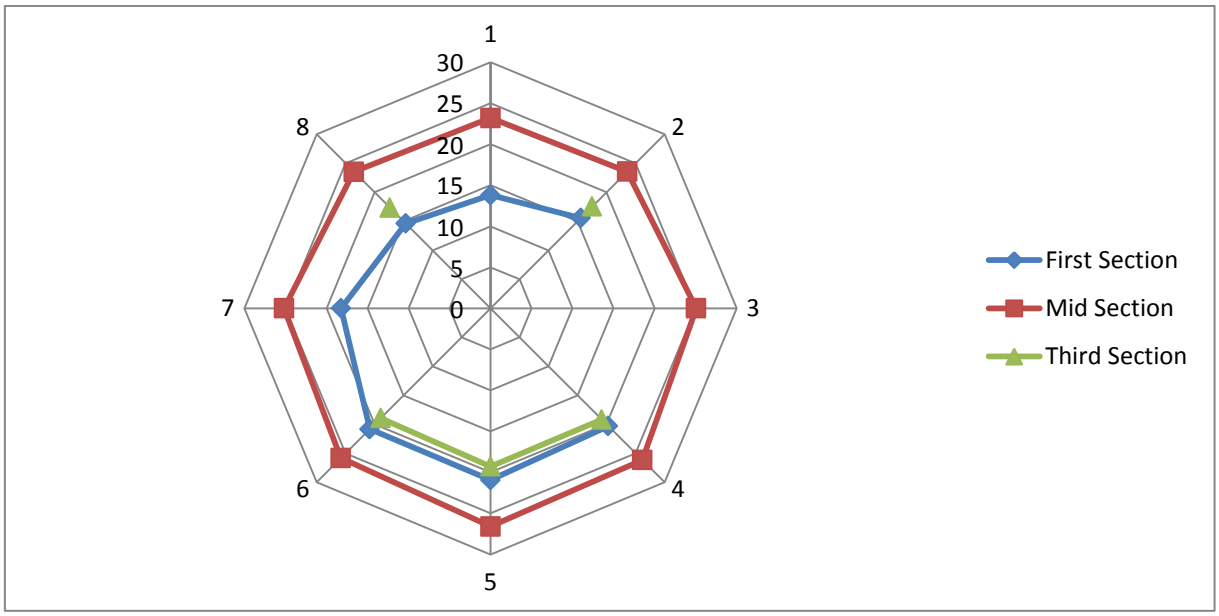

Figure 5.43: Outer wall temperature profile [°C] for $x = 0{,}4$

The second figure, represents the situation when 40% of the mass flow is composed of gas. The temperature profile is changed, showing higher values on the bottom side of the pipe. This can be explained with a reduction of the heat transfer coefficient on the upper side due to the presence of the gas phase. In fact with so little mass flow, the momentum of the fluid is not enough to stand the buoyancy forces, and the two

phase flow moves with a stratified flow. So the gas is concentrated on the upper side of the test pipe increasing the thermal resistance.

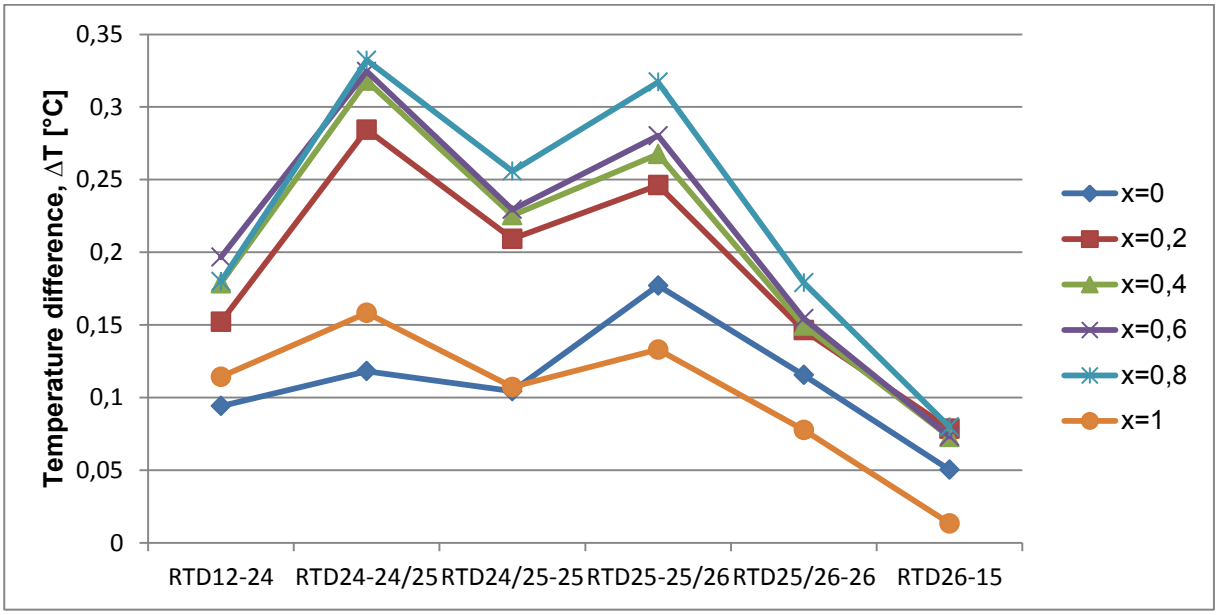

Figure 5.44: Temperature difference between each section of the shell side

The temperature difference between the measurement section of the shell side behaves as expected. Liquid and gas only measurement show the same trend as in the previous tests, taking in account the reduced mass flow. The two phase points have the same “V” trend as in the previous tests, but even with little heat exchanged, the relative difference between the temperature differences is greater, probably due to the stratification of the flow.

6 CONCLUSIONS

The commissioning of a test section for the calculation of the in-tube heat transfer coefficient was carried out. Several tests meant to prove the functioning of the test rig have been performed using isopropanol as working fluid.

The tests brought to light that the configuration of the sub-pipes delivering the coolant in the shell side of the heat exchanger allows an inlet effect to occur. This increases the htc oil side changing the equilibrium of the heat exchange process in that spot. The supply of the cooling fluid plays therefore and important role.

In addition, it has been discovered that the capillary pipes supporting the TC's of the mid measurement section are generating a turbulence which varies the htc of the shell side downstream. These two effects combined together let the heat exchange process to be not homogeneous.

For these reason in counter flow configuration only the first measurement section results reliable with local heat transfer coefficient averagely $7{,}8\%$ smaller than the Petukhov correlation, taken as reference. In direct flow configuration, the effects presented above act differently, and the reliable measurement sections are the second and the third with mean discrepancy of $2{,}9\%$ and $10{,}8\%$.

A simplified uncertainty propagation for the liquid tests is reported, showing that the measured htc has smaller uncertainty than the calculated one. This is mainly caused by the uncertainty assumed for the thermal proprieties of the fluids since no exact values were reported in literature. Nevertheless the discrepancy between this two values is not comprehended in the uncertainty interval.

Gas tests were performed in direct flow condition. In this case the reliable sections (second and third) have a discrepancy of -8% and 13% over the expected value.

Two-phase test were carried out in direct flow configuration too and to analyze the results the correlation used so far are adapted with the homogeneous model. Local htc values results good results in the first measurement section with discrepancy of $-0{,}5\%$ to the adapted Petukhov correlation, still considered as reference. Second and third measurement section behave worse with discrepancy generally increasing with vapor quality and mean values averagely 55% and 14% more than the reference value.

In the light of what has been proved in the tests, the shell side of the heat exchanger needs to be changed. In order to avoid the inlet effect identified the sub-pipes must

be moved far from the first and third measurement section and a new configuration for them is suggested. By placing them tangentially to the sell pipe with a pitch angle of $90°$, the coolant should reach measurement section with an homogeneous flow.
The mid measurement section is important for the purpose of the project but the actual construction is strongly affecting the behavior of the heat exchanger, therefore, a proper solution is still object of test.
Temperature trend of the coolant in direct flow condition is still not fully understood and needs to be studied in future tests.

7 REFERENCES

[1] Commission of the European Communities: Limiting Global Climate Change to 2 degrees Celsius. The way ahead for 2020 and beyond; Brussels 2007

[2] BP p.l.c.: BP Statistical Review of World Energy – June 2013; London 2013

[3] Verein Deutscher Ingenieure: VDI-Heat Atlas; Springer; Berlin 2010

[4] Bonacina, C.; Cavallini, A.; Mattarolo, L.: Trasmissione del Calore; Cleup Editore; Padua 1992

[5] ISO ENV 13005: “Guide to the expression of uncertainty in measurement (GUM)”

[6] Kim, D.; Ghajar, A.J.; Dougherty, R.L.; Ryali, V.K.: Comparison of 20 Two-Phase Heat Transfer Correlation with Seven Sets of Experimental Data, Including Flow Pattern and Tube Inclination Effects; Heat transfer engineering; vol.20; no.1; 1999

[7] Shao, W.; Granryd, E.: Flow Condensation of Pure and Oil Contaminated Refrigerant HFC134a in a Horizontal Tube; International Refrigeration and Air Conditioning Conference; 1994

[8] Coppetti, J.B.; Macagnan, M.H.; Kunsler, N.: Boiling of R-134a in horizontal mini tube; J. Braz. Soc. Mech. Sci. & Eng.; vol.33; no. 1 Rio de Janeiro 2011

[9] Robinson D.M.; Thome J.R.: Local Bundle Boiling Heat Transfer Coefficients on a Plain Tube Bundle; HVAC&R Research; 10; 2004; pp. 33-51

[10] Hemmerling, K., Luke, A.: Inbetriebnahme einer Versuchsanlage zur Untersuchung des Wärmeübergangs von Kohlenwasserstoffen in horizontalen Rohren; Technische Thermodinamik, Universität Kassel; 2014

[11] Fischer, P.; Luke, A.: Theoretische Auslegung und Inbetriebnahme einer Anlage zur Messung des Wärmeübergangs bei der Kondensation von Gemischen; Technische Thermodinamik, Universität Kassel; 2013

[12] Huang, X.; Ding, G; Hu., H.; Zhu, Y.; Peng, H.; Gao, Y.; Deng, B.: Influence of oil on flow condensation heat transfer of a R410a inside 4,18 mm and 1.6 mm inner diameter horizontal smooth tubes; Proc. 13th Int. Heat Transfer Conference; Sydney 2006; KN-21

[13] Thome, J.R.: Wolverine Engineering Data Book III; Wolverine Tube Inc.

[14] Park, K.j.; Jung, D.; Deo, T.: Flow condensation heat transfer characteristic of hydrocarbon refrigerant and dimethyl ether inside a horizontal plain tube; Internationa Journal of Multiphase Flow; 34; 2008, pp. 628-635

[15] Shah, M. M.: A general correlation fo heat transfer during film condensing inside pipes; International Journal of Heat and Mass Transfer; 22; 1979, pp. 547-556

[16] Tandon, T. N.; Varma, H. K.; Gupta, C.: Heat transfer during forced convection condensation inside horizontal tube; International Journal of Refrigeration; 18; 3; 1995; pp.210-214

[17] Rotta, J.: Turbulente Stroemungen, Verlag Teubner, Stuttgart, 1972

[18] Friedel, L.: Pressure drop during gas/vapor-liquid flow in pipes; International Chemical Engineering; 20; 1980; pp.193-213

[19] Lockhart, R. W.; Martinelli, R. C.: Proposed Correlation of Data for Isothermal Two-Phase, Two-Component Flow in Pipe; Chem. Eng. Prog.; 45; 1949; pp.39-48

[20] Smith, S.L.: Void Fractions in Two-Phase Flow: A Correlation Based upon an Equal Velocity Head Model; Proceedings of the Institution of Mechanical Engineers; vol. 184; no. 1; June 1969; pp.647-664

[21] Ghajar, A.J.: Non-Boiling Heat Transfer in Gas-Liquid Flow in Pipes – a Tutorial; Journal of the Brazilian Society of Mechanical Scientists & Engineers; January-March 2005; 27; 1; pp.46-73

8 APPENDIX

8.1 Pressure Losses

- Single phase flow

In its flow, the fluid is prone to frictional forces caused by the resistance to flow, that will lead to a pressure drop along the pipe. In order to sustain the internal flow this pressure drop must be evaluated. Through the momentum balance of an infinitesimal flow part, the whole drop can be estimated through the pressure gradient and then divided in three different parts: one due to momentum variation, one due to gravity, and one due to friction losses:

$$(-\Delta p)_{tot} = (-\Delta p)_m + (-\Delta p)_g + (-\Delta p)_f \qquad 8.1$$

- $(-\Delta p)_m = G^2 \cdot \left(\frac{1}{\rho_{out}} - \frac{1}{\rho_{in}}\right)$, where G is the specific mass flux;
- $(-\Delta p)_g = g \cdot \rho \cdot L \cdot sin\,\beta$, where *g* is the acceleration of gravity and *β* the slope of the pipe;
- $(-\Delta p)_f = 2 \cdot f \cdot \frac{L}{D_h} \cdot \frac{G^2}{\rho}$, where f is the frictional factor.

These contributions change a lot according to the type of process happening in the considered section. For example momentum contribution is negligible when no phase change is occurring, and gravity contribution is negligible when the pipe is horizontal. The friction factor is strictly bounded with the type of flow, so there is a specific formula for every case.

- Two phase flow

Between the types of two phase flow, gas/liquid flow is the most complex configuration since the interface is deformable and the gaseous phase is compressible. Therefore the calculation of pressure drop in this case needs to be simplified. There are two ways of handle the problem, supposing that the phases are flowing homogeneously or heterogeneously.

Used in this work is the homogeneous model, based on the hypothesis that the gas phase and the liquid phase are flowing with the same speed $w_g = w_f$, so like a compressible one-phase flow. It follows, that every formula describing two phase behavior has changed, introducing homogeneous proprieties:

- $\varepsilon_{OM} = \frac{x}{\rho_g} \Big/ \left(\frac{x}{\rho_g} + \frac{1-x}{\rho_l}\right)$ Homogeneous void fraction [20]

- $\rho_m = \rho_{OM} = \varepsilon_{OM} \cdot \rho_g + (1 - \varepsilon_{OM}) \cdot \rho_l = \left(\frac{x}{\rho_g} + \frac{1-x}{\rho_l}\right)^{-1}$ Homogeneous density
- $\nu_{OM} = x \cdot \nu_g + (1 - x) \cdot \nu_l$ Homogeneous specific volume
- $\mu_{OM} = x \cdot \mu_g \cdot \rho_{OM}/\rho_g + (1 - x) \cdot \mu_l \cdot \rho_{OM}/\rho_l$ Homogeneous viscosity [20]

According to the homogeneous model, the contributions of the total pressure drop are now expressed with homogeneous properties. Gravity and Momentum contributions are simply calculated with the previous properties. Friction is evaluated with an empirical correlation similar to the ones of single phase flow:

- $(-\Delta p)_{m,OM} = G^2 \cdot \left(\frac{1}{\rho_{OM,out}} - \frac{1}{\rho_{OM,in}}\right)$;
- $(-\Delta p)_{g,OM} = g \cdot \rho_{OM} \cdot L \cdot \sin\beta$;
- $(-\Delta p)_{f,OM} = 2 \cdot f_{OM} \cdot \frac{L}{D_h} \cdot \frac{G^2}{\rho_{OM}}$,
  - $f_{OM} = 0{,}079 \cdot {Re_{OM}}^{-0{,}25}$ is the homogeneous frictional factor function of the homogeneous Raynolds

8.2 Therminol proprieties

- $\rho\left[\frac{kg}{m^3}\right] = A + B \cdot T(℃) + C \cdot T^2(℃) + D \cdot T^3(℃)$
- $c_p\left[\frac{kJ}{kg \cdot K}\right] = A + B \cdot T(℃) + C \cdot T^2(℃) + D \cdot T^3(℃) + E \cdot T^4(℃)$
- $\lambda\left[\frac{W}{m \cdot K}\right] = A + B \cdot T(℃) + C \cdot T^2(℃)$
- $\mu\left[\frac{mm^2}{s}\right] = e^{\left(\frac{A}{T(℃)+B} + C\right)}$

	A	B	C	D	E
ρ	776,257	−0,696982	−0,000131384	$-2{,}09079 \cdot 10^{-6}$	
c_p	2,01422	0,00386884	$2{,}05029 \cdot 10^{-6}$	$-1{,}12621 \cdot 10^{-8}$	$3{,}86282 \cdot 10^{-11}$
λ	0,112994	−0,00014781	$1{,}61429 \cdot 10^{-7}$		
μ	−3562,69	146,4	−2,68168		

8.3 Sensitivity indexes

$$Nu_{PP} = \frac{f/8 \cdot (Re - 1000) \cdot Pr}{C + 12{,}7 \cdot (f/8)^{\frac{1}{2}} \left(Pr^{\frac{2}{3}} - 1\right)} \cdot \left[1 + \left(\frac{D_h}{L}\right)^{\frac{2}{3}}\right]$$

$$\frac{\partial Nu_{PP,GN}}{\partial Re} = \frac{f/8 \cdot Pr}{C + 12{,}7 \cdot (f/8)^{\frac{1}{2}} \left(Pr^{\frac{2}{3}} - 1\right)} \cdot \left[1 + \left(\frac{D_h}{L}\right)^{\frac{2}{3}}\right]$$

$$\frac{\partial Nu_{PP,GN}}{\partial D_h} = \frac{f/8 \cdot (Re - 1000) \cdot Pr}{C + 12{,}7 \cdot (f/8)^{\frac{1}{2}} \left(Pr^{\frac{2}{3}} - 1\right)} \cdot \frac{2}{3 \cdot D_h} \cdot \left(\frac{D_h}{L}\right)^{\frac{2}{3}}$$

$$\frac{\partial Nu_{PP,GN}}{\partial L} = \frac{f/8 \cdot (Re - 1000) \cdot Pr}{C + 12{,}7 \cdot (f/8)^{\frac{1}{2}} \left(Pr^{\frac{2}{3}} - 1\right)} \cdot \left(\frac{-2}{3 \cdot L}\right) \cdot \left(\frac{D_h}{L}\right)^{\frac{2}{3}}$$

$$\frac{\partial Nu_{PP,GN}}{\partial Pr} = \frac{f/8 \cdot (Re - 1000) \cdot \left[1 + \left(\frac{D_h}{L}\right)^{\frac{2}{3}}\right]}{\left[C + 12{,}7 \cdot (f/8)^{\frac{1}{2}} \left(Pr^{\frac{2}{3}} - 1\right)\right]^2} \cdot \left\{C + 12{,}7 \cdot (f/8)^{\frac{1}{2}} \cdot \left[\frac{Pr^{\frac{2}{3}}}{3} - 1\right]\right\}$$

$$\frac{\partial Nu_{PP,GN}}{\partial f} = \frac{Pr/8 \cdot (Re - 1000) \cdot \left[1 + \left(\frac{D_h}{L}\right)^{\frac{2}{3}}\right]}{\left[C + 12{,}7 \cdot (f/8)^{\frac{1}{2}} \left(Pr^{\frac{2}{3}} - 1\right)\right]^2} \cdot \left\{C + \frac{12{,}7}{2} \cdot (f/8)^{\frac{1}{2}} \cdot \left[Pr^{\frac{2}{3}} - 1\right]\right\}$$

$$\frac{\partial Nu_{PP}}{\partial C} = \frac{-f/8 \cdot Pr \cdot (Re - 1000)}{\left[C + 12{,}7 \cdot (f/8)^{\frac{1}{2}} \left(Pr^{\frac{2}{3}} - 1\right)\right]^2} \cdot \left[1 + \left(\frac{D_h}{L}\right)^{\frac{2}{3}}\right]$$

$$f = (1{,}82 \cdot logRe - 1{,}64)^{-2} \qquad \frac{\partial f}{\partial Re} = \frac{-2 \cdot 1{,}82}{Re \cdot (1{,}82 \cdot \log(Re) - 1{,}64)^3}$$

$$C = 1{,}07 + \frac{900}{Re} - \frac{0{,}63}{1 + 10 \cdot Pr}$$

$$\frac{\partial C}{\partial Re} = -\frac{900}{Re^2} \qquad \frac{\partial C}{\partial Pr} = \frac{6{,}3}{(1 + 10 \cdot Pr)^2}$$

$$Nu_{DB} = 0{,}026 \cdot Re^{0{,}8} \cdot Pr^{0{,}3}$$

$$\frac{\partial Nu_{DB}}{\partial Re} = 0{,}026 \cdot 0{,}8 \cdot Re^{-0{,}2} \cdot Pr^{0{,}3} \qquad \frac{\partial Nu_{DB}}{\partial Pr} = 0{,}026 \cdot Re^{0{,}8} \cdot 0{,}3 \cdot Pr^{-0{,}7}$$

$$Nu_{Ha} = a \cdot (Re^b - c) \cdot Pr^{0,4} \cdot \left[1 + \left(\frac{D_h}{L}\right)^{\frac{2}{3}}\right]$$

$$\frac{\partial Nu_{Ha}}{\partial Re} = a \cdot b \cdot Re^{b-1} \cdot Pr^{0,4} \cdot \left[1 + \left(\frac{D_h}{L}\right)^{\frac{2}{3}}\right] \qquad \frac{\partial Nu_{Ha}}{\partial Pr} = a \cdot (Re^b - c) \cdot 0{,}4 \cdot Pr^{-0,6} \cdot \left[1 + \left(\frac{D_h}{L}\right)^{\frac{2}{3}}\right]$$

$$\frac{\partial Nu_{Ha}}{\partial D_h} = a \cdot b \cdot Re^{b-1} \cdot Pr^{0,4} \cdot \frac{2}{3 \cdot D_h} \cdot \left(\frac{D_h}{L}\right)^{\frac{2}{3}} \qquad \frac{\partial Nu_{Ha}}{\partial L} = a \cdot b \cdot Re^{b-1} \cdot Pr^{0,4} \cdot \left(\frac{-2}{3 \cdot L}\right) \cdot \left(\frac{D_h}{L}\right)^{\frac{2}{3}}$$

$Pr = \frac{c_p \cdot \mu}{\lambda}$	$Re = \frac{G \cdot D_h}{\mu}$	$Nu = \frac{Nu \cdot \lambda}{L}$
$\frac{\partial Pr}{\partial c_p} = \frac{\mu}{\lambda}$ $\frac{\partial Pr}{\partial \mu} = \frac{c_p}{\lambda}$ $\frac{\partial Pr}{\partial \lambda} = -\frac{c_p \cdot \mu}{\lambda^2}$	$\frac{\partial Re}{\partial D_h} = \frac{G}{\mu}$ $\frac{\partial Re}{\partial G} = \frac{D_h}{\mu}$ $\frac{\partial Re}{\partial \mu} = -\frac{G \cdot D_h}{\mu^2}$	$\frac{\partial \alpha}{\partial Nu} = \frac{\lambda}{L}$ $\frac{\partial \alpha}{\partial \lambda} = \frac{Nu}{L}$ $\frac{\partial \alpha}{\partial L} = -\frac{Nu \cdot \lambda}{L^2}$
$G = \frac{\dot{m}}{A}$	$\frac{\partial G}{\partial A} = -\frac{\dot{m}}{A^2}$	$\frac{\partial G}{\partial \dot{m}} = \frac{1}{A}$
$A = \frac{\pi \cdot D^2}{4}$	$\frac{\partial A}{\partial D} = \frac{\pi \cdot D}{2}$	

$$R_{Corr} = \frac{\ln \frac{D_{n+1}}{D_n} \cdot D_{int}}{2 \cdot \lambda_n}$$

$$\frac{\partial R_{corr}}{\partial D_{n+1}} = \frac{D_{int}}{D_{n+1} \cdot 2 \cdot \lambda_n} \qquad \frac{\partial R_{corr}}{\partial D_n} = \frac{-D_{int}}{D_n \cdot 2 \cdot \lambda_n} \qquad \frac{\partial R_{corr}}{\partial D_1} = \frac{\ln\left(\frac{D_2}{D_1}\right) - 1}{2 \cdot \lambda_1}$$

$$\frac{\partial R_{wall}}{\partial D_{int}} = \frac{\ln\left(\frac{D_{ext}}{D_{int}}\right) - 1}{2 \cdot \lambda_1} \qquad \frac{\partial R_{corr}}{\partial \lambda_n} = -\frac{\ln\left(\frac{D_{n+1}}{D_n}\right) \cdot D_{int}}{2 \cdot {\lambda_n}^2}$$

$$T_{WF,i} = T_{WF,in} - \frac{\dot{m}_{Th} \cdot c_{p,Th} \cdot \Delta T_{th}}{\dot{m}_{WF} \cdot c_{p,WF}}$$

$$\frac{\partial T_{WF,i}}{\partial \dot{m}_{Th}} = -\frac{c_{p,Th} \cdot \Delta T_{th}}{\dot{m}_{WF} \cdot c_{p,WF}} \qquad \frac{\partial T_{WF,i}}{\partial c_{p,Th}} = -\frac{\dot{m}_{Th} \cdot \Delta T_{th}}{\dot{m}_{WF} \cdot c_{p,WF}} \qquad \frac{\partial T_{WF,i}}{\partial \Delta T_{th}} = -\frac{\dot{m}_{Th} \cdot c_{p,Th}}{\dot{m}_{WF} \cdot c_{p,WF}}$$

$$\frac{\partial T_{WF,i}}{\partial \dot{m}_{WF}} = \frac{\dot{m}_{Th} \cdot c_{p,Th} \cdot \Delta T_{th}}{{\dot{m}_{WF}}^2 \cdot c_{p,WF}} \qquad \frac{\partial T_{WF,i}}{\partial c_{p,WF}} = \frac{\dot{m}_{Th} \cdot c_{p,Th} \cdot \Delta T_{th}}{\dot{m}_{WF} \cdot {c_{p,WF}}^2}$$

$A = \pi \cdot D \cdot L$	$\frac{\partial A}{\partial D} = \pi \cdot L$	$\frac{\partial A}{\partial L} = \pi \cdot D$

$$Q = \dot{m}_{WF} \cdot c_{p,WF} \cdot \Delta T_{WF}$$

$$\frac{\partial Q}{\partial \dot{m}_{WF}} = c_{p,WF} \cdot \Delta T_{WF} \qquad \frac{\partial Q}{\partial c_{p,WF}} = \dot{m}_{WF} \cdot \Delta T_{WF} \qquad \frac{\partial Q}{\partial \Delta T_{WF}} = \dot{m}_{WF} \cdot c_{p,WF}$$

$$\Delta T = \frac{\Delta_1 - \Delta_2}{ln\frac{\Delta_1}{\Delta_2}}$$

$$\frac{\partial \Delta T}{\partial \Delta_1} = \frac{ln\frac{\Delta_1}{\Delta_2} - \frac{\Delta_1 - \Delta_2}{\Delta_1}}{\left(ln\frac{\Delta_1}{\Delta_2}\right)^2} \qquad \frac{\partial \Delta T}{\partial \Delta_2} = \frac{\frac{\Delta_1 - \Delta_2}{\Delta_2} - ln\frac{\Delta_1}{\Delta_2}}{\left(ln\frac{\Delta_1}{\Delta_2}\right)^2}$$

$$\alpha_{int,1-3} = \left(\frac{A_{1-3} \cdot \Delta T_{ln,1-3}}{\dot{Q}_{1-3}} - R_{wall}\right)^{-1}$$

$$\frac{\partial \alpha}{\partial A} = -\frac{\Delta T_{ln} \cdot \dot{Q}}{\left(\dot{Q} \cdot R_{wall} - \Delta T_{ln} \cdot A\right)^2} \qquad \frac{\partial \alpha}{\partial \Delta T_{ln}} = -\frac{A \cdot \dot{Q}}{\left(\dot{Q} \cdot R_{wall} - \Delta T_{ln} \cdot A\right)^2}$$

$$\frac{\partial \alpha}{\partial \dot{Q}} = \frac{\Delta T_{ln} \cdot A}{\left(\Delta T_{ln} \cdot A - \dot{Q} \cdot R_{wall}\right)^2} \qquad \frac{\partial \alpha}{\partial R_{wall}} = \frac{\dot{Q}}{\left(\Delta T_{ln} \cdot A - \dot{Q} \cdot R_{wall}\right)^2}$$

$$\dot{q}_{z,i} = \frac{\dot{m}_{WF} \cdot c_{p,th}}{\pi \cdot D_{int}} \cdot T_{f(z)}$$

$$\frac{\partial \dot{q}_{z,i}}{\partial \dot{m}_{WF}} = \frac{c_{p,th}}{\pi \cdot D_{int}} \cdot T_{f(z)} \qquad \frac{\partial \dot{q}_{z,i}}{\partial c_{p,th}} = \frac{\dot{m}_{WF}}{\pi \cdot D_{int}} \cdot T_{f(z)}$$

$$\frac{\partial \dot{q}_{z,i}}{\partial z} = \frac{\dot{m}_{WF} \cdot c_{p,th}}{\pi \cdot D_{int}} \cdot \frac{dT_{f(z)}}{dz} \qquad \frac{\partial \dot{q}_{z,i}}{\partial D_{int}} = -\frac{\dot{m}_{WF} \cdot c_{p,th}}{\pi \cdot {D_{int}}^2} \cdot T_{f(z)}$$

$$\alpha_{int,i} = \left(\frac{\Delta T_i}{\dot{q}_{z,i}} - R_{corr,in}\right)^{-1}$$

$$\frac{\partial \alpha}{\partial \Delta T_i} = -\frac{\dot{q}_{z,i}}{\left(\Delta T_i - \dot{q}_{z,i} \cdot R_{corr}\right)^2} \qquad \frac{\partial \alpha}{\partial \dot{q}_{z,i}} = \frac{\Delta T_i}{\left(\Delta T_i - \dot{q}_{z,i} \cdot R_{corr}\right)^2} \qquad \frac{\partial \alpha}{\partial R_{corr}} = \frac{{\dot{q}_{z,i}}^2}{\left(\Delta T_i - \dot{q}_{z,i} \cdot R_{corr}\right)^2}$$

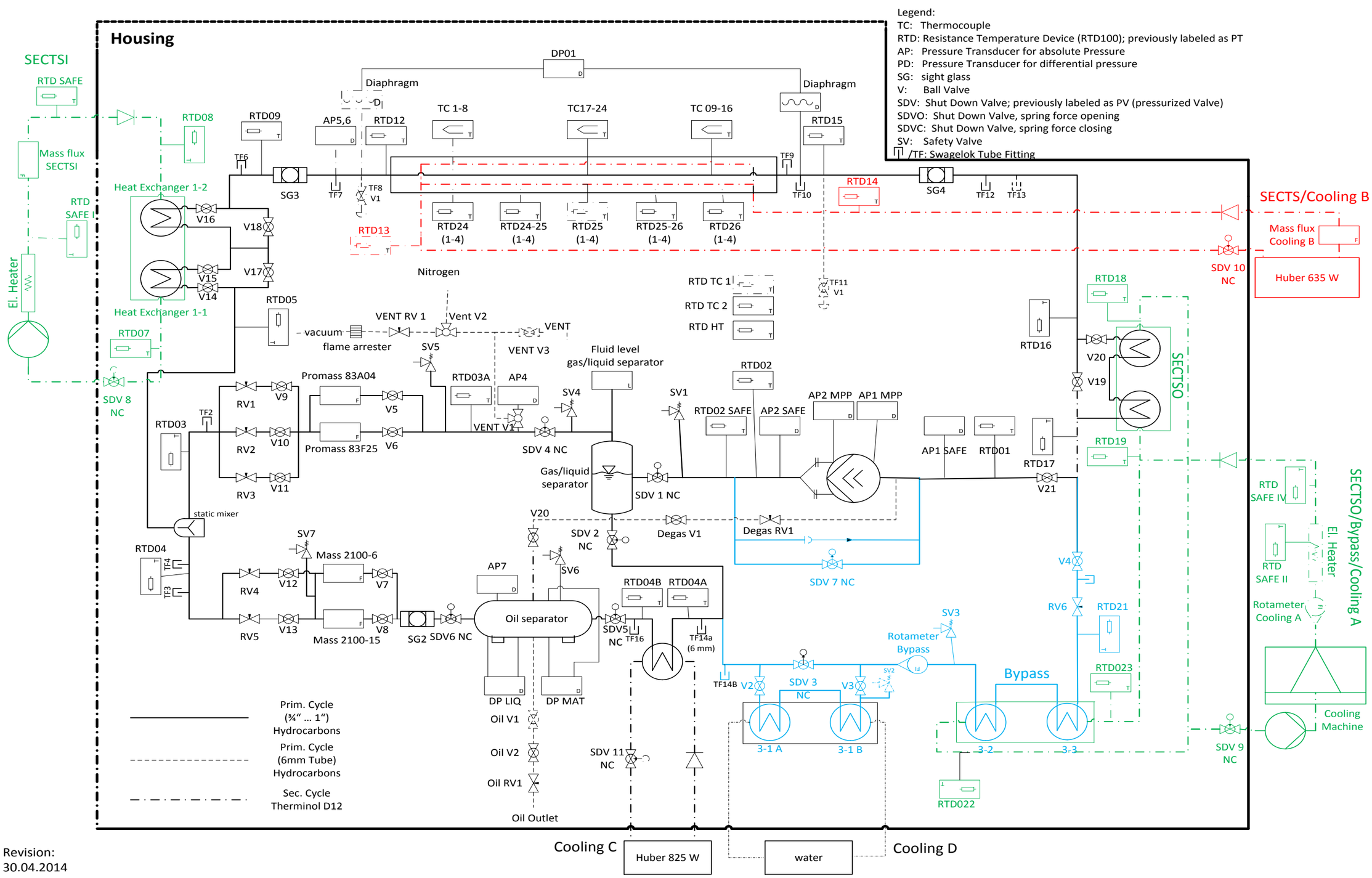

Legend:
TC: Thermocouple
RTD: Resistance Temperature Device (RTD100); previously labeled as PT
AP: Pressure Transducer for absolute Pressure
PD: Pressure Transducer for differential pressure
SG: sight glass
V: Ball Valve
SDV: Shut Down Valve; previously labeled as PV (pressurized Valve)
SDVO: Shut Down Valve, spring force opening
SDVC: Shut Down Valve, spring force closing
SV: Safety Valve
/TF: Swagelok Tube Fitting

Revision:
30.04.2014

Figure 8.1: Flow sheet of the test facility